This is to certify that the

dissertation entitled

STRUCTURE STUDIES OF ^{11}Li AND ^{10}Li

presented by

Brian Matthew Young

has been accepted towards fulfillment
of the requirements for

Ph.D. degree in Nuclear Physics

Walter Benenson
Major professor

Date DEC 23 1993

STRUCTURE STUDIES OF ^{11}Li AND ^{10}Li

By

Brian Matthew Young

A DISSERTATION

Submitted to
Michigan State University
in partial fulfillment of the requirements
for the Degree of

DOCTOR OF PHILOSOPHY

Department of Physics and Astronomy

1993

ABSTRACT

STRUCTURE STUDIES OF ^{11}Li AND ^{10}Li

By

Brian Matthew Young

The nucleus ^{11}Li, only recently available for extensive study with the advent of facilities that produce radioactive nuclear beams, has presented nuclear theorists and experimentalists with an intriguing puzzle. Experimental evidence indicates that ^{11}Li consists of a ^{9}Li core and a "halo" of two loosely bound neutrons, the matter radius of which extends well beyond that observed in most nuclei. Theoretical models have been developed which utilize this picture and predict a very sensitive dependence of the ^{11}Li two–neutron binding energy on the nature of the n–^{9}Li interaction. The mass of ^{11}Li has been determined from a measurement of the Q–value of the reaction ^{14}C(^{11}B,^{11}Li)^{14}O at $E/A \approx 32$ MeV. The results, which indicate a two–neutron separation energy of $S_{2n}(^{11}\mathrm{Li}) = 295 \pm 35$ keV, put this basic quantity on a firm basis for use in these theoretical models. Experimental measurements and theoretical predictions of the low–lying structure of the unbound nucleus ^{10}Li have presented sometimes conflicting, but mounting evidence that ^{10}Li has a ground state consisting of a low–lying $2s\frac{1}{2}$ neutron resonance and at least one excited state consisting of a $1p\frac{1}{2}$ neutron resonance unbound by between 400 and 800 keV. Momentum spectra have been measured for the reaction ^{11}B(^{7}Li,^{8}B)^{10}Li at $E/A \approx 19$ MeV and laboratory angles of 5° and 3.5°. The results indicate the existence of a broad state in ^{10}Li, corresponding to a single p–wave neutron resonance unbound to neutron decay by 538 ± 62 keV with width $\Gamma_{\mathrm{lab}} = 358 \pm 23$ keV. There is also evidence that the ^{10}Li

ground state is either an s- or a p-wave resonance barely unbound to neutron decay with $S_n \geq -100$ keV and $\Gamma_{\rm lab} < 230$ keV.

Dedicated to my wife, Kathryn.

ACKNOWLEDGEMENTS

During my stay at the NSCL, I have had the privilege to work with many truly fine individuals. What follows is a woefully incomplete list of folk who have helped me during my four–plus years here.

I would like to thank my advisor, Walter Benenson, for his help and what now seem like almost superhuman displays of patience and calm during my work here. I would also like to thank Alex Brown, George Bertsch, and Mikhail Zhukov for innumerable helpful discussions and for entertaining equally innumerable questions about nuclear structure and resonance calculations. Toshiyuki Kubo, Henning Esbensen, Ian Thompson, and Rubby Sherr also lent a great deal of assistance without which the work contained in this dissertation would not have been possible.

Maggie Hellström is one of the dearest friends I have ever known. Her support and encouragement during a particularly murky period of my life have meant more to me than she will ever know. Maggie is always willing to lend a hand and advice when asked, and, perhaps more importantly, has the uncanny ability to inject good–humored sanity into *any* situation. Such injections were frequently needed and greatly appreciated, and I consider myself very lucky to know and to have worked with her. I would also like to thank Sherry Yennello for her encouragement and kindness during the whole nightmarish postdoc search.

I am especially grateful to Brad Sherrill, Michael Thoennessen, John Stevenson, David Morrissey, Jim Clayton, and Mike Mohar for teaching me so much about the *right* way to conduct nuclear physics experiments.

Among the most enjoyable experiences I've had here are the beer–brewing sessions with Phil Zecher, Mathias Steiner, Damian Handzy, and David McGrew. Phil and I often colored these sessions with discussions of libertarianism, the philosophy and

novels of Ayn Rand, and the financial aspects of chaos theory (or was it the chaotic aspects of financial theory). For two years I shared an office with Mathias, something for which I think he deserves a medal. I mercilessly inflicted upon him my infernal libertarian views, my equally infernal musical tastes, and (even worse) daily doses of Rush Limbaugh. Although I think he realized the last was predominantly for theatrical effects: Mathias on an indignant tirade was infinitely more entertaining than Limbaugh ever could have been. It was quite entertaining to share with Damian his *first* reading of Atlas Shrugged; although I'm sure he got as much enjoyment out of my first reading of Tolkien's ring trilogy. My basement, in addition to providing fermenting space for homebrews, also managed to contain the hellish noises that David and I were wont to make with guitars and other bits of electronic gadgetry. I think between the two of us we managed to set musical evolution back several millenia. Michael Fauerbach, Raman Pfaff, Don Sackett, Easwar Ramakrishnan, John "Ned" Kelley, Jeff Winger, Daniel Bazin, and Nigel Orr have also shared countless shifts, beers, pizzas, parties, annoying songs, and interminable meetings with me and have in no small way made lab life tolerable. I would also like to thank the students of the Physics 231 class that I taught while I was writing this dissertation. I realize that none of them will ever read this, but it was with them that I learned just how much fun it is to teach a group of students, to make the connection, and to actually have them leave the classroom knowing more than they did fifty minutes before.

You have all made my time here incredibly rewarding and enjoyable, and I will miss you all.

My parents have a picture of me on Career Day in fifth grade. Most of the other kids wanted to be rock stars, pilots, baseball players, and policemen; then here's Brian in a lab coat (actually, it was my mom's old raincoat) holding a vial of something (pump oil, maybe, or liquid scintillator). When I told my parents I wanted to be a physicist, they had no idea what one looked like. Their best guess was the lab coat and the vial. I must have scared the living daylights out of them. I shudder to think how much money I cost them with my penchant for taking apart various household appliances and applying magnets to the television to figure out where the colors came from. I owe my parents an immeasurable amount of gratitude for putting up with my antics, questions, and destructive experiments when I was growing up. Thanks a million, you guys.

Finally, I would like to thank my wife, Kathryn, for everything. For not getting upset when I came dragging in at all hours of the morning, for fielding phone calls while I was working, for bringing me dinner at the lab, for tolerating my positively annoying habit of brainstorming while strolling around our apartment playing the banjo, for coming up here to this frozen wasteland to live with me for four and a half years. What can I say? She deserves just as much credit as I do for the work contained in these pages. Thank you, Ryn, you've given me so much, and made it all worthwhile.

Contents

List of Tables

List of Figures

Chapter 1

Introduction–Motivation and Overview

Recent advances in accelerator and spectrometer design have made possible the production of intense radioactive nuclear beams. This has greatly expanded the region of experimentally obtainable nuclei to encompass nuclear species far from stability. The availability of these unstable nuclei has resulted in a large amount of exploration and mapping of the neutron and proton drip lines, the boundaries marking the upper limits on neutron and proton numbers beyond which nuclei become particle unstable. Experiments which involve nuclei near the drip lines have revealed structures and dynamic systems very different from those previously studied. These new systems have presented a challenge to nuclear models which were developed to describe phenomena exhibited by nuclei closer to the valley of stability.

One of the most interesting nuclei to challenge traditional models is ^{11}Li. A large body of experimental work has been carried out in an attempt to understand its structure. These experiments have indicated that ^{11}Li consists of a ^{9}Li core and a "halo" of two loosely bound neutrons, the matter radius of which extends well beyond that observed in most nuclei. With these ideas as a starting point, several calculations have been made which treat ^{11}Li as a three–body system comprising a ^{9}Li core and

2 neutrons. Hansen and Jonson have demonstrated in [Hans 87] that in the simplest model of ^{11}Li, a quasi–deuteron consisting of a ^{9}Li core coupled to a dineutron ^{2}n, the binding energy is the only variable needed to find the momentum and spatial distributions of particles within the nucleus. More complex models have also shown that the radius, and even the existence, of a neutron halo is intimately dependent on the binding energy of the halo neutrons. For this reason, an accurate experimental value for the ^{11}Li binding energy is of vital importance to the understanding of the halo phenomena.

There is however, some uncertainty in the value of the mass of ^{11}Li. The three measurements to date have yielded two–neutron separations energies ranging from 170 to 340 keV with uncertainties from 50 to 120 keV. The substantial disagreement between these measurements as well as the magnitude of their uncertainties limits their usefulness in theoretical calculations. In September of 1992, the ^{11}Li mass was deduced from the Q–value of the ^{14}C(^{11}B,^{11}Li)^{14}O reaction measured with the A1200 fragment separator at the NSCL. In Chapter 2 of this work, a more detailed discussion of previous experiments pertaining to ^{11}Li is presented along with a discussion of several two– and three–body models that have been developed to reproduce the results of these experiments. Chapter 3 contains a detailed description of the NSCL ^{11}Li mass measurement. The computer code, RELMASS, used in the analysis of the data from this experiment, is presented in Appendix A.

Central to the models described above is the interaction of a single neutron with the ^{9}Li core. The fact that ^{11}Li is loosely bound while ^{10}Li, with one less neutron, is unbound implies that the interaction between the valence neutrons plays a vital role in the stability and structure of ^{11}Li. For this reason, there is considerable interest in the unbound nucleus ^{10}Li. The low–lying structure of ^{10}Li is the subject of much debate, however. There has been a great deal of effort, both experimental and theoretical, directed towards understanding the structure of this nucleus. These efforts have resulted in claims that the ^{10}Li ground state, a resonance of a single unbound neutron in a ^{9}Li well, is unbound by as little as 60 keV and as much as 800 keV. It is expected, in analogy with other $N = 7$ nuclei, that the ^{10}Li ground state resonance should be either a $1p\frac{1}{2}$ or a $2s\frac{1}{2}$ neutron state. In addition to significant uncertainty regarding the resonance energy, there is also a great deal of disagreement on the spectroscopic nature of the ^{10}Li ground state. In May of 1992, the low-lying structure of ^{10}Li was determined from momentum spectra which were collected from the reaction ^{11}B(^{7}Li,^{8}B)^{10}Li at the NSCL. Chapter 4 of the present work contains a review of the existing measurements of the low-lying structure of ^{10}Li as well as a detailed description of our measurement. Computer codes for calculating the shapes of the ^{10}Li neutron resonances and for fitting the resonance shapes to the experimental data are presented in Appendices B and C respectively.

The experimental results presented in this work will be summarized in Chapter 5. The three–body models described above predict a sensitive dependence of several observables on not only the resonance energies of the lowest ^{10}Li states, but also their spectroscopic nature. Most calculations assume that the ^{10}Li ground state is a $1p\frac{1}{2}$ neutron resonance. However, very recent calculations by Thompson and Zhukov have included a $2s\frac{1}{2}$ states as well as a $1p\frac{1}{2}$ state in the n–^{9}Li interaction. The results of these calculations and their agreement with our experimental data will also be discussed.

Chapter 2

History of ^{11}Li

I Introduction

This chapter contains a description of the main trends of experimental and theoretical research that have been directed towards ^{11}Li. Experimental results are discussed in section II. Measurements of parallel and transverse momentum distributions of ^{9}Li fragments from the breakup of ^{11}Li are described as are measurements of neutrons observed in coincidence with the ^{9}Li fragments, and measurements of Coulomb dissociation cross sections of ^{11}Li. It is seen that the experimental evidence indicates that ^{11}Li can be described as a three-body system consisting of a ^{9}Li core with a spatially broad "halo" of two loosely bound neutrons. Based on the three–body picture described above, several theoretical models have been developed. A sketch of these models and some of their results are presented in section III. In particular, it is shown that these models predict that the radius, and even the existence, of a neutron halo is intimately dependent on the binding energy of the halo neutrons. A brief discussion is presented in section IV concerning the low–lying structure of ^{10}Li and its effects on the results of these models. A more detailed discussion of this topic is presented in Chapter 5. The sensitive dependence of halo phenomena on the neutron binding energy emphasizes the necessity for an accurate measurement of the

^{11}Li binding energy. The three existing measurements of the ^{11}Li mass are detailed in section V.

II Structure of ^{11}Li – Experimental Results

The existence of ^{11}Li as a particle–stable drip line nucleus was known for quite some time [Posk 66, Klap 69]. It was not until 1985, however, that evidence was found that ^{11}Li might have a structure radically different from that predicted by traditional nuclear models [Tani 85a]. Tanihata *et al.* report the results of interaction cross section measurements for several lithium isotopes (^{6}Li - ^{11}Li) as well as ^{7}Be, ^{9}Be, and ^{10}Be. These measurements were performed with a beam energy of E/A = 790 MeV and targets of beryllium, carbon, and aluminum. The lithium and beryllium projectiles were produced as secondary beams by fragmenting beams (E/A = 800 MeV) of ^{11}B and ^{20}Ne on a beryllium production target. The isotopes in the secondary beam were separated by magnetic rigidity and identified by velocity, from time–of–flight measurements, and by charge, from pulse height measurements in scintillation counters, before incidence on the reaction target. The interaction cross section, defined as the total reaction cross section for changing the proton and/or neutron number in the incident nucleus, was measured using the high–acceptance spectrometer described in [Tani 85b]. It was found that the interaction cross section could be separated into contributions from the projectile and target

$$\sigma = \pi \left[R_{\mathrm{T}} + R_{\mathrm{P}}\right]^2 \tag{2.1}$$

where R_{T} and R_{P} are the radii of the target and projectile, respectively. The measured radii of most of the projectiles were between 2.09 and 2.46 fm, a result that is in good agreement with the empirical relation derived from the liquid drop model of a nucleus with mass number A, $R = (1.2 \text{ fm}) \cdot A^{1/3}$ [Blat 52]. The measured radius of ^{11}Li, however, was 3.14 fm, a value much larger than that of other nuclei in this mass region. It is suggested in [Tani 85a] that this large radius indicates a large deformation or a long tail in the matter distribution of ^{11}Li.

To further understand the structure of ^{11}Li, and in particular the large matter radius, experiments have been performed to measure the momentum distributions of ^{9}Li from the fragmentation of ^{11}Li projectiles. It has long been known that the momentum distributions of fragmentation reaction products exhibit an isotropic Gaussian distribution in the projectile rest frame [Grei 75]. The width of this distribution can be interpreted in terms of Fermi motion and/or nuclear binding energy [Gold 74], or in terms of the momentum distribution of the fragment inside the projectile [Hüfn 81, Shim 87]. Based on these ideas, it is hoped that information about the momentum distributions from fragmentation of ^{11}Li may shed some light on its structure.

In the first measurement of the momentum distributions of products from ^{11}Li fragmentation [Koba 88], Kobayashi *et al.* fragmented primary beams of ^{20}Ne and ^{22}Ne at E/A = 800 MeV to produce secondary beams of 790 MeV/nucleon ^{11}Li, ^{8}He, and ^{6}He. The secondary beams were then fragmented on carbon and lead targets. The reaction products were analyzed using the HISS magnetic spectrometer at the Bevalac in the Lawrence Berkeley Laboratory. The transverse–momentum (i.e. perpendicular to the beam axis) distributions of several projectile fragments are presented and analyzed in [Koba 88]. The momentum distributions for most of the fragments exhibited the expected Gaussian shape. An example of this is shown in part a) of Figure 2.1, which depicts the transverse–momentum distribution of ^{6}He fragments from ^{8}He projectiles on a carbon target. The width of the fitted Gaussian is σ = 77 MeV/c. It has been shown by Goldhaber [Gold 74], that the width σ of fragmentation momentum distributions can be parametrized by a single parameter

σ_0 as

$$\sigma^2 = \sigma_0^2 \frac{A_\mathrm{F}(A_\mathrm{P} - A_\mathrm{F})}{A_\mathrm{P} - 1} \tag{2.2}$$

where A_P and A_F are the mass numbers of the projectile and fragment, respectively, and σ_0 is the reduced width. The reduced width for the ^{6}He data is 59 MeV/c.

A decidedly different result was observed for the ^{9}Li momentum distribution, shown in part b) of Figure 2.1. For the ^{9}Li data, there was a two–Gaussian peak structure. The wide component corresponds to a reduced width of 53 MeV/c, in good agreement with the values obtained from the ^{6}He data as well as the data collected from other fragmentation reactions. The narrow component corresponds to a reduced width of 17 MeV/c. According to Goldhaber, the reduced width can be related to the Fermi momentum P_F of the projectile by $\sigma_0 = \sqrt{5}\,P_F$. In this picture, the existence of two reduced widths implies two Fermi momenta, an unphysical conclusion.

To interpret their data, Kobayashi *et al.* relied on the models developed by Hüfner and Nemes [Hüfn 81] and Shimoura *et al.* [Shim 87]. In their models, which approximate the fragment momentum distribution by the Fourier transform of the asymptotic wave function of the projectile, the reduced width can be related to the fragment separation energy $\langle \varepsilon \rangle$ by

$$\sigma^2 = M_p \langle \varepsilon \rangle \frac{A_\mathrm{P} - 1}{A_\mathrm{P}} \tag{2.3}$$

Under this interpretation, the narrow momentum component in the ^{9}Li data corresponds to $\langle \varepsilon \rangle = 0.34$ MeV. When compared with the one– and two–neutron separation energies of ^{10}Li and ^{11}Li, this result indicates that the ^{9}Li fragments in the narrow peak come from reactions in which two weakly bound outer neutrons are removed from ^{11}Li. The broad momentum component comes from removal of two less weakly bound neutrons, decay of excited ^{9}Li, and neutron decay of ^{10}Li. This observation

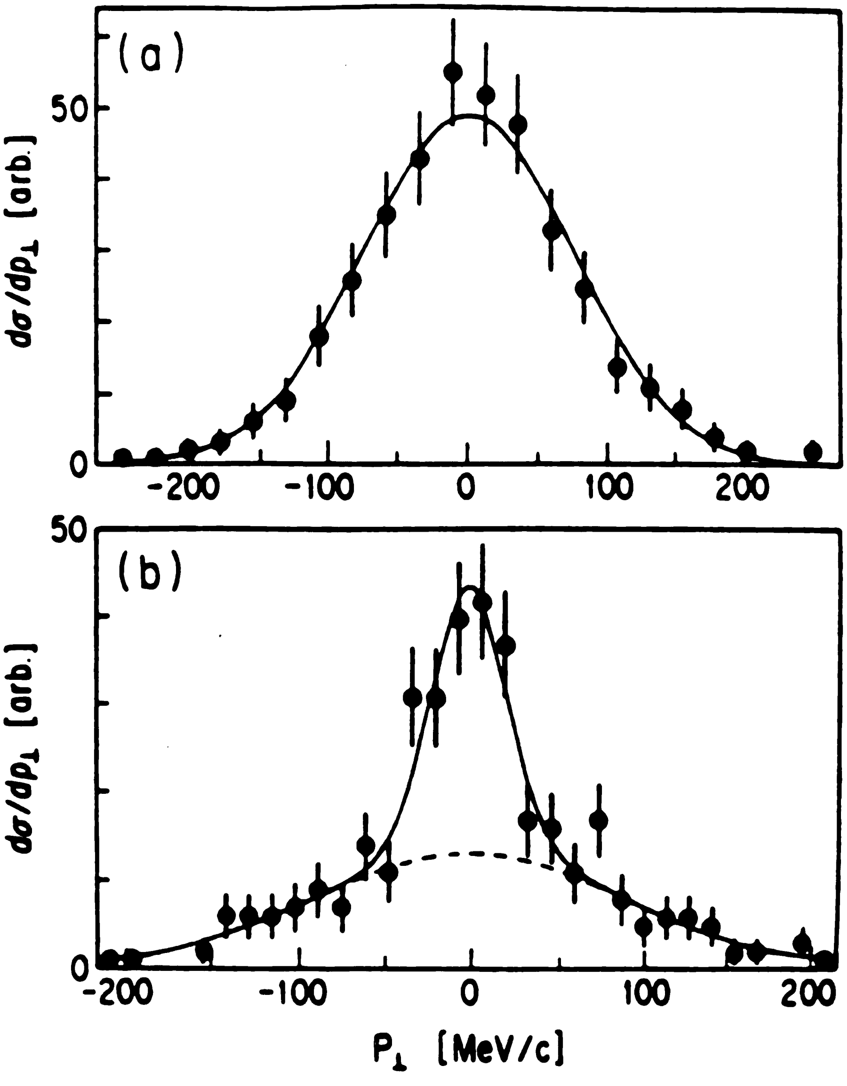

Figure 2.1: [Koba 88] a) Transverse–momentum distribution of ^{6}He fragments from the reaction of ^{8}He at $E/A = 790$ MeV on a C target. The solid line is a fitted Gaussian distribution with a width $\sigma \approx 80$ MeV/c. b) Transverse–momentum distribution of ^{9}Li fragments from reactions of ^{11}Li at $E/A = 790$ MeV on a C target. The dotted line is a contribution from the wide component of the ^{9}Li distribution. The solid line is the sum of the narrow and wide components. The widths of these components are $\sigma = 23$ MeV/c and $\sigma = 95$ MeV/c.

also provides an understanding of the large ^{11}Li matter radius measured by Tanihata *et al.*. By the Heisenberg Uncertainty Principle, a narrow momentum component corresponds to a broad spatial component, and vice versa. Thus, the narrow component in the ^{9}Li comes from a broad spatial distribution attributable to a long tail in the probability distribution for the two loosely bound neutrons in ^{11}Li. It is this long tail which dominated the matter radius measurements of Tanihata *et al.*.

Of particular importance, given this measurement, is the question of whether the momentum distributions of projectile fragmentation products reflect the structure of the projectile only or also depend on the fragmentation reaction itself. A possible avenue of inquiry is to study fragmentation reactions from low–Z and high–Z targets, in which the contributions to the total reaction from Coulomb interactions and nuclear interactions differ strongly. However, for reactions on a high–Z target, narrow structures in the transverse–momentum distribution, of the type observed by Kobayashi *et al.*, would become washed out by Coulomb deflection and multiple scattering. Parallel–momentum distributions, which, since the total momentum distribution is isotropic, are known to have widths similar to those of transverse–momentum distributions for the same reaction, do not suffer from these drawbacks. In 1992, Orr *et al.* measured the parallel–momentum distributions of ^{9}Li nuclei from projectile fragmentation reactions of ^{11}Li on targets of ^{9}Be, ^{93}Nb, and ^{181}Ta at $E/A = 66$ MeV [Orr 92]. Their results indicate that the momentum widths do not depend strongly on the Z of the target. For all targets, parallel–momentum widths of $\sigma \approx 19$ MeV/c were observed. Assuming this momentum component comes from a two–neutron spatial distribution having a Yukawa functional form ($\exp(-r/\rho)/r$), this momentum width yields an rms radius of 6.2 fm.

In addition to the effort described above, experiments have been performed by Anne, Riisager and collaborators [Anne 90, Riis 92] in which the spatial extent of the outer two neutrons in ^{11}Li has been deduced from the angular distributions of neutrons from the fragmentation of ^{11}Li. In these experiments, secondary beams of ^{11}Li at $E/A = 29$ MeV were collided with targets of beryllium, nickel, and gold. The angular distributions of single neutrons from the (^{11}Li,^{9}Li) reactions, reported in [Anne 90], are shown in Figure 2.2. By assuming that each of the outer two ^{11}Li neutrons is represented by a Yukawa wave function with a range parameter ρ and transforming this spatial distribution to momentum space, it was found that the angular distributions of the neutrons should have a Lorentzian shape. When this functional form was fitted to the data (as depicted with the solid lines in Figure 2.2), the range parameter ρ was found to be approximately 12 fm for all three targets, a value which corresponds to an rms radius of 8.5 fm. Further analysis of this data, reported in [Riis 92], support these conclusions.

Based on experiments such as these, the nucleus ^{11}Li has come to be viewed as a three–body system consisting of a ^{9}Li core and a "halo" of two loosely bound neutrons as depicted in Figure 2.3. While the radius of ^{9}Li is approximately 2.5 fm, the experimental evidence has indicated that the rms radius of the two halo neutrons is between 6 and 10 fm. One of the more interesting phenomena predicted by theoretical models which incorporate this picture, some of which will be discussed in the next section, is the "soft" mode of the giant dipole resonance. In nuclei closer to the valley of stability, the (isovector) giant dipole resonance is an excitation mode in which the protons and neutrons in the nucleus oscillate collectively about the nuclear center–of–mass but in opposite phase with each other [Gold 48, Wong 90]. In a nucleus of mass A, the giant dipole resonance (GDR) energy is found to be roughly proportional to $A^{-1/3}$. For nuclei with mass near $A = 10$, the GDR energy is approximately 22 MeV. However, for a halo nucleus, such as ^{11}Li, it has been proposed [Hans 87] that two GDR excitations exist. One, dubbed the "hard" or "normal" mode, involves the

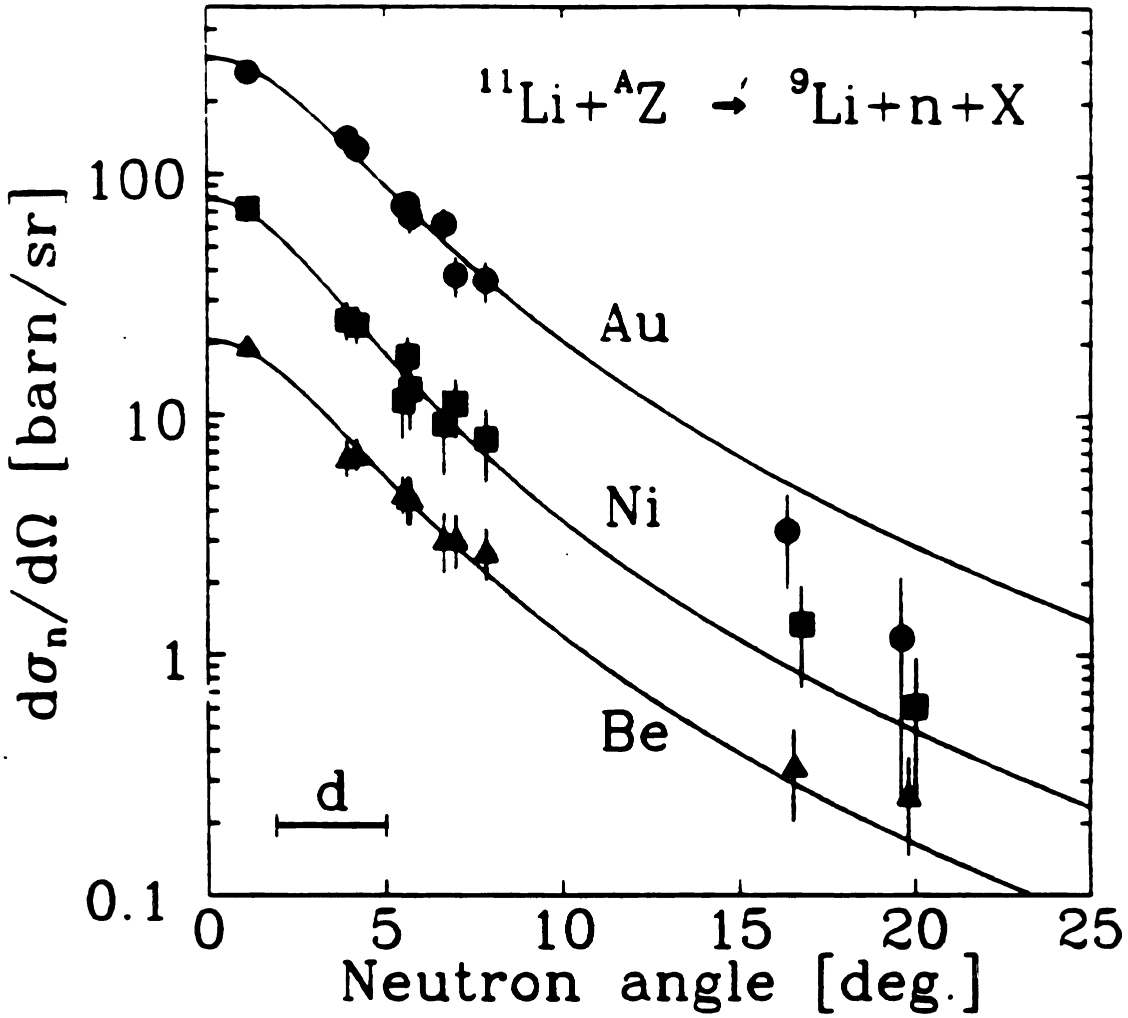

Figure 2.2: [Anne 90] Angular distributions of single neutrons from the (^{11}Li,^{9}Li) reaction on Be, Ni, and Au targets at $E/A = 29$ MeV [Anne 90, Riis 92]. The solid lines are Lorentzian functional forms, derived from the assumption that both of the outer two ^{11}Li neutrons have a Yukawa wave function.

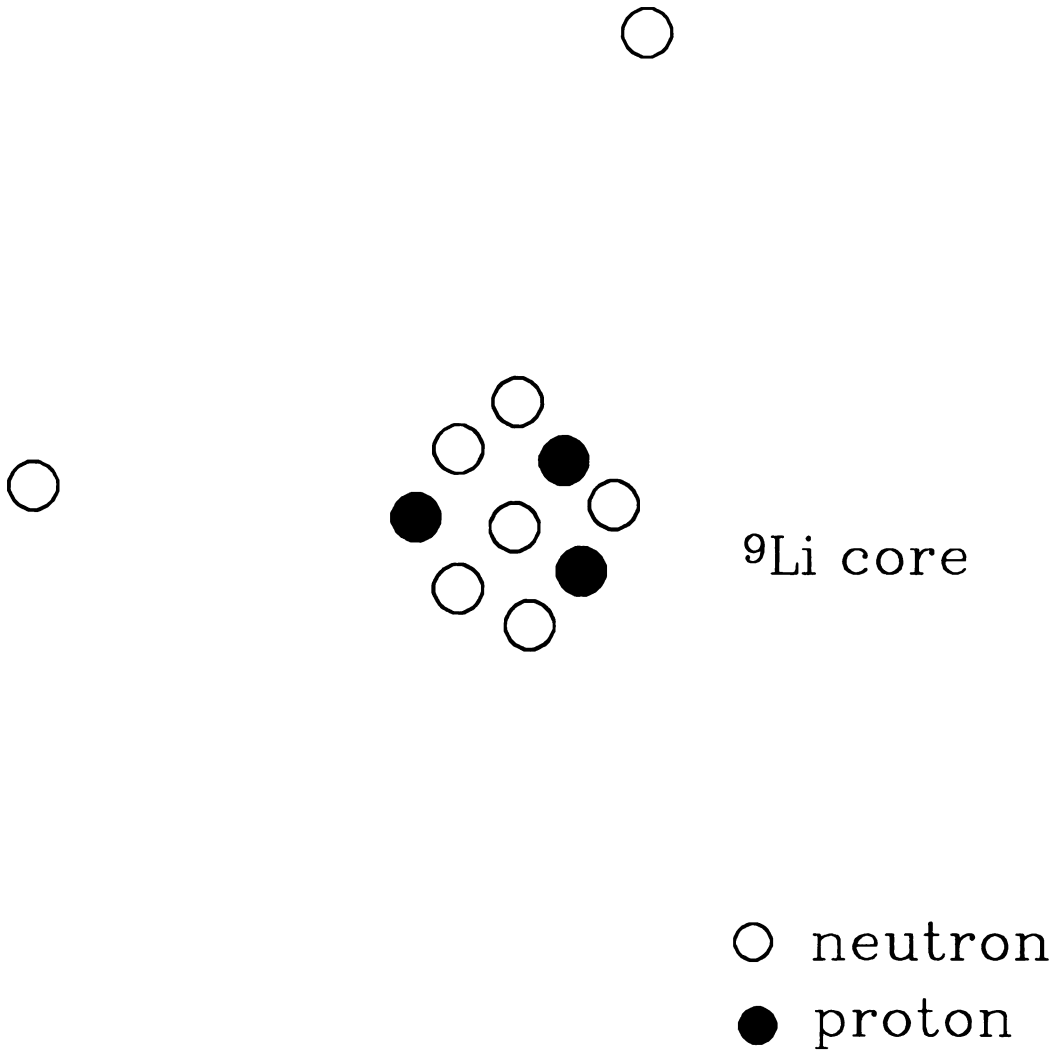

Figure 2.3: Schematic diagram of ^{11}Li halo structure. Experimental evidence has indicated that ^{11}Li is a three–body system consisting of a ^{9}Li core and a halo of two loosely bound neutrons.

traditional GDR of the *core* nucleus only, leaving the halo neutrons unaffected. The energy of this resonance is expected to be very close to the GDR energy of the naked core nucleus. The other mode is labelled the "soft" mode, and has the core nucleus and the neutron halo oscillating against one another. The restoring force for such an oscillation is very small, and consequently the energy of this resonance is expected to be quite small (roughly 1.0 MeV for ^{11}Li).

Experimental evidence for the existence of this soft GDR presents a tantalizing problem. The first possible evidence for such an excitation was reported by Kobayashi *et al.* in 1989 [Koba 89]. Secondary beams of ^{11}Li were collided with targets of beryllium, carbon, copper, aluminum, and lead at $E/A = 800$ MeV. From the dependence of the interaction cross section, defined as the total cross section for changing the proton and/or neutron number of the projectile, on the target proton number, the electromagnetic dissociation (EMD) cross section was deduced. The measured EMD cross section for ^{11}Li on the heavier targets was much larger than that for the less neutron–rich projectile, ^{12}C.

To explain this result, the EMD cross section was calculated as a product of the known photo–nuclear cross section $\sigma_{\gamma\mathrm{N}}(E_\gamma)$ and the theoretically calculated virtual–photon spectrum $N_{\mathrm{V}\gamma}(E_\gamma)$

$$\sigma^{\mathrm{EMD}} = \int_{E_{\mathrm{th}}}^{\infty} N_{\mathrm{V}\gamma}(E_\gamma)\sigma_{\gamma\mathrm{N}}(E_\gamma)dE_\gamma \tag{2.4}$$

where E_{th} is the threshold energy for particle emission [Heck 76]. When the photo–nuclear cross section was assumed to have a simple Lorentzian form, the data were best reproduced by a ^{11}Li GDR energy of 4.6 MeV. Additional calculations were performed by assuming that the photo–nuclear cross section consisted of two GDR peaks. One was located at 22 MeV, as expected for ^{9}Li. The other peak was taken as a free parameter and was assumed to correspond to the soft dipole mode. When the contributions from both GDR peaks were weighted by the virtual-photon spectrum, which fell off very rapidly with photon energy, and by the Thomas–Reche–Kuhn sum rule [Wong 90], it was found that the EMD cross section was dominated by the soft dipole peak. This is illustrated in Figure 2.4. Under this assumption, the data were best reproduced by a ^{11}Li soft GDR energy of 0.9 MeV.

Further measurements by Blank *et al.* [Blan 91], utilizing the same systems as above, but at a beam energy of $E/A = 80$ MeV, corroborate the large EMD cross section for ^{11}Li on heavy targets, as well as the GDR energy of 4.6 MeV as found in the model described above. It was found, however, that the soft GDR model predicted a much larger dependence of the EMD cross section on energy than that which was measured. Very recent measurements by Ieki and collaborators [Ieki 93] of ^{11}Li on a lead target at $E/A = 28$ MeV also corroborate the large EMD cross section and the GDR energy of approximately 4.6 MeV. Application of the soft GDR model yields a soft GDR energy of 0.7 MeV. It is noted in their report that such a GDR energy corresponds to a classical oscillation period of 1240 fm/c. The measurements of Ieki *et al.* are kinematically complete, and it is observed that the ^{9}Li fragments from the ^{11}Li breakup suffer a significant Coulomb acceleration in the electric field of the lead target nucleus. Such a large acceleration implies that the ^{11}Li projectiles break up very near to the target and consequently that the soft GDR, if it exists, lives for an extremely short time. A quantitative treatment of the data places the upper limit on the soft GDR lifetime at 85 fm/c, a value significantly less than the classical oscillation period. This raises the question of whether the soft GDR exists. It is possible that the breakup actually took place, not via excitation of a soft GDR, but through a more direct channel. If not, the question still remains as to whether it make sense to speak of the existence of a resonance that decays well before one oscillation period.

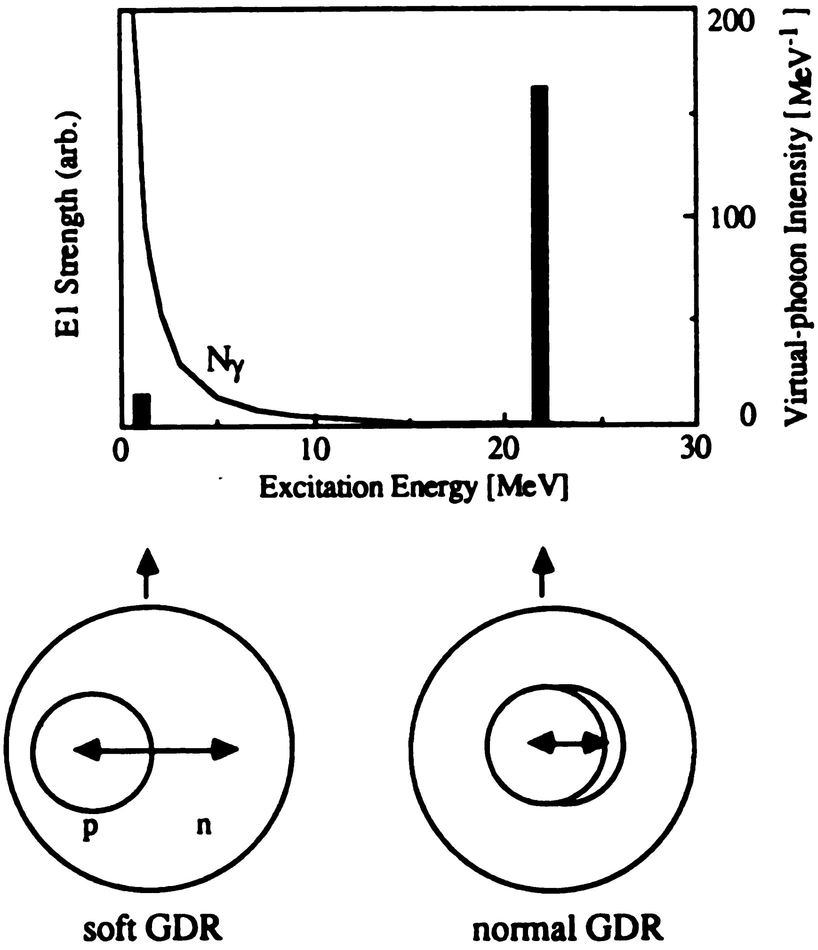

Figure 2.4: [Koba 89] Schematic representation and intensities of soft and normal giant dipole resonances in ^{11}Li. The solid line in the graph is the virtual-photon spectrum for ^{11}Li on lead at E/A = 800 MeV. The energies and intensities, as calculated from the TRK sum rule, of the two dipole resonance modes is shown by the black bars. Even though the normal GDR has a greater intensity as predicted by TKR, when weighted by the virtual-photon spectrum, the soft GDR dominates.

Clearly, ^{11}Li presents entirely new nuclear behavior and exhibits phenomena which challenge traditional nuclear models. It has been shown [Hans 87] that, qualitatively, the existence of a neutron halo has a very sensitive dependence on the binding energy of the halo neutrons. For this reason, it is expected that halo behavior should be exhibited by a large number of drip–line nuclei. Indeed, experimental evidence [Fuku 91, Tani 92, Riis 92] has indicated halo phenomena in the nuclei ^{14}Be, ^{11}Be, ^{8}He, and ^{6}He. It is apparent that neutron halos are by no means isolated phenomena, and that as further experiments are performed, more nuclei will be found to posses halos. It is becoming increasingly important that the structures of these nuclei be understood.

III Structure of ^{11}Li – Theory

Experimental evidence, some of which was presented in the previous section, has led to the theoretical treatment of ^{11}Li as a three–body system comprising a ^{9}Li core and a diffuse halo of two loosely bound neutrons. The first, and qualitatively the simplest, such treatment was presented by Hansen and Jonsen in [Hans 87]. In their model, ^{11}Li is assumed to be a quasi–deuteron consisting of a structureless ^{9}Li core nucleus coupled to a dineutron ^{2}n. The nuclear potential for this system is idealized as a radial square well. Under these assumptions, it was found that, outside the well, the radial wave function is

$$\Psi(r) = (2\pi\rho)^{-1/2}\left[\frac{\exp(-r/\rho)}{r}\right]\left[\frac{\exp(R/\rho)}{(1+R/\rho)^{1/2}}\right] \tag{2.5}$$

where r denotes the distance between ^{9}Li and the dineutron, and R the radius of the square well. The decay parameter ρ is given by

$$\rho = \hbar/(2\mu E_{\mathrm{B}})^{1/2} \tag{2.6}$$

where μ and E_{B} are the reduced mass and binding energy of the system. The matter distribution, given by $|\Psi(r)|^2$, then decays outside the well as $\exp(-2r/\rho)/r^2$. This simple model indicates that the existence of the neutron halo, that is, the large radius of the neutron distribution, arises from the very small binding energy of the two halo neutrons. The Fourier transform of the wave function given above yields the momentum probability distribution $f(p)$ [Boyd 93]

$$f(p) \propto \frac{1}{[p^2 + (\hbar/\rho)^2]^2} \tag{2.7}$$

By inserting the appropriate values for ^{11}Li ($\mu = \frac{18}{11}(931.5\ \mathrm{MeV/c^2})$ and $E_{\mathrm{B}} \approx 0.3$ MeV) into these expressions, it is found that $\rho \approx 6.5$ fm and $\Gamma_p \approx 30$ MeV/c. Both results are in reasonably good agreement with experimental data.

Hansen and Jonsen proceed further with their model and postulate the existence of a low–energy soft dipole excitation, discussed in the previous section, in analogy with the deuteron. It was found that the Coulomb dissociation cross section for collisions with a target Z_{targ} and relative velocity v is proportional to

$$\frac{Z_{\mathrm{targ}}^2}{E_{\mathrm{B}} v^2} \tag{2.8}$$

and, for low beam energies and heavy targets, should therefore be quite large (e.g. on the order of 5 barns for $E/A = 100$ MeV incident on uranium). Such a large cross section has been confirmed experimentally; however, there is still some question concerning experimental measurements of the lifetime of, and hence the existence of, the soft dipole excitation as a means of Coulomb dissociation.

Johannsen, Jensen, and Hansen [Joha 90] extended this model by introducing structure to the dineutron system. In their model, ^{11}Li is treated as a system of three interacting particles. More specifically, the dineutron is assumed to be in an $S = 0$ state, and any spin–dependent interactions between the halo neutrons and the ^{9}Li core, which is assumed to be structureless, are ignored. Both the neutron–neutron and neutron–^{9}Li interactions are taken as simple Gaussian radial wells. The depths and widths of the wells are chosen to reproduce the low-energy n–n scattering data and the approximate size of the ^{9}Li nucleus. The ground state wave function is then determined variationally for different n–^{9}Li well depths. These calculations reproduce the sensitive dependence of the matter and momentum distributions on the neutron binding energy, but disagree somewhat with experiment. Calculations of the Coulomb dissociation cross section also reproduce the observed trend but again disagree somewhat with the data. Perhaps the most interesting result of their calculations, however, is the prediction of strong correlations between the two neutrons in ^{11}Li. This raises the possibility that, although the isolated dineutron system has no bound state, such a state may indeed exist in the nuclear medium.

Bertsch, Esbensen and Ieki [Bert 91, Esbe 93] approach the dineutron problem in a different manner. Their model is conceptually similar to that described in [Joha 90], but more realistic potentials are used for the n–n and n–^{9}Li interactions. The n–^{9}Li interaction was taken to be a sum of Coulomb and centrifugal terms along with a Woods–Saxon nuclear well and a Thomas–type spin–orbit term. The parameters of this potential were adjusted to reproduce the binding energies of other nuclei with neutron and proton numbers similar to those of ^{11}Li. The single–particle states of this well were used as the space of basis states for the calculation. The n–n interaction was taken to be a density–dependent contact interaction

$$V_{nn} = \delta(\mathbf{r}_1, \mathbf{r}_2)\,(v_0 + v_\rho(\rho(\mathbf{r}_1, \mathbf{r}_2))) \tag{2.9}$$

where $\mathbf{r}_1$ and $\mathbf{r}_2$ are the positions of the two neutrons. The parameters of this reaction were also adjusted in a manner similar to that described above. The ground state wave function and binding energy were found by using the two–particle Green's function, which was expressed as an expansion in the single particle states of the n–^{9}Li well. Their model also exhibits a sensitive relation between the ^{11}Li binding energy and matter radius, as well as a large Coulomb dissociation cross section. The results of these calculations are also compared with the kinematically complete measurements of Ieki and collaborators [Ieki 93]. It was found that the calculations were in agreement with the measured single–neutron and two–neutron momentum distributions, but that the predicted ^{9}Li momentum distributions were narrower than those observed by Ieki and collaborators.

Many other calculations have been performed with other three–body models similar to the ones described above [Tosa 90, Zhuk 91, Bang 92, Thom 93a]. A detailed review of these models is given in [Zhuk 93]. All of these models have succeeded in reproducing experimental observables such as the ^{11}Li binding energy, halo radius, and momentum distribution widths to within a factor of two, but they also show substantial disagreement with one another. One of the most striking points of disagreement is on the degree to which the halo neutrons are correlated within ^{11}Li. The discrepancies between these models points up the need for more accurate and complete experimental data for use as input parameters in the calculations as well as for comparison with model predictions.

IV Predicted ^{11}Li mass and ^{10}Li

All of the three–body models that have been used to describe ^{11}Li assume some form for the n–^{9}Li interaction. Only until very recently, it was believed that this system only has one low–lying resonance state, a $1p\frac{1}{2}$ neutron state unbound by 800 keV [Wilc 75, Bark 77]. However, as will be discussed in Chapter 4, there is newer evidence which calls into question the energy of this state as well as the possible existence of

Reference	$S_{2n}(^{11}\mathrm{Li})$ (keV)
Thibault *et al.*, 1975 [Thib 75]	170 ± 80
Wouters *et al.*, 1988 [Wout 88]	320 ± 120
Kobayashi *et al.*, 1992 [Koba 92]	340 ± 50

Table 2.1: Summary of existing measurements of the two–neutron separation energy of ^{11}Li.

a lower–lying $2s\frac{1}{2}$ state. The calculations of Bertsch and Esbensen have indicated that the predicted ^{11}Li binding energy is quite sensitive to the energy of the ^{10}Li $1p\frac{1}{2}$ state, as illustrated in Figure 2.5. Very recent calculations performed by Thompson and Zhukov [Thom 93a, Thom 93b, Zhuk 93] have included a $2s\frac{1}{2}$ state as well as a $1p\frac{1}{2}$ state in the n–^{9}Li interaction. Their results indicate that the inclusion of both states, as well as the energies of these states, has profound effects on the predicted ^{11}Li binding energy, as shown in Figure 2.6, as well as other observables. These issues will be discussed in more detail in Chapter 5.

V Previous ^{11}Li mass measurements

As discussed earlier in this chapter, the existing models of halo nuclei, and in particular ^{11}Li, all predict a very sensitive dependence of the signature halo phenomena, such as the halo radius and momentum distributions, on the binding energy of the halo neutrons. For this reason, it is essential to the understanding of the structure of ^{11}Li and halo nuclei in general that the mass of ^{11}Li be known as accurately as possible. There is some uncertainty on the value of the ^{11}Li mass, as can be seen in Table 2.1, which lists all of the existing measurements.

In 1975, Thibault *et al.* [Thib 75] reported the first measurement of the mass of ^{11}Li. In their measurement, lithium ions were produced by 24 GeV protons incident

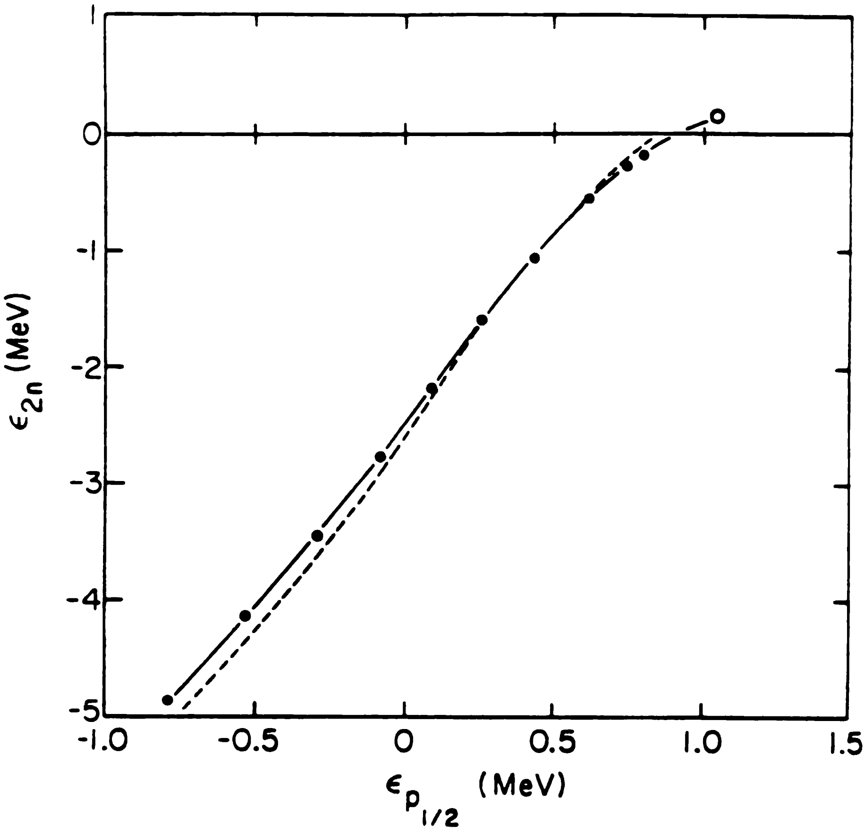

Figure 2.5: [Bert 91] Sensitive dependence of ^{11}Li binding energy on ^{10}Li $1p\frac{1}{2}$ state energy as predicted by Bertsch and Esbensen. The solid and dashed lines indicate calculations assuming correlated and uncorrelated neutrons respectively. Both calculations assume the n–^{9}Li system has only a single $1p\frac{1}{2}$ state, the energy of which was treated as a variable parameter.

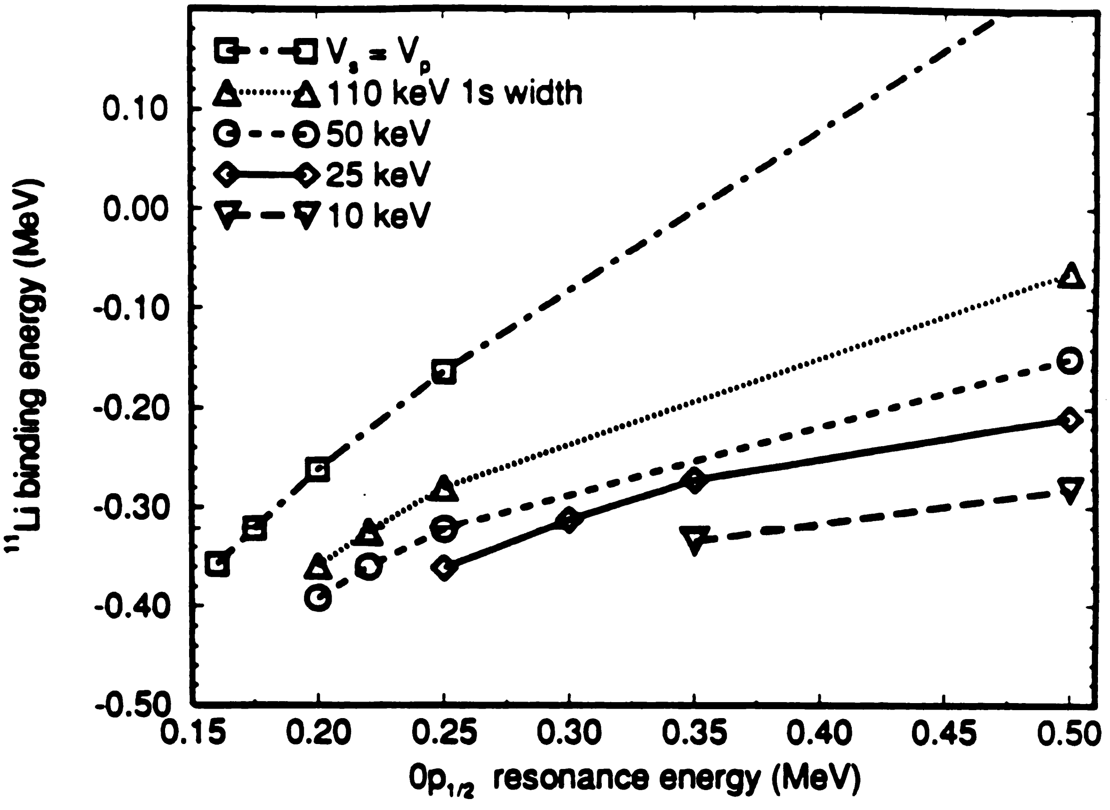

Figure 2.6: [Thom 93b] Dependence of ^{11}Li binding energy on ^{10}Li $1p\frac{1}{2}$ and $2s\frac{1}{2}$ state energies as predicted by Thompson and Zhukov. The ordinate is the predicted two-neutron binding energy of ^{11}Li. The input parameters of these models are the $1p\frac{1}{2}$ neutron resonance energy of the ^{10}Li first excited state (the abscissa) and the $2s\frac{1}{2}$ resonance energy of the ^{10}Li ground state (shown with various plotting symbols). In these calculations, two potentials were assumed for the n–^{9}Li system, one for $1p\frac{1}{2}$ the interaction, and one for the $2s\frac{1}{2}$ interaction. Also shown in this figure are the predicted results assuming the same potential for both interactions (ie. $V_s = V_p$).

on iridium foils in a target–ion source. The ions were then accelerated by a DC voltage through a series of slits and magnetic elements into a shielded counter. The ^{11}Li mass was deduced by comparing the voltages necessary to transport ^{9}Li, the mass of which is well known, and ^{11}Li through identical trajectories of the optical system. In 1988, Wouters *et al.* [Wout 88] measured the mass of ^{11}Li nuclei produced from fragmentation reactions of 800 MeV protons on a thorium target. The mass of the fragments was determined using the TOFI spectrometer at LAMPF. The value frequently used in theoretical calculations is the more recent result of Kobayashi *et al.* [Koba 92]. In their measurement, the ^{11}Li mass was determined from the measured Q-value of the pion double charge–exchange reaction ^{11}B(π^-,π^+)^{11}Li. This work, however, has never been accepted for publication, and the details of the measurement and particularly the sources of the uncertainty are not known. The substantial disagreement between these measurements as well as the magnitude of their uncertainties limits their usefulness in theoretical calculations. Chapter 3 contains a description of a measurement of the ^{11}Li mass that was performed at the National Superconducting Cyclotron Laboratory in late 1992.

Chapter 3

The Mass of ^{11}Li from the ^{14}C(^{11}B,^{11}Li)^{14}O Reaction

I Introduction

As indicated in the previous chapter, a central quantity to the understanding of the structure of ^{11}Li is its binding energy. From the theoretical point of view, the current state of knowledge of this quantity is unsatisfactory and presents a hindrance to development of more accurate models. In September of 1992, the ^{11}Li mass was measured via the Q–value of the ^{14}C(^{11}B,^{11}Li)^{14}O reaction analyzed in the A1200 fragment separator at the NSCL. The details of this measurement are presented in this chapter. A brief description of the A1200 and its operation as a spectrometer is presented in section II. Section III contains details of the experimental procedures, including the calibration of the spectrometer and collection of the production data. The analysis of the experimental data is discussed in section IV. The analysis relied heavily on the computer code RELMASS, a description of which is given in Appendix A. Particular attention will also be paid to calibration of the A1200 dipole magnets. Finally, the results of the measurement will be presented in section V.

II Description of A1200

Brought online in 1991, the A1200 is a series of magnets and a standardized array of detectors integrated into a device used primarily for the separation of radioactive beams at the NSCL [Sher 91]. The device consists of four superconducting 22.5° dipole bending magnets and several superconducting quadrupole focusing magnets grouped into sets of two and three. Four room–temperature sextupole magnets are also used to correct for optical aberrations. The layout of the magnets in the A1200, which is located in the K1200 beamline immediately downstream of the K1200 cyclotron, is shown in Figure 3.1. The magnets are controlled, singly or in gangs, with a computer program communicating with the magnet power supplies via ARCNET. Accurate calibration of the magnetic fields versus the power supply current allows easy manipulation of the magnetic fields, and hence the magnetic rigidity, of the device. The dipole fields, the most critical values in determining the rigidity of the device, are continuously monitored by eight NMR probes located in the four dipole magnets – two probes per magnet, one for high fields and the other for weak fields.

In addition to the magnets, the A1200 also includes a standardized array of detectors for use in analyzing filtered reaction products. This setup consists of a thin plastic scintillator detector located at Image 1, four parallel–plate–avalanche–counters (PPACs), with cathodes segmented to achieve position resolution in x and in y, located in pairs at Image 2 and the Focal Plane, and a 10 cm plastic scintillator detector located at the Focal Plane. Time–of–flight information is obtained, on a particle–by–particle basis, from the fast signals of the plastic scintillator detectors located at Image 1 and the Focal Plane. The signal from the thick plastic scintillator at the Focal Plane is also used to obtain the total energy of the reaction products. The PPACs provide position information for each fragment particle, and, when used in pairs, can

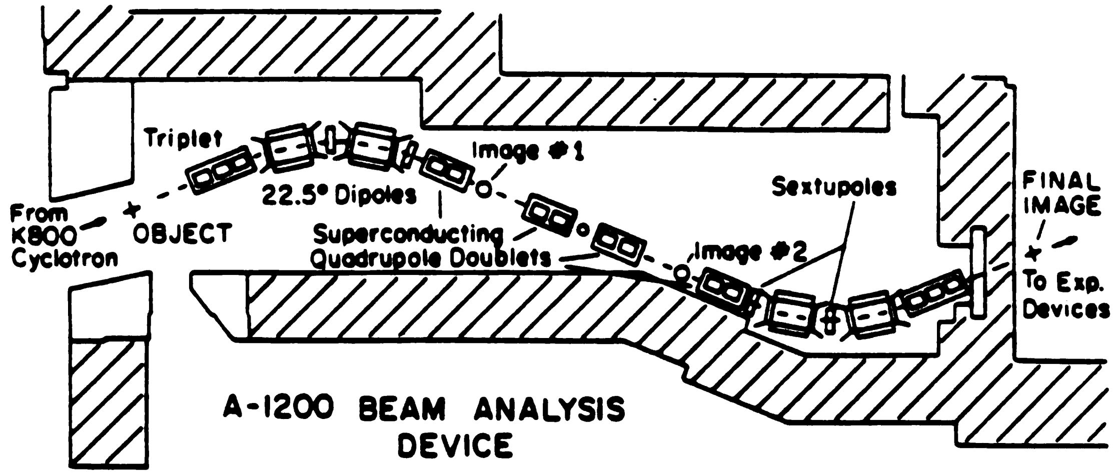

Figure 3.1: [Sher 91] Schematic layout of the A1200. The device consists of four superconducting 22.5° dipole bending magnets and several superconducting quadrupole focusing magnets grouped into sets of two and three. Also used in experiments are a standardized array of detectors (located at Image 1, Image 2 and the Final Image) and several retractable platforms, located at several places throughout the device, for holding other hardware such as targets, degrader wedges, and scintillator screens.

provide information about the angle of a particle's path off the central axis. This standard setup is very frequently augmented by one or more energy loss detectors, usually located at the Focal Plane. Examples of such detectors are 5×5 cm silicon PIN diodes, silicon surface-barrier transmission detectors, and ion chambers. The energy loss information from these detectors can be combined with the total energy information or with the time-of-flight information from the plastic scintillator(s) to obtain particle identification.

Typically, the A1200 is run in an achromatic optical mode. There are two such modes, distinguished by the momentum resolving power of the mode and the angular acceptance of the device. The most commonly used optical mode is medium-acceptance mode, in which the device subtends a solid angle of 0.8 mSr as seen from the target. High-acceptance mode is functionally equivalent to medium-acceptance mode except that the device subtends a solid angle of 4.3 mSr and the momentum resolving power is only $\frac{1}{3}$ that of medium-acceptance mode. This means that, while high-acceptance mode can provide higher overall beam intensities than medium-acceptance mode, due to its larger angular acceptance, its lower resolving power will not provide fragment separation as fine as the medium-acceptance mode. Both of these modes are achromatic, which means that all momentum components (i.e. fragment species) are focused to the same point at the Focal Plane. In both of these modes, Image 1 and Image 2 are dispersive, meaning that momentum components are separated at those points. The dispersion is inverted in the bend-plane (i.e. the high-rigidity and low-rigidity sides are flipped) at the midpoint of the device. This inversion, located between the dipole pairs, which bend in opposite directions, allows the dispersions of the dipole pairs to cancel each other out, and produces the achromaticity of these modes. It is at these locations, particularly Image 2, that detectors and aperture plates are placed to distinguish and filter reaction products.

For the experiment described in this chapter, a new optical mode was developed by B. M. Sherrill and J. Stetson at the NSCL. The chief requirements for this mode, labelled the "high-acceptance chromatic" mode or "spectrometer" mode, were twofold. To overcome the low cross-section for ^{11}Li production, as high an angular acceptance as possible was needed; and, in order to use the device as a momentum spectrometer, a dispersive (i.e. chromatic) image was needed at the Focal Plane. In this mode, there are no images other than the dispersive one at the focal plane. The dispersion is inverted inside the second dipole pair. The location of this single inversion allows the dispersions of the dipole pairs to reinforce each other, thereby producing a dispersive image at the Focal Plane. Development of this mode involved extensive optical calculations, performed by Stetson and Sherrill, as well as several experimental tests of these calculations.

III Description of experiment

The experiment was performed with an $E/A = 32.137 \pm 0.024$ MeV, ^{11}B^{5+} beam from the K1200 cyclotron, focused onto a self-supporting ^{14}C foil target, 0.450 mg/cm^2 thick. The reaction products were analyzed with the A1200 fragment separator set to a high-angular-acceptance chromatic mode as described in the previous section. For this experiment, the A1200 detectors were, with the exception of those in the Focal Plane, identical to those of the standard setup described earlier. The A1200 Focal Plane detectors consisted of one PPAC, a 0.5mm thick silicon position-sensitive detector, which was located at the focal point of the device, and a 10 cm scintillating plastic stopping detector. Redundant and unambiguous particle identification was obtained by combining the energy loss signal from the silicon detector with the total energy signal from the plastic and with the time-of-flight information obtained from the scintillator signal relative to the cyclotron rf. Position information at the dispersive focus was obtained from the silicon detector and was combined with position information from the PPAC, located 50 cm upstream, to find the angle of each particle's trajectory.

^{11}Li production reaction

The ^{11}Li nuclei were produced from the ^{14}C(^{11}B,^{11}Li)^{14}O reaction. The experiment consisted of, in addition to the calibration runs described below, two production runs of approximately 50 hours each, separated by a period during which the beam was refocused onto the target and the A1200 magnetic field settings were changed slightly in order to observe the ^{14}O excited state simultaneously with the ground state. The cross section for this reaction was determined from the 149 ^{11}Li nuclei obtained in both runs to be 24 ± 2 nb/Sr at 0° in the laboratory frame.

The particle–identification (PID) spectrum from the first run, obtained by histogramming the energy loss (ΔE) signal from the silicon detector versus the time–of–flight (TOF) information obtained from the 10 cm scintillator detector and the cyclotron accelerating rf, is shown in Figure 3.2. The PID spectrum from the second run has identical features. In addition to ^{11}Li particles, ^{10}Be^{3+} particles were seen in the Focal Plane. In the notation used here, the 3+ indicates that the ^{10}Be nucleus had a charge of $+3e$, as opposed to a ^{10}Be fully stripped of its electrons, which would have a charge of $+4e$. These nuclei were produced in the ^{14}C(^{11}B,^{10}Be)^{15}N reaction and were used for calibration of the A1200, as described below. Several other nuclear species were also seen in the Focal Plane during these runs, and are labelled in Figure 3.2. The extreme cleanliness of the PID spectrum is to a large part due to the very high rigidity of the ^{11}Li particles. Most species produced prolifically have a much lower rigidity and are not transported to the Focal Plane.

The momentum spectra for the first and second production runs are shown in

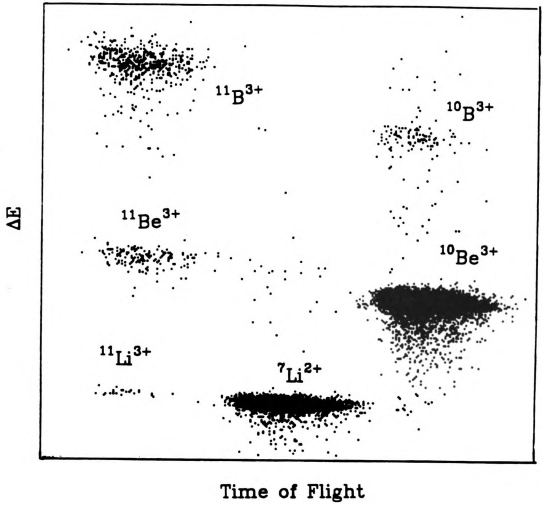

Figure 3.2: Particle–identification spectrum from ^{11}Li production run. The spectrum was obtained by histogramming ΔE and TOF information taken from the silicon detector and the thick plastic scintillator detector respectively. In addition to ^{11}Li nuclei, ^{10}Be^{3+} particles, which were used for calibration of the A1200, and several other nuclei were observed as well.

the bottom part of Figure 3.3. For both runs, there is literally no background in the spectra. In addition to the primary peaks, corresponding to the ground states of both ^{11}Li and ^{14}O, another peak, corresponding to unresolved states in ^{14}O near 6.3 MeV excitation energy, is seen in the data from the second run. While it is possible that an excited state of ^{11}Li could also be embedded in this peak, it is clear from the data that there is no indication of such a state at higher excitation energies.

Calibration reactions

In addition to data from the ^{11}Li production reaction, data were also collected from the ^{14}C(^{11}B,^{10}Be)^{15}N reaction simultaneous to the production data. This reaction, which has a well-known Q-value, was used to calibrate the A1200. The calibration momentum spectra from both runs are shown in the top part of Figure 3.3. The ground state and unresolved 5.3 MeV doublet states of ^{15}N were used as the primary calibration points. Also seen in the calibration spectra are a cluster of ^{15}N and ^{10}Be excited states, corresponding to a total excitation energy between 8.0 and 10.0 MeV, and the 3.37 MeV first excited state of ^{10}Be, which shows marked kinematic broadening due to the recoil from the isotropic in-flight gamma decay. Also studied was the ^{14}C(^{11}B,^{9}Li)^{16}O reaction, the data from which was combined, as described in the next section, with the calibration data to determine the beam energy.

IV Analysis

Analysis of the experimental data consisted of a multi-step process that culminated in two experimental measurements of the Q-value of the ^{14}C(^{11}B,^{11}Li)^{14}O reaction, from which the mass, or equivalently, the two-neutron separation energy, of ^{11}Li was deduced. This process, described below, was greatly simplified by the computer code RELMASS, written by Toshiyuki Kubo with suggestions from Ed Kashy. A

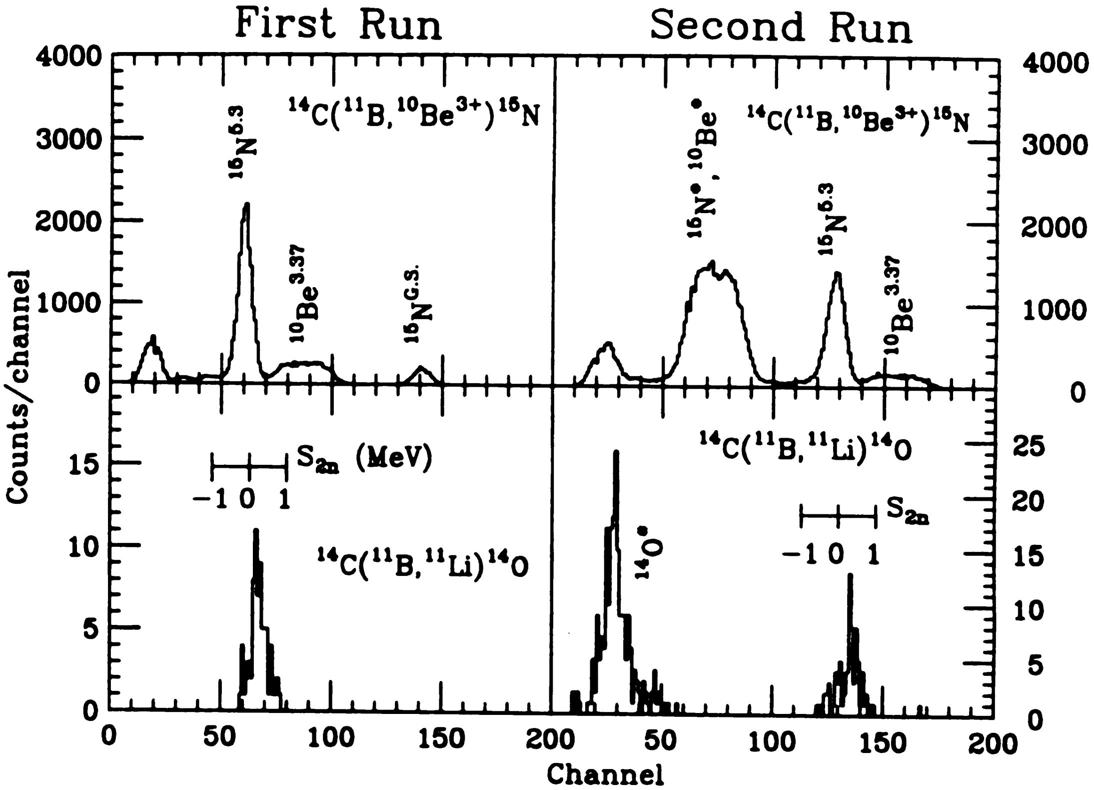

Figure 3.3: Momentum spectra from ^{11}Li production and calibration runs. The data from the first and second runs are shown in the left and right portions of the figure, respectively. The momentum spectra from the reaction $^{14}C(^{11}B,^{10}Be^{3+})^{15}N^*$ are shown in the top part of the figure. The ground state and unresolved 5.3 MeV doublet states of ^{15}N were used as the primary calibration points. Other features in the calibration spectra are a cluster of ^{15}N and ^{10}Be excited states, and the 3.37 MeV first excited state of ^{10}Be. The momentum spectra collected from the reaction $^{14}C(^{11}B,^{11}Li)^{14}O$ are shown in the bottom part of the figure. It is important to note that both the calibration and ^{11}Li spectra were collected simultaneously.

description of the code's operation is given in Appendix A.

The first run was analyzed first. For a given beam energy, the kinetic energy of the ^{10}Be ejectile from the ^{14}C(^{11}B,^{10}Be)^{15}N calibration reaction can be found, after including energy loss effects of the beam and ejectile in the target material, from the well-known Q-value of the reaction. The magnetic rigidity, defined for a particle with charge Q and momentum p moving in a uniform magnetic field as the product of bend radius and field strength, can be found by balancing the Lorentz force with the centrifugal force

$$\mathrm{B}\rho = \frac{p}{Q} \tag{3.1}$$

From this definition, it is clear that the ejectile particle's magnetic rigidity can also be found from its kinetic energy. For a given A1200 magnetic field, particles with different momenta have different bend radii and arrive at different positions in the Focal Plane. The data from the ^{14}C(^{11}B,^{10}Be)^{15}N reaction were used to calibrate the focal plane position as a linear function of bend radius, obtained from the known rigidities and magnetic field. Since the radius-position (ρ vs x) line is a property of the spectrometer, independent of the reactions studied, all reaction products must lie on this line.

Since the ^{14}C(^{11}B,^{9}Li)^{16}O reaction also has a well-known Q-value, the beam energy uniquely determines the rigidity of the ^{9}Li ejectile. Utilizing this fact, the beam energy was obtained by requiring that the measured position and the calculated bend radius of the ^{9}Li particles lie on the same calibration line as the two states from the ^{14}C(^{11}B,^{10}Be)^{15}N reaction, as shown in Figure 3.4. The beam energy determined in this manner was $E/A = 32.137 \pm 0.024$ MeV. The uncertainty of the beam energy reflects the statistical uncertainty of the position measurement of the ^{9}Li ejectiles. From the calibration curve, the ^{11}Li rigidity can then be determined from its measured Focal Plane position. The rigidity can then be combined with the beam energy to obtain the measured Q-value for the production reaction, from which can be deduced the ^{11}Li mass.

The second run was analyzed in a manner similar to that described above. Before the second run, the beam was refocused onto the target, and the magnetic fields of the A1200 were decreased slightly. Both of these actions affected the calibration curve. As the magnetic field was decreased, the momentum spectra shifted to the right on the Focal Plane, as seen in Figure 3.3, with the result that only one calibration peak, corresponding to the 5.3 MeV doublet in ^{15}N, remained on the Focal Plane. When the beam was refocused onto the target, the position of the beam spot was changed. This change would affect the *offset* of the calibration line, but not the slope, which reflects a property of the A1200 magnets and optics, namely the degree to which a change in a particle's bend radius changes the particle's Focal Plane position. Thus, the calibration line for the second run was obtained by keeping the same slope as before, and determining the new offset from the single calibration peak. This new calibration curve was then used to determine the Q-value of the ^{14}C(^{11}B,^{11}Li)^{14}O reaction for the second run.

Central to all A1200 measurements is knowledge of the dipole magnetic fields, for these determine the magnetic rigidity of the particles which arrive at the Focal Plane. The dipole fields are measured by NMR probes in each of the magnets. These probes, however, measure the field at only *one* point in each dipole magnet, whereas, in actuality, the desired quantity is the average field over the trajectory of a given particle. The difference between this effective field and the field measured by the NMR probe is typically less than 0.1% and for most purposes, such as the production of a radioactive beam or the measurement of a fragment momentum distribution, is negligible. However, for the measurement reported here, this difference, which varies

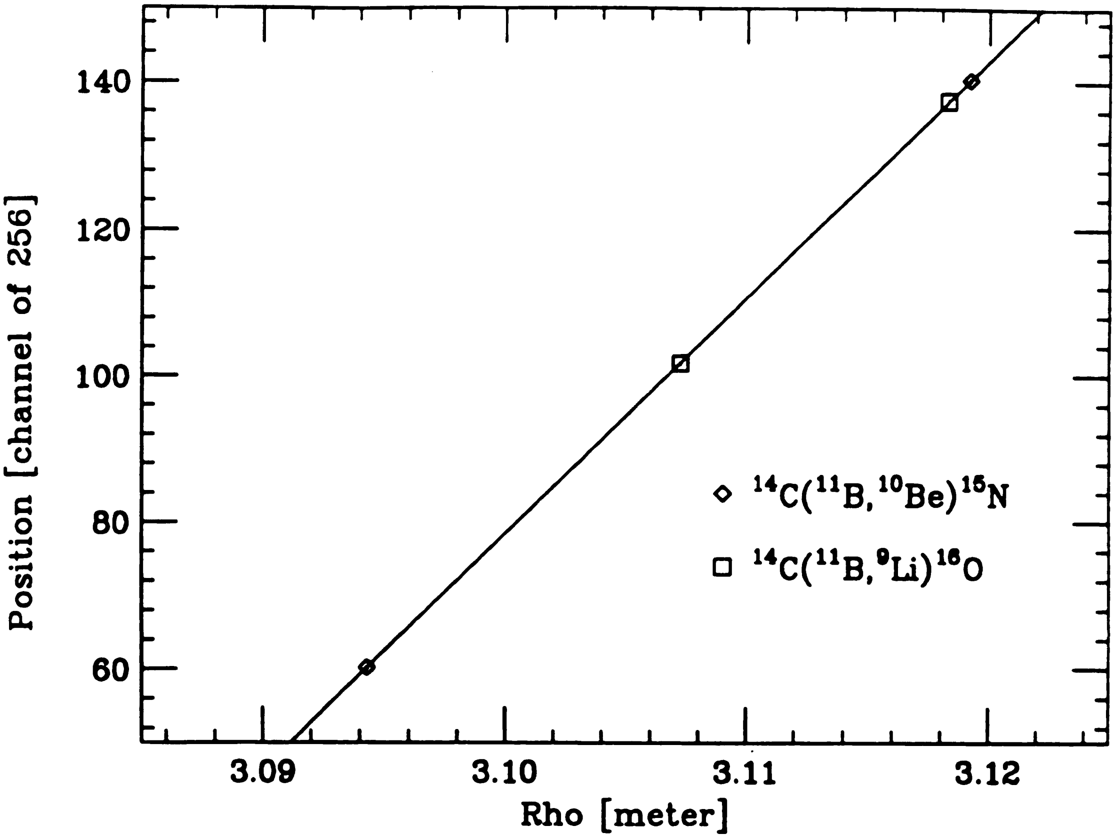

Figure 3.4: ρ vs x calibration of A1200 Focal Plane for first ^{11}Li production run. A line was fitted to the two points from the $^{14}C(^{11}B,^{10}Be)^{15}N$ reaction, shown as diamonds in the figure. The beam energy was determined by requiring that the $^{14}C(^{11}B,^{9}Li)^{16}O$ points, shown as squares, lie on the calibration line. The error bars for the points are approximately one fourth the size of the symbols used for plotting.

with the strength of the field and is attributable to fringe field effects and to the magnetic properties of the iron from which the magnets are made, is quite important.

The dependence of the effective field B_{eff} on the field as measured by the NMR probes B_{NMR} was measured using two techniques. The following discussion assumes that the two quantities, B_{eff} and B_{NMR}, are related by a correction term η which is dependent on B_{NMR}

$$B_{eff} = B_{NMR} \left[1 + \eta(B_{NMR})\right] . \tag{3.2}$$

The first technique involved the calibration of the S320 magnetic spectrograph, described in the next chapter, using the momentum-matching method detailed in [Nole 74]. A molecular beam $(H\text{-}He)^{2+}$ and its constituent nuclei, H^{1+} and He^{2+}, obtained by fragmenting the molecular beam on a thin aluminum foil located at the target position of the A1200, were then transported through the A1200 and into the S320. The A1200 magnets were then calibrated by comparing the rigidities of the particles, as measured with the S320, with the A1200 magnetic fields B_{NMR}, as measured by the NMR probes in the A1200 dipoles. The three data points obtained in this way are shown as diamonds in Figure 3.5. In the second technique, a beam of $^{238}U^{35+}$ with energy $E/A = 20.08 \pm 0.02$ MeV was focused onto a thin aluminum foil at the target position of the A1200. By interacting with the target material, the uranium particles lost electrons and emerged with a broad distribution of charge states which were then transported through the A1200. The A1200 magnets were calibrated by comparing the known rigidities of these charge states with the measured B_{NMR} values. The data points thus obtained are shown as squares in Figure 3.5. A polynomial curve was fitted to the data and is shown as the solid line in the figure. Also indicated, by the vertical lines, is the range of fields over which the ^{11}Li mass measurement was performed. It is seen that the effective magnetic field has a weak dependence on the

NMR value in this region.

V Results

The deduced values for the two-neutron separation energy of ^{11}Li from the first and second runs are $S_{2n}(^{11}\text{Li}) = 301 \pm 24$ keV and $S_{2n}(^{11}\text{Li}) = 288 \pm 26$ keV respectively. The uncertainties in these values reflect statistical uncertainties in determination of the centroids of the ^{11}Li peaks. The average of these two values is $S_{2n}(^{11}\text{Li}) = 295 \pm 18$ keV. The uncertainty here is also only statistical. To take into account the uncertainty in the beam energy, the data were re–analyzed with the incident energy increased by one sigma. It was found that this contributed an uncertainty to the ^{11}Li binding energy of 23 keV. Uncertainty in the calibration of the A1200 dipole fields was also found to have an 11 keV contribution.

There is an additional contribution from the ρ vs x calibration due to uncertainty about the relative strengths with which the states of the unresolved ^{15}N doublet were populated. The two states have excitation energies of 5.270 and 5.299 MeV. In the analysis, it was assumed that these states were populated equally, and that the peak corresponded to the average excitation energy of 5.285 MeV. The contribution to the final uncertainty from this assumption, obtained by re–analyzing the data twice assuming 100% population of one or the other of the doublet states, was found to be 15 keV. The above analyses were performed assuming the ejectiles were detected at 0° in the laboratory frame. Although the A1200 subtends a finite solid angle in the forward cone centered about 0° in the laboratory frame, and therefore the average laboratory angle of the reaction products is not 0°, it was found that this made a negligible difference in the final result.

The individual contributions to the overall uncertainty are listed in Table 3.1.

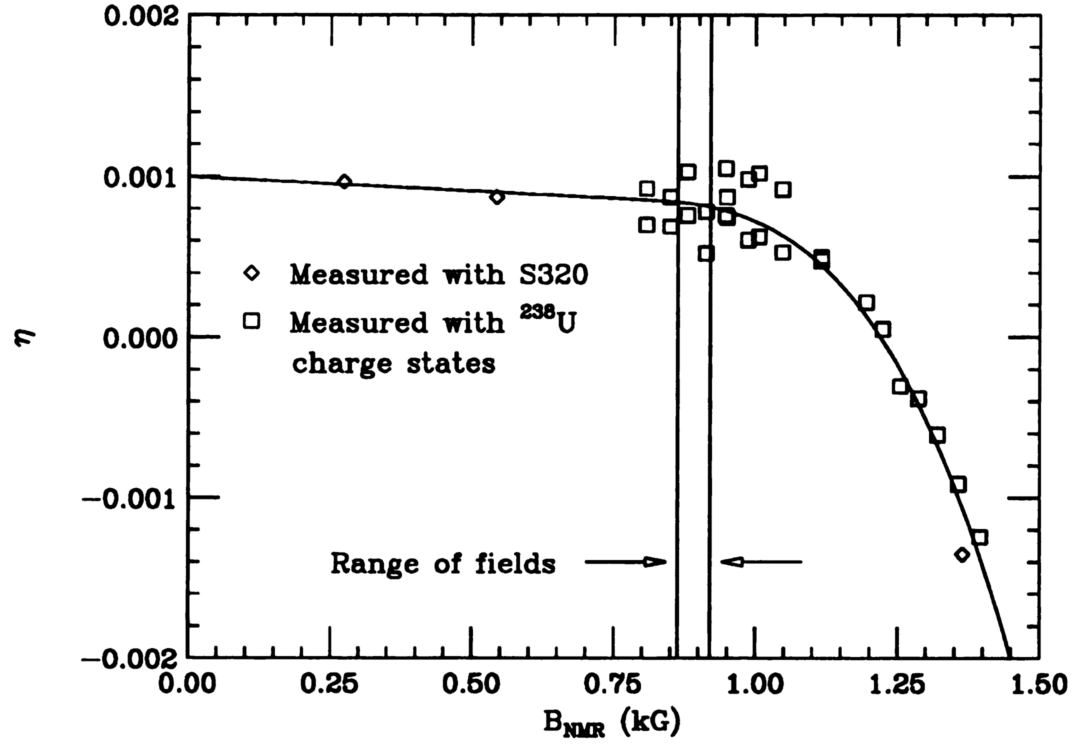

Figure 3.5: Calibration of A1200 dipole magnets. The effective A1200 magnetic field B_{eff} is related to the field B_{NMR} as measured by the NMR probes by $B_{eff} = (1 + \eta)B_{NMR}$. The diamonds are those data points obtained by comparing B_{NMR} with rigidities as measured with the S320. The squares are those data points obtained from rigidity measurements of uranium charge states. The solid curve is a polynomial fit to the data. The range of fields over which the ^{11}Li measurement was performed is indicated by the vertical lines. The central radius of the A1200 is 3.104 meters. The error bars for the points are approximately one tenth the size of the symbols used for plotting.

Source of uncertainty	σ (keV)
statistics	18
beam energy	23
magnetic field correction	11
^{15}N excited state population in calibration	15
total uncertainty	35

Table 3.1: Sources of experimental uncertainty in ^{11}Li mass measurement. The four uncertainties listed are added in quadrature to yield the total uncertainty.

When these values are added in quadrature to obtain the final uncertainty, the resulting two–neutron separation energy for ^{11}Li is $S_{2n}(^{11}\text{Li}) = 295 \pm 35$ keV. The corresponding Q–value for the ^{14}C(^{11}B,^{11}Li)^{14}O reaction is -37.120 ± 0.035 MeV. As can be seen in Table 3.2 this result is in good agreement with the previous measurements while substantially lowering the uncertainty. Using the existing four measurements, the weighted best values for the ^{11}Li mass excess and two–neutron separation energy are 40.802 ± 0.026 MeV and 295 ± 26 keV respectively. This places the accuracy of these quantities, which are essential to the understanding of the structure of ^{11}Li and halo nuclei in general, on a level high enough to be used with confidence in nuclear halo models.

Reference	$S_{2n}(^{11}\mathrm{Li})$ (keV)
Thibault *et al.*, 1975 [Thib 75]	170 ± 80
Wouters *et al.*, 1988 [Wout 88]	320 ± 120
Kobayashi *et al.*, 1992 [Koba 92]	340 ± 50
Present work	295 ± 35
Average value	295 ± 26

Table 3.2: Summary of existing measurements of the two–neutron separation energy of ^{11}Li, including the present work. Also listed is the weighted average of the four existing measurements.

Chapter 4

Structure Studies of ^{10}Li

I Introduction

All of the three-body models that have been used to describe ^{11}Li assume some form for the n–^{9}Li interaction. Until very recently, it was believed that this system only has one low-lying resonance state, a $1p\frac{1}{2}$ neutron state unbound by 800 keV. However, new evidence calls into question the energy of this state and also raises the possibility that a $2s\frac{1}{2}$ state exists at a much lower energy. Calculations performed by Bertsch and Esbensen[Bert 91] and Thompson and Zhukov [Thom 93a, Thom 93b, Zhuk 93] have shown that the predicted ^{11}Li binding energy is very sensitive to the number of low-lying ^{10}Li states as well as their energies and spectroscopic structures. Thus, a thorough understanding of the structure of ^{10}Li will shed a great deal of light on the structure of ^{11}Li. A review of the existing measurements of the ^{10}Li ground and/or first excited states is presented in section II. In May of 1992, the low-lying structure of ^{10}Li was measured from the momentum spectra and Q-value of the ^{11}B(^{7}Li,^{8}B)^{10}Li reaction analyzed with the S320 magnetic spectrometer at the NSCL. Sections III and IV contain a description of the S320 and the details of the experimental procedures, respectively. The analysis of the experimental data is discussed in section V. Part of the analysis consisted of determination of the shapes of the ^{10}Li neutron resonances. The theoretical assumptions and computer codes used in these calculations are presented in Appendix B. The ^{11}B(^{7}Li,^{8}B)^{10}Li reaction, populating the low-lying states of ^{10}Li was found to have a cross section of approximately 9.5 ± 0.7 μb/Sr at 5° in the laboratory frame. Such a low cross section resulted in very poor statistics (i.e. less than 15 events per channel) in the collected momentum spectrum. For this reason, the standard least-squares fitting technique, the statistical assumptions for which rely on a large number of events per channel, was inapplicable to the data. A more general maximum-likelihood fitting technique was employed. This technique, and the computer code through which it was implemented, is presented in Appendix C. The results of this analysis and the conclusions that can be drawn from the data are discussed in section VI.

II History of ^{10}Li

If the neutron configuration of ^{10}Li is taken to be that of other $N = 7$ nuclei, such as ^{11}Be and ^{12}B, then the lowest states should have 6 neutrons in their lowest shell model orbits and the seventh neutron in the $1p\frac{1}{2}$ or the $2s\frac{1}{2}$ orbits as illustrated in Figure 4.1. The combination of these two possible neutron orbits with the $1p\frac{3}{2}$ orbit occupied by the third proton in ^{11}Li yields four possible J^{π} values for the lowest states of ^{10}Li: 1^{+}, 1^{-}, 2^{+}, and 2^{-}. In the first measurement of the ^{10}Li neutron separation energy, Wilcox *et al.*[Wilc 75] determined the energy of ^{8}B in coincidence with ^{9}Li (from the breakup of ^{10}Li) produced in the reaction ^{9}Be(^{9}Be,^{8}B)^{10}Li at 121 MeV. The ^{8}B ejectile and the ^{9}Li recoil daughter were observed in semiconductor detector telescopes positioned respectively at 14° and approximately 10° in the laboratory and approximately 50 cm from the target. Their energy spectrum, shown in Figure 4.2, exhibits a pronounced peak corresponding to a neutron-unbound state with separation energy $S_n = -0.80 \pm 0.25$ MeV and width $\Gamma_{\text{c.m.}} = 1.2 \pm 0.3$ MeV. It was assumed that this

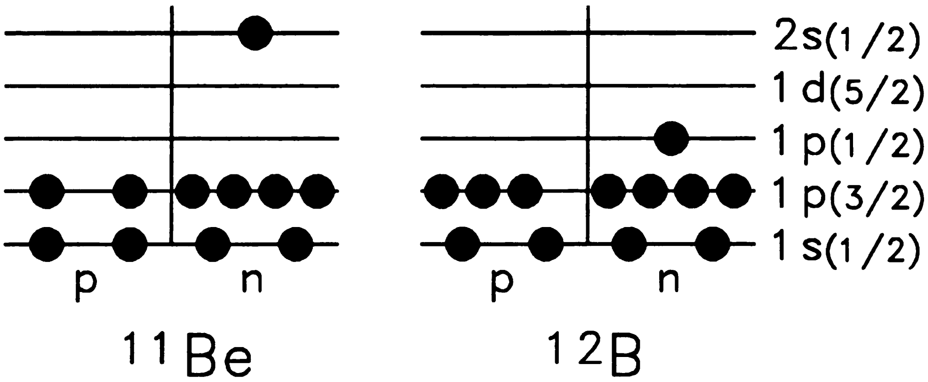

Figure 4.1: Shell structure of the $N = 7$ nuclei ^{11}Be and ^{12}B. The ^{11}Be ground state has the seventh neutron in the $2s\frac{1}{2}$ orbit. The ^{12}B ground and first excited states (as well as the ^{11}Be first excited state) have the seventh neutron in the $1p\frac{1}{2}$ orbit.

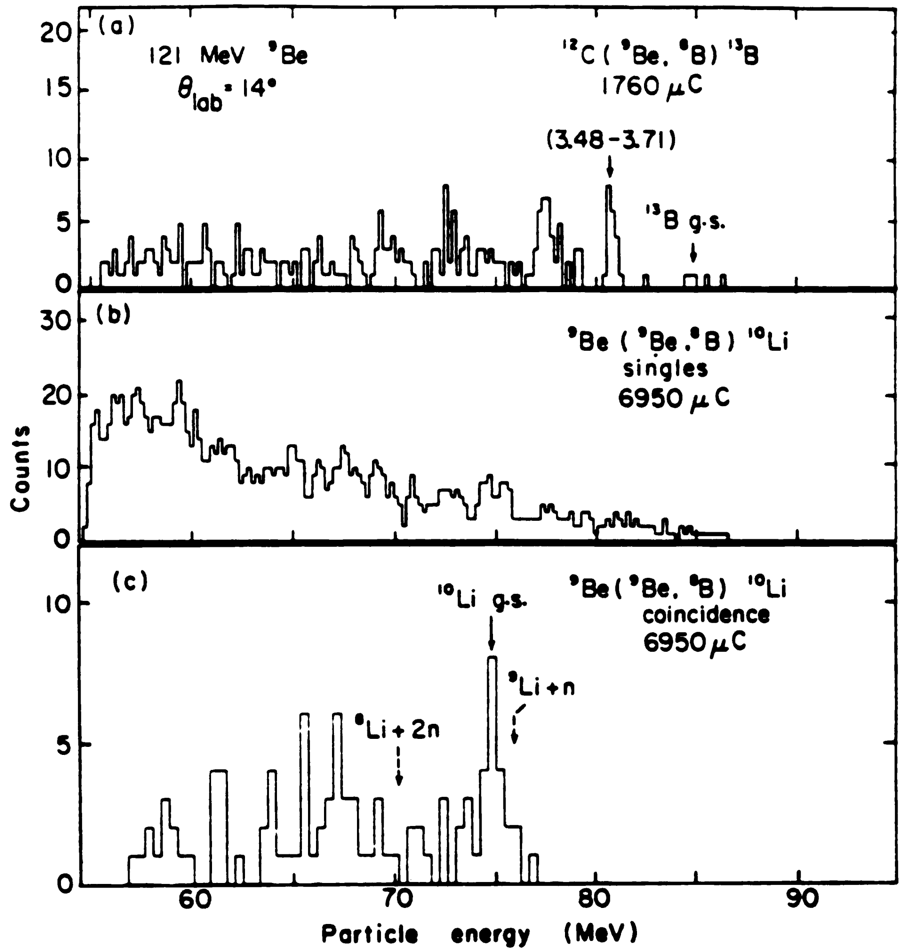

Figure 4.2: [Wilc 75] Energy spectra of ^{8}B from the ^{12}C(^{9}Be,^{8}B)^{13}B and ^{9}Be(^{9}Be,^{8}B)^{10}Li reactions at E/A =13.4 MeV and θ_{lab} = 14°. a) Calibration spectrum of ^{8}B from the ^{12}C(^{9}Be,^{8}B)^{13}B reaction. b) and c) Energy spectra of ^{8}B from the ^{9}Be(^{9}Be,^{8}B)^{10}Li reaction, singly and in coincidence with ^{9}Li from the breakup of the recoiling ^{10}Li. The coincidence spectrum shows a peak corresponding to a neutron-unbound state with separation energy $S_n = -0.80 \pm 0.25$ MeV and width $\Gamma_{\text{c.m.}} = 1.2 \pm 0.3$ MeV.

was the ground state of ^{10}Li. Soon thereafter, Barker and Hickey [Bark 77] argued, from a systematic study of the energies and parities of excited states of known $N = 7$ nuclei, that the ^{10}Li ground state should be a $\nu 2s\frac{1}{2}$ state which is narrow and much less unbound to neutron decay. They further suggested that the state observed by Wilcox *et al.* was an excited $\nu 1p\frac{1}{2}$ state.

In 1990, Amelin *et al.* measured the inclusive spectrum of protons produced in absorption of π^- by ^{11}B nuclei, shown in Figure 4.3, and reported the observation of a state in ^{10}Li unbound to neutron decay by approximately 150 keV [Amel 90]. In late 1992, Kryger *et al.* analyzed the relative velocity spectrum of neutrons collected in coincidence with ^{9}Li fragments from the decay of ^{10}Li [Kryg 93]. Their spectrum is shown in Figure 4.4. The dotted curve in the figure is the expected spectrum from a thermal neutron background. The solid curve represents the background added to the expected line shape from a low–energy decay very similar to that reported by Amelin *et al.*. It is important to note that while this curve fits the data quite well, such a peak in the relative velocity spectrum only indicates the presence of a very low–energy neutron decay which could either be a low–lying ^{10}Li state decaying to the ^{9}Li ground state, or a ^{10}Li excited state at $S_n \simeq -2.5$ MeV decaying to the first excited state of ^{9}Li. The dashed curve is the expected spectrum from a broad state unbound by 800 keV, similar to that reported by Wilcox and collaborators. The two–peaked structure in this calculated spectrum arises from the fact that, as the ^{10}Li decays in flight, the acceptance defined by the experimental apparatus allows detection of only those n–^{9}Li events where the decay is parallel or antiparallel to the beam axis. The absence of such a two–peaked structure in the data fails to corroborate the observation of Wilcox and collaborators of a broad ^{10}Li state unbound by 800 keV. An observation similar to that of Kryger *et al.* has also been reported by Kobayashi and collaborators [Koba 93].

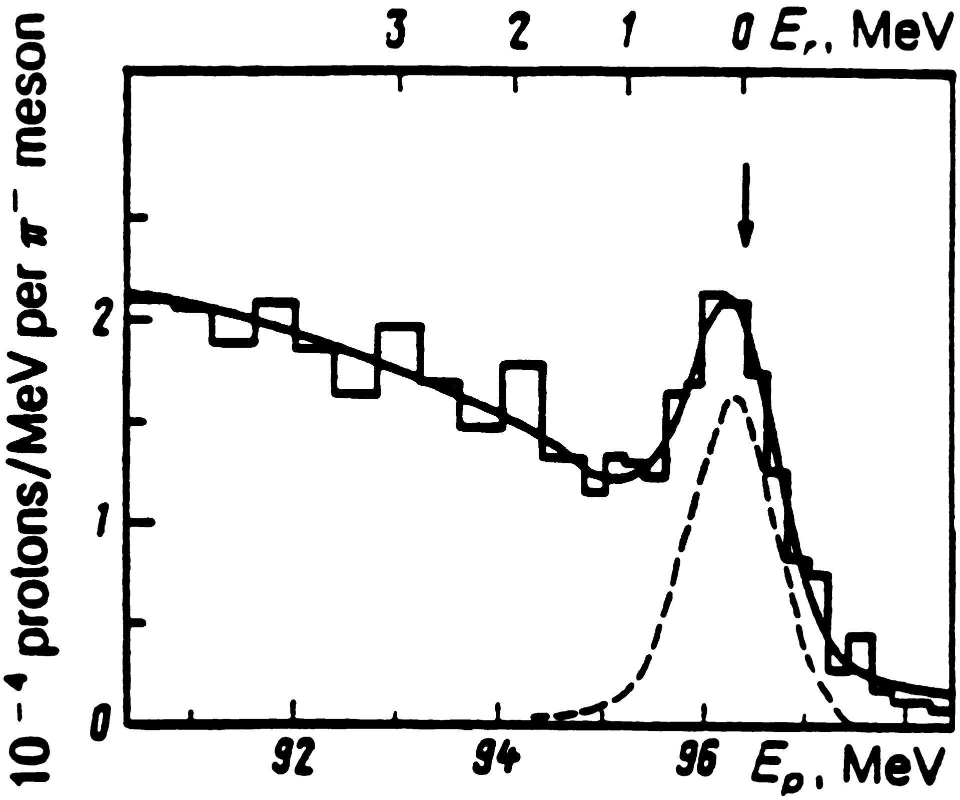

Figure 4.3: [Amel 90] Energy spectrum of protons from the reaction ^{11}B(π^-,p)^{10}Li. The dashed curve is a theoretical calculation, a Breit–Wigner form folded with the resolution of the spectrometer, of the shape of a low-lying neutron resonance. The solid curve is a sum of the dotted curve and a three–body phase space background, also folded with the spectrometer resolution. The peak corresponds to a neutron-unbound state with separation energy $S_n = -0.15 \pm 0.15$ MeV and width $\Gamma_{\mathrm{c.m.}} < 0.4$ MeV.

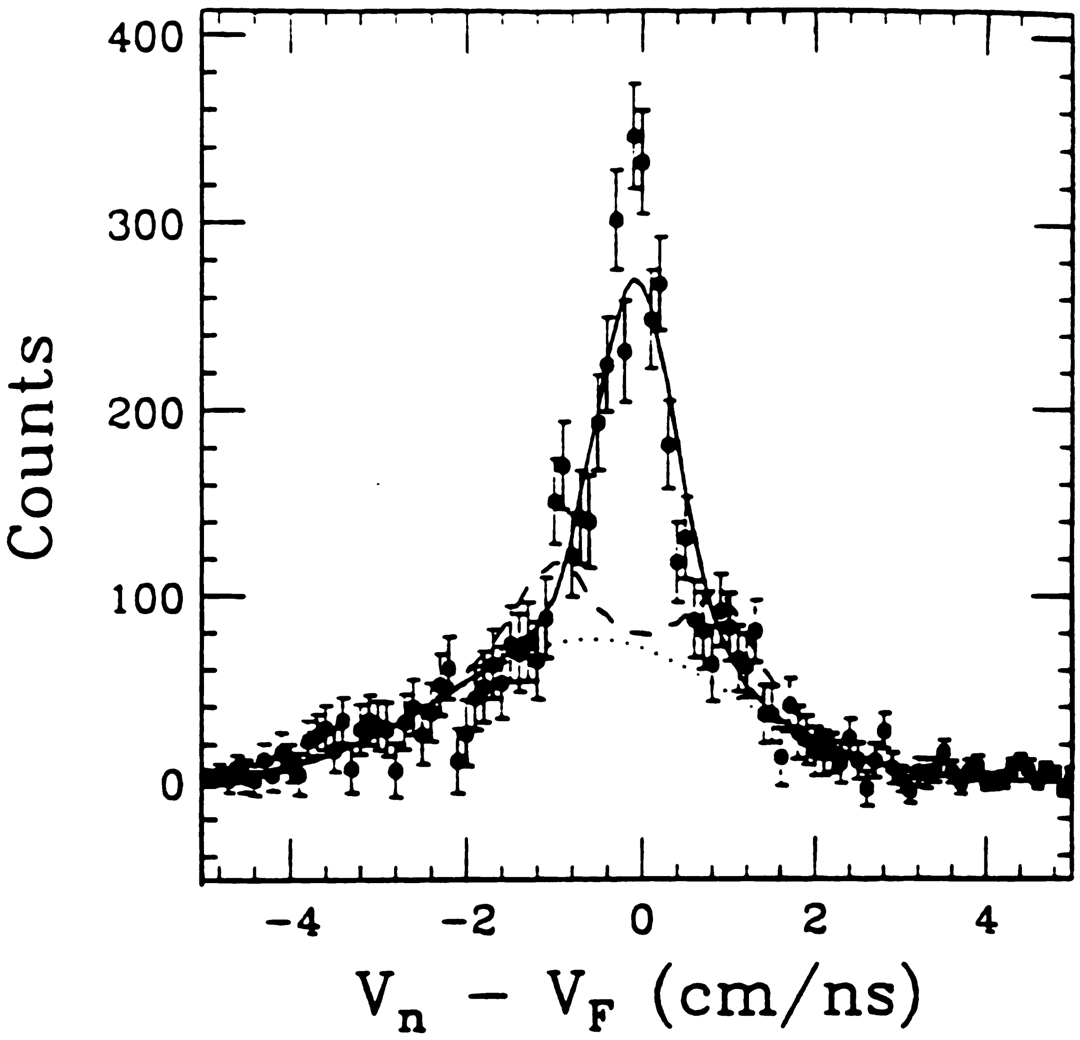

Figure 4.4: [Kryg 93] Relative velocity spectrum of neutrons collected in coincidence with ^{9}Li fragments from the decay of ^{10}Li. The dotted curve in the figure is the expected spectrum from a thermal neutron background. The solid curve represents the background added to the expected line shape from a low-energy state unbound by approximately 150 keV. The dashed curve is the expected spectrum from a broad state unbound by 800 keV.

Bohlen and collaborators have recently reported on Q-value measurements of the ^{9}Be(^{13}C,^{12}N)^{10}Li and ^{13}C(^{14}C,^{17}F)^{10}Li reactions at energies of E/A =25.8 MeV and E/A =24.1 MeV, respectively [Bohl 93]. The data from these reactions, collected with the Q3D magnetic spectrograph at the Hahn-Meitner-Institut, are shown in Figures 4.5 and 4.6. Both spectra contain broad peaks which Bohlen *et al.* claim consist of two ^{10}Li states: one, the ground state, neutron-unbound by 0.420 ± 0.050 MeV, and the other, the first excited state, unbound by 0.800 ± 0.094 MeV. Arguing from reaction systematics, the authors further assert that both states are $1p\frac{1}{2}$ neutron states with J^{π} values of 1^{+} for the ground state and 2^{+} for the excited state. Bohlen *et al.* speculate that Wilcox and collaborators observed the first excited state and not the ground state.

The experimental results published to date, summarized in Table 4.2, reflect a substantial disagreement concerning the energy and spectroscopic nature of the ^{10}Li ground and first excited states. It seems fairly certain that the state observed by Wilcox and collaborators is not the ^{10}Li ground state. Several groups [Amel 90, Kryg 93, Koba 93] have presented evidence for a weakly unbound ^{10}Li ground state. The existence of a weakly unbound $\nu 2s\frac{1}{2}$ ground state would be in agreement with the suggestions of Barker and Hickey, as well as the shell model predictions of Warburton and Brown[Brow 92, Warb 92]; these shell model calculations, however, also predict that the $\nu 1p\frac{1}{2}$ first excited state should have an excitation energy of only about 100 keV. Also supporting the existence of this state is the observation by Abramovich *et al.*[Abra 73] of a $T = 2$ state in ^{10}Be which, with Coulomb energy systematics, gives $S_n = -60$ keV for ^{10}Li. Bohlen and collaborators, however, claim that the ^{10}Li ground state is neither weakly unbound nor a $\nu 2s\frac{1}{2}$ state. In the work reported in the following sections, the low-lying structure of ^{10}Li was deduced from the momentum spectra and Q-value of the ^{11}B(^{7}Li,^{8}B)^{10}Li reaction measured with the S320 magnetic

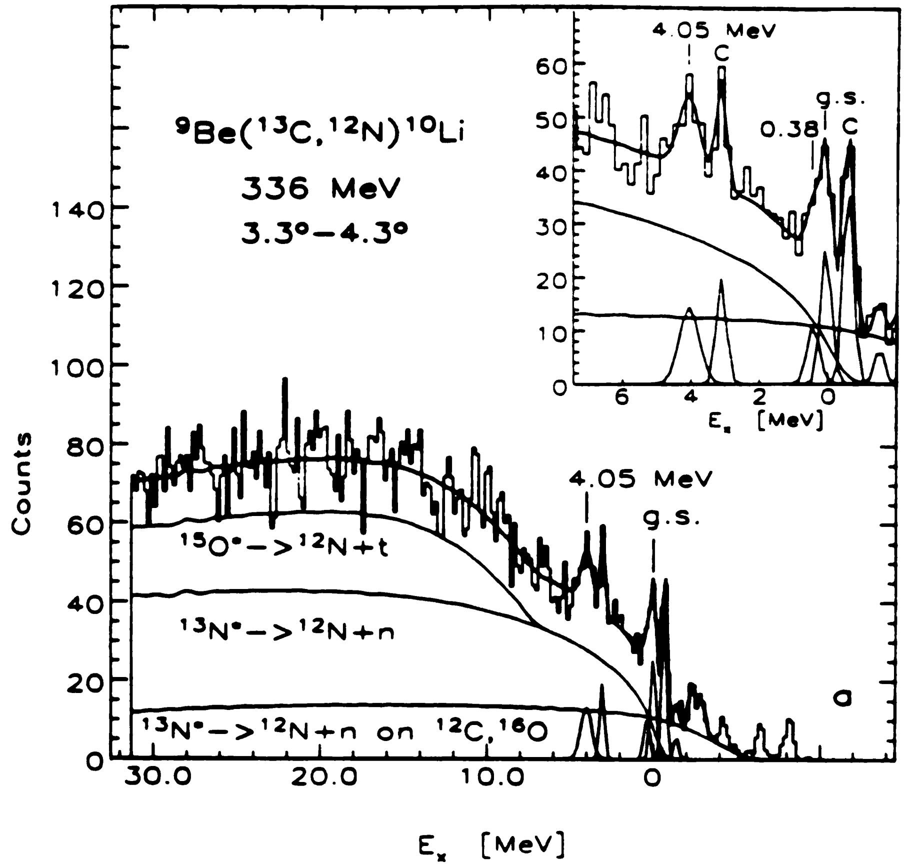

Figure 4.5: [Bohl 93] Energy spectrum of ${}^{12}N$ from the ${}^9Be({}^{13}C,{}^{12}N){}^{10}Li$ reaction at E/A =25.8 MeV and $\theta_{lab} = 3.8°$. The spectrum near low excitation energy contains, in addition to a peak from a target contaminant, a broad peak which the authors claim comprises two ${}^{10}Li$ states. The peaks are fitted with symmetric line shapes, the widths of which are determined from R-matrix calculations.

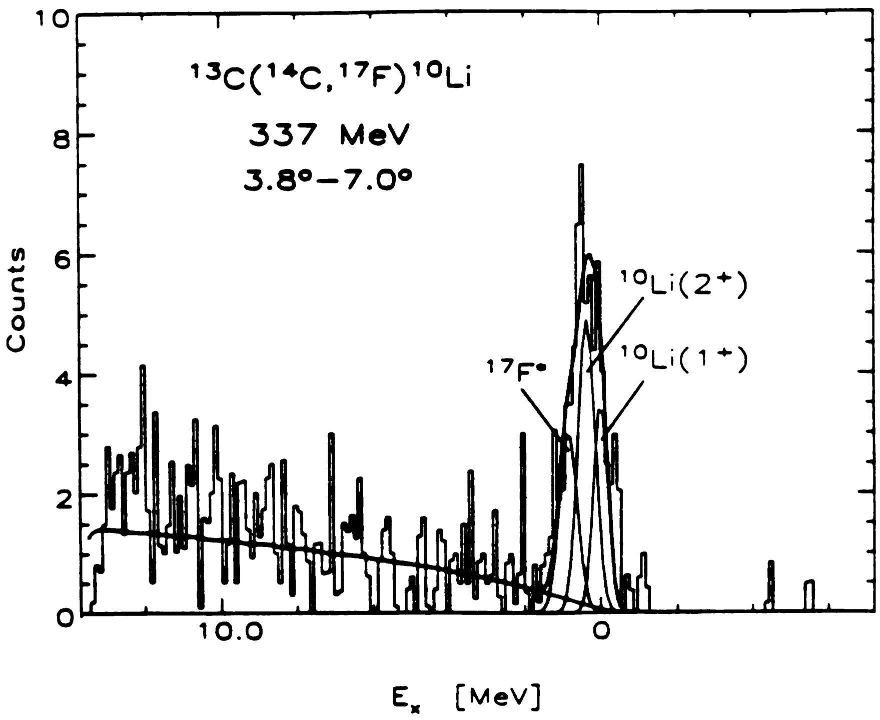

Figure 4.6: [Bohl 93] Energy spectrum of ^{17}F from the $^{13}C(^{14}C,^{17}F)^{10}Li$ reaction at E/A =24.1 MeV and $\theta_{lab} = 5.4°$. The spectrum contains a very broad peak which the authors assert consists of the same two ^{10}Li states as in the previous figure, and an excited state ($E_{ex} = 0.5$ MeV) of ^{17}F. The peaks are fitted with symmetric line shapes, the widths of which are determined from R–matrix calculations.

spectrometer at the NSCL.

III Description of S320

The S320 is a QQDMS (Quadrupole – Quadrupole – Dipole – Multipole – Sextupole; where the Multipole is an octupole) spectrometer used for nuclear reaction analysis and spectroscopy [Plic 92, Sher 83]. The separating element of the S320 is a 34.4° bending dipole magnet. The field intensities of the magnets have been accurately calibrated versus the power supply currents and are controlled via ARCNET in a manner similar to that employed with the A1200. The dipole field is continuously monitored by three probes located at one position in the dipole magnet, each probe sensitive to a different range of field strengths. The spectrometer, depicted in Figure 4.7, is located in the N1 vault at the NSCL and is mounted on a carriage that pivots about the target location to allow measurements at laboratory angles from −4° to 55°. The spectrometer subtends a solid angle that is adjustable via aperture plates to a maximum of 70 mSr. The detector box is removable, thereby allowing easy reconfiguration of the detector setup. There is, however, a standard array of particle detectors that is used for most experiments. These detectors can be configured to study fast, light ions ("light–ion mode") or slow, heavy ions ("heavy–ion mode"). For the experiment described here, the detectors were run in light–ion mode. In this mode, the standard configuration consists of a stack of five detectors: a position–sensitive single wire proportional chamber (SWPC), located at the focal position of the spectrometer, followed by two ionization chambers (IC), another SWPC, and a large composite block of scintillating plastic. The SWPC's are both 0.5 inches thick and the IC's are both 6 inches thick. All four detectors operate in the same gas volume. The scintillator block consists of a thin (0.02 inches) sheet of fast scintillator followed by a 10 cm block of slow scintillator. The light output from the scintillator

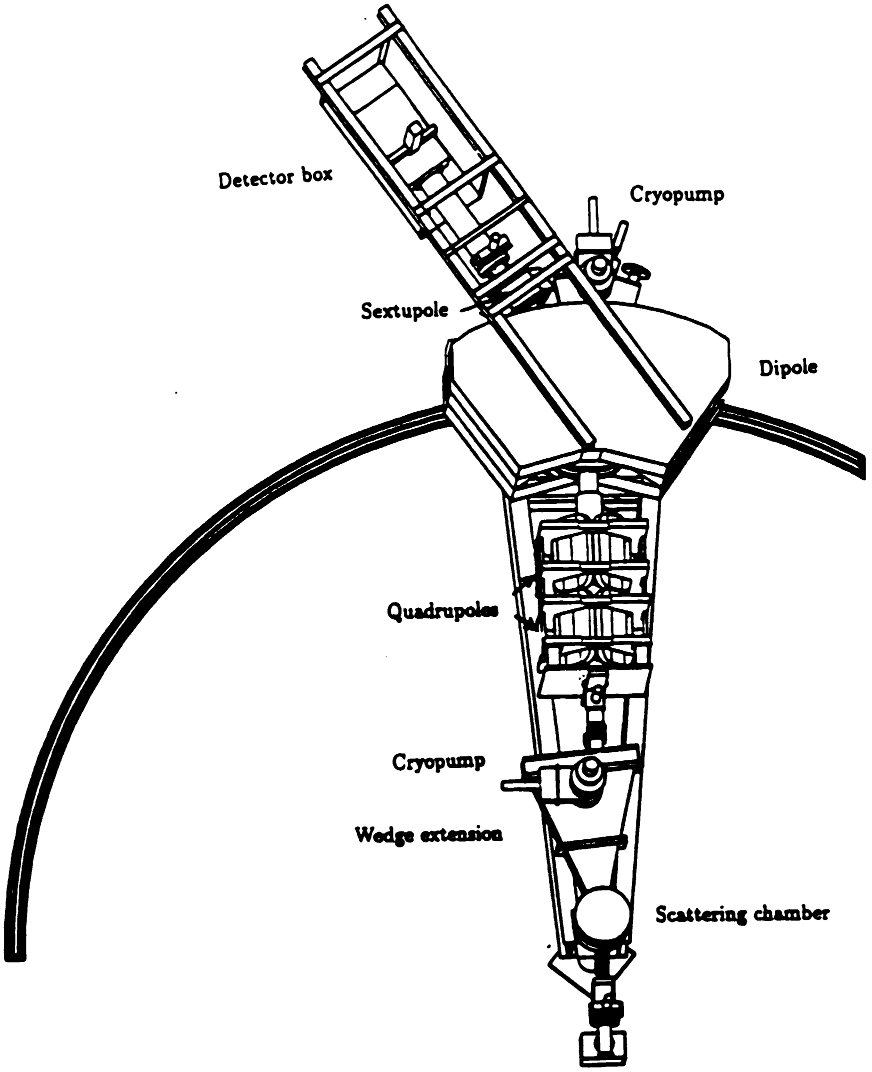

Figure 4.7: [Plic 92] Schematic layout of S320 magnetic spectrometer. the device consists of two quadrupole focusing magnets, a 34.4° bending dipole magnet, an octupole magnet (not labelled in figure, but located just after the dipole), and a sextupole magnet. While the detector box is removable to allow easy reconfiguration of the detector setup, there is a standard detector assembly that is used for most experiments. The entire spectrometer is mounted on a carriage that pivots about the target location in the scattering chamber to allow measurements at laboratory angles from −4° to 55°.

is collected by two phototubes. The SWPC's provide position information and, when used in pairs, can also provide information about a particle's angle of entry into the focal plane. Redundant energy loss information is obtained from the two IC's and total energy information is obtained from the light output of the scintillator block. Time–of–flight information is obtained from the fast signal from the scintillator and the cyclotron rf. Particle identification is found on a particle–by–particle basis by combining energy loss and time–of–flight information.

IV Description of experiment

The experiment was performed with an $E/A = 18.772 \pm 0.054$ MeV, $^{7}\mathrm{Li}^{1+}$ beam from the K1200 cyclotron. For the production runs, the beam was transported from the K1200, through the A1200, which acted as a passive beamline, and focused onto a 0.125 mg/cm^2 thick self–supporting ^{11}B foil target, located at the target position of the S320. A ^{12}C (natural) target, 0.56 mg/cm^2 thick, was used for the calibration runs. The reaction products were analyzed with the S320 magnetic spectrograph with an overall resolution (FWHM) of 0.23 MeV. The focal plane detectors were configured in the standard light–ion mode described above. The energy loss signal from the ionization chambers and the time–of–flight, taken from the scintillator signal relative to the cyclotron rf, provided unambiguous particle identification (PID). Position information was obtained from the front wire chamber, located at the focus of the spectrometer.

^{10}Li production reaction

The ^{10}Li nuclei were produced from the $^{11}\mathrm{B}(^{7}\mathrm{Li},^{8}\mathrm{B})^{10}\mathrm{Li}$ reaction. Data were collected at laboratory angles of 5.23° and 3.73° for approximately eight and ten hours, respectively. The PID spectrum from the 5.23° data, obtained from the energy loss in the first ion chamber and the time-of-flight information from the scintillator versus the cyclotron rf, is shown in Figure 4.8. The PID spectrum from the 3.73° data has identical features. In addition to ^{8}B particles, several other nuclei were observed and are labelled in the figure. The momentum spectrum for the 5.23° measurement is shown in the bottom portion of Figure 4.9. The most striking feature of this spectrum is a broad peak centered near channel 260, corresponding to a neutron separation energy of approximately -500 keV. Also notable is a weak narrow peak in the spectrum at a neutron separation energy close to zero. While this is not as well pronounced as the broad peak, it does not appear to correspond to any likely target contaminants. As discussed earlier, it is expected that the ^{10}Li ground state might have the valence neutron in the $2s\frac{1}{2}$ orbit and the first excited state could have a $1p\frac{1}{2}$ valence neutron. Since an s-wave neutron resonance at $S_n \leq -500$ keV is expected to be too broad to observe, the broad peak in the data is believed to correspond to one or more p-wave resonances, while the narrower, less unbound peak could be an s-wave resonance belonging to the ^{10}Li ground state. The cross section for the reaction at 5.23° to populate these peaks was measured to be 9.5 ± 0.7 μb/Sr. The momentum spectrum for the 3.73° run is shown in Figure 4.10. During this portion of the experiment, the beam current from the K1200 cyclotron had diminished considerably from approximately 110 nA, as was measured during the 5.23° run, to approximately 75 nA. This, combined with a smaller solid angle, due to a smaller aperture placed on the spectrometer entrance to reduce background at the more forward angle, resulted in very poor statistics for this spectrum. For this reason, the 3.73° data are not included in the subsequent analysis.

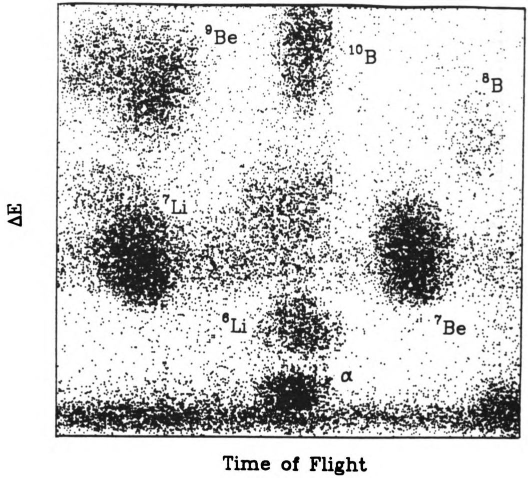

Figure 4.8: Particle–identification spectrum from ^{10}Li production run at $\theta_{\rm lab} = 5.23°$. The spectrum was obtained by histogramming ΔE and TOF information taken from the first ion chamber and the thick plastic scintillator respectively. Several nuclear species other than ^{8}B were also observed.

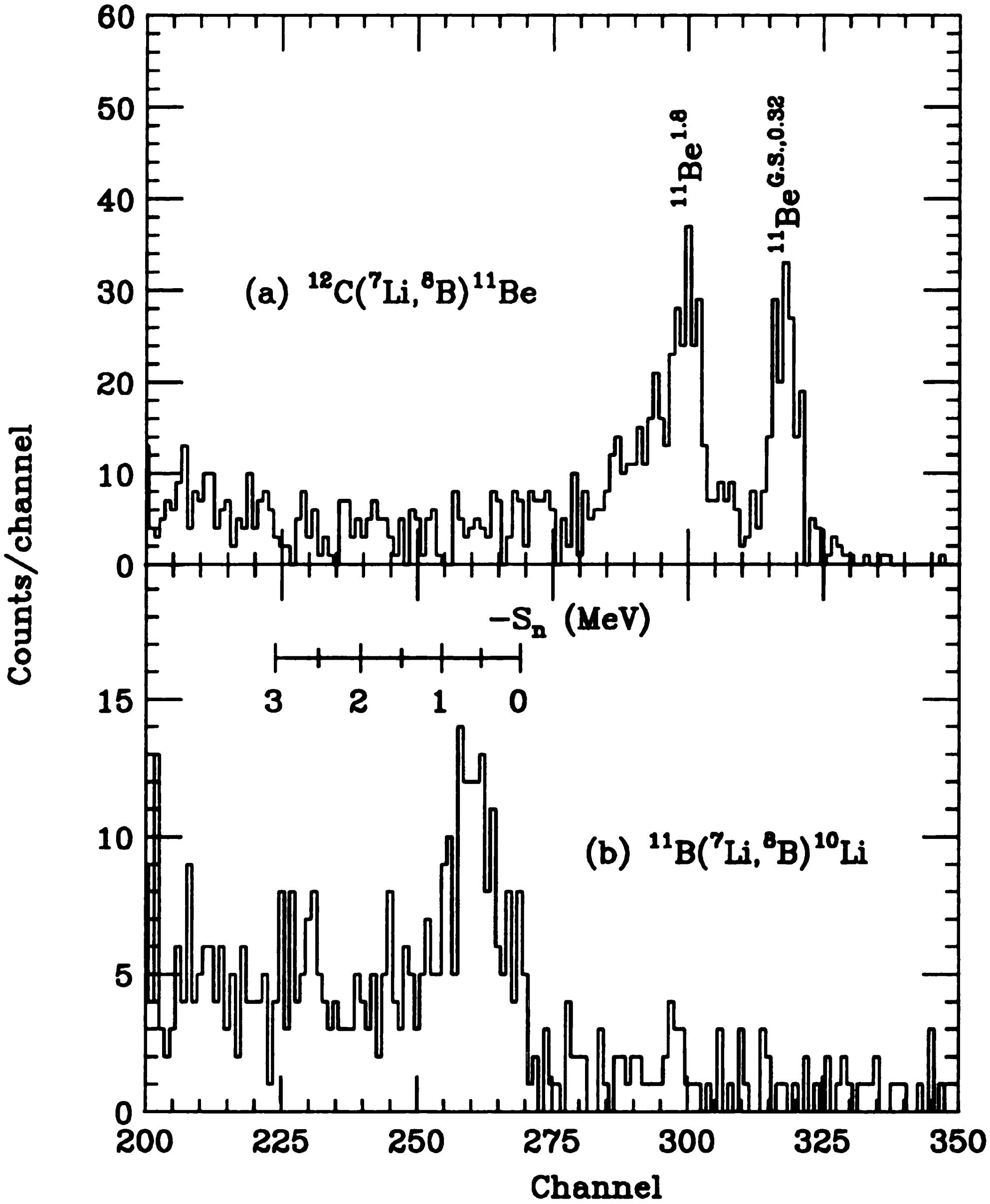

Figure 4.9: Momentum spectra from ^{10}Li production and calibration runs. Only the 5.23° data are shown here. The top part of the figure contains the momentum spectrum from the $^{12}C(^{7}Li,^{8}B)^{11}Be$ reaction. The 1.8 MeV ^{11}Be excited state was used as a primary calibration point. The bottom part of the figure contains the momentum spectrum from the $^{11}B(^{7}Li,^{8}B)^{10}Li$ reaction. Both spectra were collected at the same spectrometer field setting.

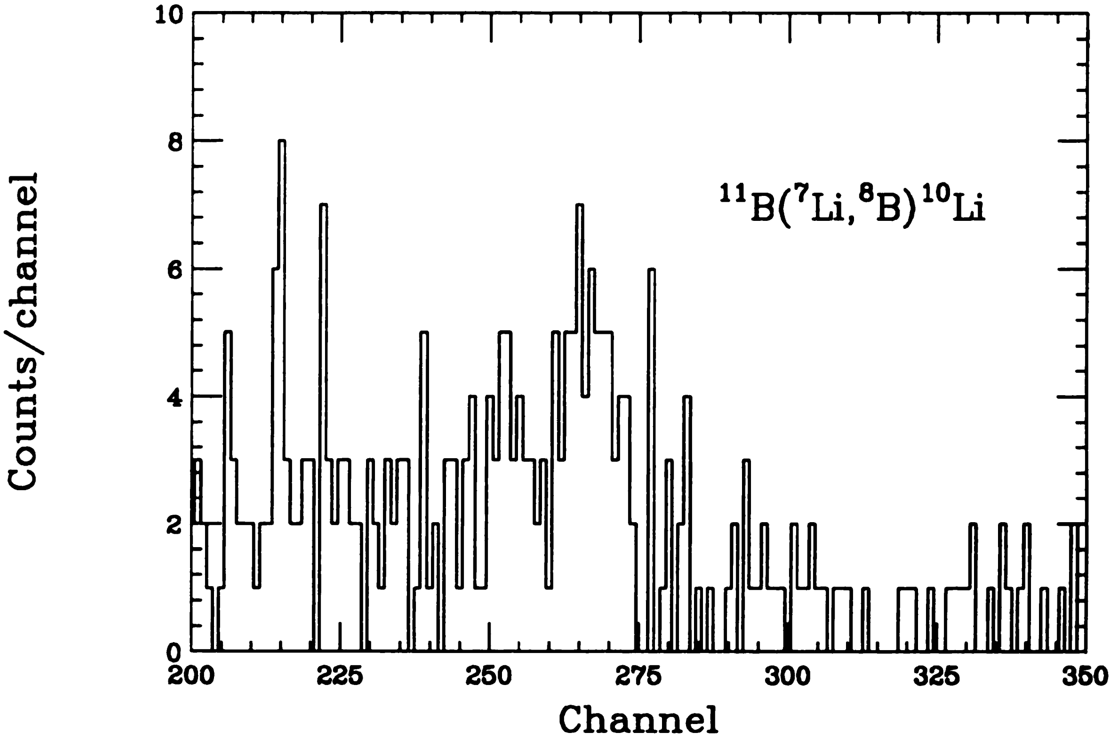

Figure 4.10: Momentum spectrum from ^{10}Li production run at $\theta_{\rm lab} = 3.73°$. Diminished beam current and spectrometer solid angle at this angle resulted in the very poor statistics evident in this spectrum. The data shown here were not included in the final analysis and mass determination of ^{10}Li.

Calibration reactions

Momentum spectra were collected for the ^{12}C(^{7}Li,^{8}B)^{11}Be reaction, which has a well-known Q-value, at the same angles and field settings as the production measurements. The spectrum collected at a laboratory angle of 5.23° is shown in the top part of Figure 4.9. The ground and first excited states of ^{11}Be are not resolved; however, the 1.778 MeV second excited state of ^{11}Be is strongly populated. The last state was used as a primary calibration point. Additional calibration points were also obtained by setting the spectrometer magnetic elements to step elastically scattered beam particles across the active area of the detector array.

V Analysis

Analysis of the data was accomplished utilizing the same procedure as described in Section IV of Chapter 4, but without the benefit of the computer code RELMASS. The beam energy, determined from the A1200 magnetic dipole fields necessary to transport the beam through the center of the device, was $E/A = 18.772 \pm 0.054$ MeV. The uncertainty of the beam energy reflects an uncertainty in the average of the NMR readings from the A1200 dipoles. The S320 spectrometer was calibrated by studying two reactions. The first was the ^{12}C(^{7}Li,^{7}Li)^{12}C reaction populating the ^{12}C ground state (i.e. elastically scattered beam) and 4.44 MeV excited state. Both states have well-known Q-values. Several runs were taken with this reaction at different spectrometer field settings so as to step the peaks from these two states across the focal plane. The rigidities of the ^{7}Li ejectile are easily calculated, and were used in conjunction with the known spectrometer fields and measured focal plane positions to amass a set of (ρ,x) points. The second calibration reaction was ^{12}C(^{7}Li,^{8}B)^{11}Be, the data for which are shown in the top part of Figure 4.9. Since the ground and 0.32 MeV first excited state of ^{11}Be are not resolved, the 1.778 MeV second excited state was used to provide an additional (ρ,x) point. A second order polynomial was fitted to this dataset and served as the focal plane calibration. This calibration curve was then used to deduce the Q–values of the states seen in the ^{11}B(^{7}Li,^{8}B)^{10}Li production reaction. To a given channel in the momentum spectrum from this reaction (bottom part of Figure 4.9) can be assigned a rigidity for the ^{8}B ejectile particle. This rigidity is then used to find a Q–value and hence a mass for ^{10}Li. Thus, a one–to–one correspondence was determined between channel number and $S_n(^{10}Li)$, the neutron separation energy of ^{10}Li. It is known that the ground and 0.32 MeV first excited states of ^{11}Be are both negligibly narrow, while the 1.778 MeV second excited state has a width of 100 keV. This information, combined with the measured width of the last state and the fact that the first two states were not resolved, was used to estimate the (FWHM) resolution of the spectrometer to be 230 keV.

To ascertain the nature and location of the peaks in the ^{10}Li data, the spectrum was fitted with a multiparameter function which consisted of several components, the first of which was a constant background. Other components were one or more p– or s–wave neutron resonances. For these, scattering calculations were performed to estimate their widths and line shapes. Details of these calculation are given in Appendix B. It was found that $2s\frac{1}{2}$ and $1p\frac{1}{2}$ states with resonance energies below 100 keV were significantly narrower than the 230 keV device resolution. For such states, the functional form used in the fitting was taken to be a Lorentzian with $\Gamma =$ 230 keV. At higher energies, s–wave resonance widths increased extremely rapidly to approximately 2 MeV at a neutron energy of 500 keV. The widths of p–wave resonances exhibited a more gradual increase with energy. Thus, s–waves above 100 keV resonance energy, calculated to be too broad to observe, were not considered in the fitting. For p–waves, the functional forms used in the fitting were parametrizations of the calculated line shapes. Finally, a 3–body phase space background, attributable to those reactions which directly produce the ^{8}B–n–^{9}Li final state, was included in the fitting. The explicit form for this phase space contribution, as a function of the center–of–mass momentum of one of the three final particles, is given in [Bloc 56]. To be applicable to the fitting of the data, the functional form given had to be transformed into the laboratory frame and the laboratory momentum of the ^{8}B ejectile had to be expressed in terms of position in the S320 focal plane (i.e. channel number). This procedure was unfeasable analytically and was done numerically. However, it was found that the resulting function could be parametrized to an accuracy of 0.03% with the expression for the upper–right quadrant of an ellipse

$$\frac{d\sigma_{\text{3body}}}{dx}(^8\text{B}) = \begin{cases} A\sqrt{1-\left(\frac{x-x_0}{x_{\text{end}}-x_0}\right)^2} & \text{if } x < x_{\text{end}} \\ 0 & \text{otherwise.} \end{cases} \tag{4.1}$$

In this expression, x is the position of the ^{8}B, x_{end} is the position corresponding to the kinematic endpoint, and x_0 is a parameter determined by fitting the expression to the calculated functional form. The parameter A is an arbitrary scaling factor and is treated as a free parameter in the fitting of the ^{10}Li data.

Because the statistics in the ^{11}B(^{7}Li,^{8}B)^{10}Li production reaction are so low, the standard least–squares fitting technique was unsuitable. A more general maximum–likelihood fitting technique was used to treat the data. This technique, presented in Appendix C, employs a figure of merit $\mathcal{L}$ which is similar to χ^2 in that it is a measure of the goodness–of–fit, and that its minimization is the objective of the fitting procedure. However, its analytical behavior is not as well known as that of the χ^2 statistic. More specifically, using $\mathcal{L}$ it is possible to compare fits with two different functional models and to determine whether one fit is better than the other; but it is not possible to assign to a given value of $\mathcal{L}$ an exact probability analogous to the chi–square distribution as described in [Pres 92].

VI Results

The best fit to the data was obtained with, in addition to a constant background and a three–body phase space component, a single $1p\frac{1}{2}$ neutron resonance at $S_n(^{10}\text{Li}) = -538 \pm 32$ keV and a narrow neutron resonance at $S_n(^{10}\text{Li}) \geq -100$ keV. This fit, shown with a solid line in Figure 4.11, yielded a figure of merit $\mathcal{L} = 106$. It was found that $\mathcal{L}$ was insensitive to the location of the narrow resonance between 0 and approximately 70 keV neutron energy. Thus, it is only possible to state with confidence that the lower state corresponds to a neutron separation energy greater than -100 keV. A fit was also performed in which the only neutron state was a single p–wave. The resulting state had a neutron separation energy of $S_n(^{10}\text{Li}) = -505 \pm 33$ keV. The figure of merit $\mathcal{L}$ for this fit, which is shown as the dashed line in Figure 4.11, was 123. A probability cannot be assigned to a given value of $\mathcal{L}$ for a fit with a certain number of degrees of freedom, and therefore an exact quantitative comparison between these two models cannot be made. However, further tests with the fitting procedure have shown that, while the model with the narrow resonance has one more fit parameter and hence one less statistical degree of freedom than the model without the narrow resonance, this difference in the number of degrees of freedom of the two models is not sufficient to account for the difference in the values of $\mathcal{L}$. This effect was explored by holding fixed the fit parameters for the two–peak model and increasing the number of channels over which the figure of merit $\mathcal{L}$ was calculated. It was found that in order to increase $\mathcal{L}$ from 106 to 123, ten additional channels (i.e. statistical degrees of freedom) were necessary. This indicates that the best fit was obtained with one p–wave resonance and one low–lying narrow resonance. Because the widths of low–energy s– and p–waves are much narrower than the device

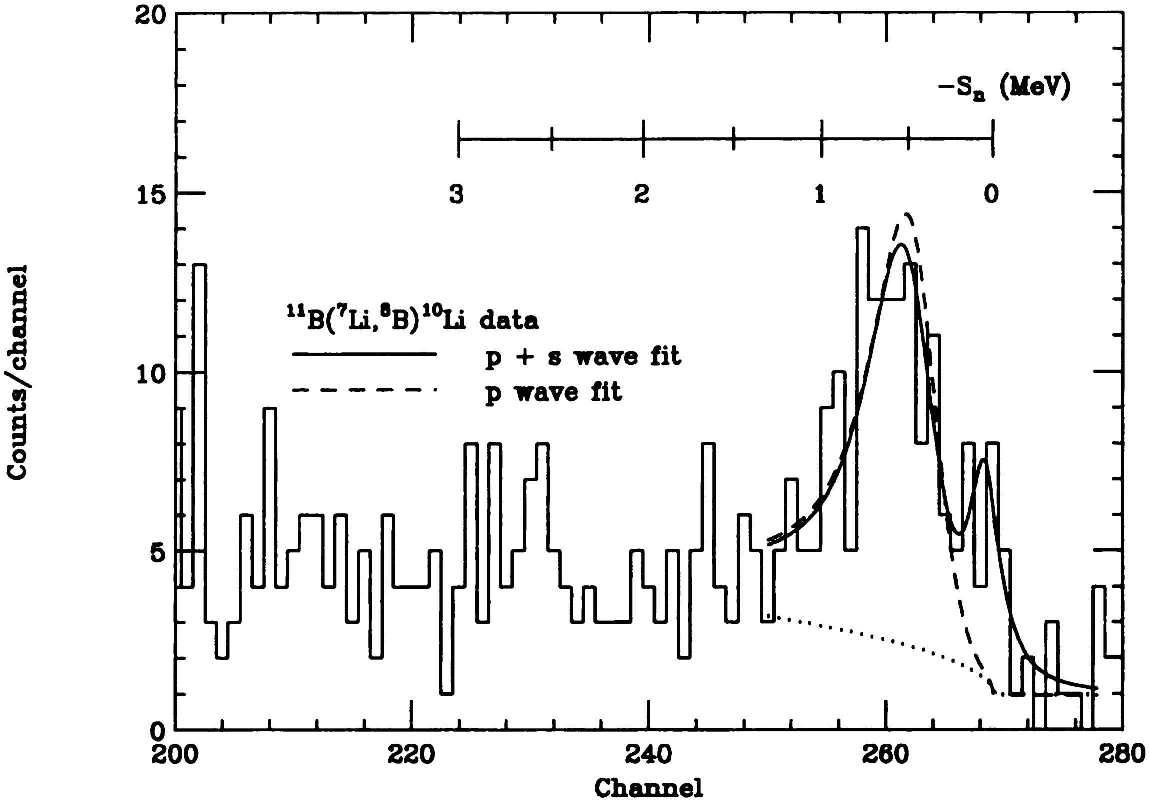

Figure 4.11: Theoretical models fitted to the collected spectrum from the reaction $^{11}B(^7Li,^8B)^{10}Li$ at $\theta_{lab} = 5.23°$. The line shape for the broad peak is obtained from resonance calculations of a p–wave neutron. The narrow state is taken to be an s–wave neutron state, the line shape of which is assumed to be a Lorentzian with width 230 keV. The details of the resonance calculations and the maximum–likelihood fitting procedure are given in Appendices B and C, respectively. The best fit, shown with the solid line, was obtained with one p–wave resonance, one s–wave resonance, a 3–body background, and a constant background. The dashed line is the fit obtained with one p–wave, a 3–body background, and a constant background. The two background terms had similar magnitudes in both models, and their sum is shown with the dotted line.

Source of uncertainty	σ (keV)
beam energy	45
spectrometer angle	27
target thicknesses	6
total nonstatistical uncertainty	53

Table 4.1: Sources of nonstatistical experimental uncertainty in ^{10}Li mass measurement. The three uncertainties listed are added in quadrature to yield the total nonstatistical uncertainty, which is further added in quadrature with the statistical uncertainties from the fitting procedure.

resolution, it is not possible to determine the spectroscopic nature of this lower state.

The uncertainties specified above reflect only statistical uncertainties from the fitting procedure. Other sources of uncertainty were experimental in nature. The data were re–analyzed with the beam energy increased by one sigma; thus determined, the contribution to the overall uncertainty from the beam energy was 45 keV. The spectrometer angle was known to within 0.05°, contributing an additional 27 keV to the final uncertainty. Finally, the thicknesses of the production and calibration targets were determined from beam energy–loss to within 1%, yielding an additional 6 keV in the final uncertainty. These contributions, which are listed in Table 4.1, are added in quadrature to yield the total nonstatistical uncertainty, which is further added in quadrature with the statistical uncertainties from the fitting procedure. The best interpretation of the data, therefore, indicates that ^{10}Li has a $1p\frac{1}{2}$ neutron state unbound to neutron decay by 538 ± 62 keV and a ground state, either a $1p\frac{1}{2}$ or a $2s\frac{1}{2}$ neutron state, unbound by less than 100 keV. The ^{10}Li mass excesses for these states are 33.563 ± 0.062 MeV and less than 33.125 MeV, respectively. The Q–values for the ^{11}B(^{7}Li,^{8}B)^{10}Li reaction to populate these states are −32.908 ± 0.062 MeV and greater than −32.471 MeV, respectively. The width of the ground state is known to

	S_n (MeV)	Γ_{lab} (MeV)	Identification
Wilcox *et al.* [Wilc 75]	-0.80 ± 0.25	1.2 ± 0.3	g.s.
Amelin *et al.* [Amel 90]	-0.15 ± 0.15	≤ 0.4	$s\frac{1}{2}$, g.s.
Kryger *et al.* [Kryg 93]	≥ -0.15 or ≈ -2.5		g.s.
Bohlen *et al.* [Bohl 93]	-0.42 ± 0.05	0.15 ± 0.07	$p\frac{1}{2}$, g.s.
	-0.80 ± 0.06	0.30 ± 0.10	$p\frac{1}{2}$
Present work	≥ -0.10	< 0.23	g.s.
	-0.54 ± 0.06	0.36 ± 0.02	$p\frac{1}{2}$

Table 4.2: Summary of experimental data on low–lying structure of ^{10}Li published to date, including the present work. The neutron separation energy and width are given for each state. Also given for each state is the identification (if any) claimed by the experimenters.

be much smaller than the resolution of the spectrometer, 230 keV. The width of the $1p\frac{1}{2}$ excited state, determined from the measured excitation energy and the calculated width at that energy, is $\Gamma_{\text{lab}} = 358 \pm 23$ keV. These values are summarized, together with the existing measurements, in Table 4.2.

An attempt was also made to fit the broad structure near −500 keV with two p–wave resonances, as was done by Bohlen *et al.*. With this model, the best fit corresponded to a minimum $\mathcal{L}$ value of 124 and put both of the resonances at the same energy as the single p–wave fit described above. Further investigations found that it was possible to keep $\mathcal{L}$ within unity of its minimum value only by placing the resonances less than 170 keV apart and centered near −520 keV separation energy. It is important to note that under no circumstances could a reasonable fit be made with a resonance unbound by more than 650 keV. Both of these results, the possible existence of a low–lying neutron state, and the fact that the broad peak in the data can only be fit by a single $1p\frac{1}{2}$ neutron resonance or by two such resonances separated by less than 170 keV, do not corroborate the results of Bohlen *et al.*. A possible explanation for this is the fact that, although the spectra collected by Bohlen *et al.* are very similar to that in the present work, particularly the data from the ^{9}Be(^{13}C,^{12}N)^{10}Li reaction shown if Figure 4.5, the theoretical p-wave line shapes used in their paper are symmetric and relatively narrow ($\Gamma_{\rm lab}$ $\simeq$200 keV) whereas the line shapes used here are asymmetric and fairly broad ($\Gamma_{\rm lab}$ $\simeq$400 keV). It seems plausible that a peak at S_n = -800 keV is artificially necessitated in order to fit the high-energy tail of the data with narrow, symmetric p-waves. Although the existence of a low-lying ^{10}Li ground state has been observed here as well as by Amelin *et al.* [Amel 90] and possibly by Kryger *et al.* [Kryg 93], it is still unclear whether this state is an s-wave or a p-wave neutron resonance. However, mounting expectations from systematic and theoretical considerations indicate that an s-wave contribution dominates the n-^{9}Li interaction.

Chapter 5

Conclusions–The Present and Future of ^{11}Li and ^{10}Li

One of the most interesting nuclei that have been made available for study by the production of intense radioactive nuclear beams is ^{11}Li. This nucleus has exhibited many remarkable properties which can be explained, both qualitatively and quantitatively, by viewing the nucleus as a three–body system, which comprises a ^{9}Li core and a halo of two loosely bound neutrons. Measurements of the rms radius of the halo neutrons have yielded values of between 6 and 10 fm. One of the most basic quantities used by theoretical models based on this three–body picture is the mass of ^{11}Li. The measurement of the ^{11}Li mass presented in this dissertation is the most accurate value to date. The current best estimate of the ^{11}Li mass excess, obtained by averaging the value reported here with the three previous measurements, is 40.802 $\pm$ 0.026 MeV. This corresponds to a two–neutron separation energy of 295 $\pm$ 26 keV. This quantity, which is basic to the understanding of the structure of ^{11}Li is now known to sufficient accuracy for precise comparison with theoretical models.

Another important factor in the three–body models of ^{11}Li is the nature of the n–^{9}Li interaction. Recent attention has focused on the low–lying structure of the neutron–unstable nucleus ^{10}Li. The experimental evidence pertaining to this nucleus does not present a clear picture. Various mass measurements have determined the ^{10}Li ground state to be unbound by as little as 150 keV and as much as 800 keV. In addition to uncertainty regarding the energy of the ground state resonance, there is also considerable disagreement over the spectroscopic nature of the ground state, which is expected to be either a $1p\frac{1}{2}$ or a $2s\frac{1}{2}$ neutron state. The existence of a broad ($\Gamma \geq 300$ keV) ^{10}Li state unbound to neutron decay by greater than 400 keV has been well established. But there is mounting evidence that there is a much lower-lying, barely unbound state. This evidence includes the observation by Amelin *et al.* of a state unbound by 150 ± 150 keV, independent observations by Kryger *et al.* and Kobayashi *et al.* of a peak corresponding to close to zero relative n–^{9}Li velocity from the decay of ^{10}Li, and the observation of a narrow state in ^{10}Be by Abramovich *et al.* believed to be the isobaric analog of a ^{10}Li state unbound by 60 keV. The experimental evidence presented in this work is the first *simultaneous* observation of both a broad, relatively high-lying ^{10}Li state and a second barely unbound state. Although the statistics in the present spectrum are rather poor, extensive resonance calculations and the employment of a statistically accurate maximum-likelihood fitting technique have allowed quantitative estimates of the low-lying structure of ^{10}Li. The best interpretation of the data indicates that ^{10}Li has a $\nu 1p\frac{1}{2}$ excited state unbound to neutron decay by 538 ± 62 keV (corresponding to a ^{10}Li mass excess of 33.563 ± 0.062 MeV) with a width of 358 ± 23 and a ground state unbound by less than 100 keV (^{10}Li mass excess less than 33.125 MeV). The spectroscopic nature of the low-lying state could not be determined from the data. However, theoretical evidence, by Barker and Hickey as well as Warburton and Brown, indicate that this low-lying state could be a $2s\frac{1}{2}$ neutron state. This would not be too surprizing since the neighboring nucleus ^{11}Be has a $2s\frac{1}{2}$ neutron state for its ground state.

The three-body models that have been used to describe ^{11}Li rely on assumed forms for the particle–particle interactions between the three constituent bodies. In the initial calculations, the n–^{9}Li interaction was chosen to recreate a $1p\frac{1}{2}$ neutron resonance at an energy of 800 keV, in accordance with the measurements in [Wilc 75]. Recent Fadeev calculations performed by Bang and Thompson [Bang 92], under these assumptions, failed to reproduce simultaneously the experimentally observed neutron binding energy, the widths of the ^{9}Li momentum distributions from ^{11}Li breakup, and the energy of the 3–body breakup peak. It was found [Thom 93b] that the binding energy and rms matter radius could be reproduced only if the single n-^{9}Li p–wave state was at approximately 200 keV. The ^{9}Li momentum widths predicted from those p–wave–dominated Fadeev wavefunctions that reproduced the rms ^{11}Li radius were approximately three times larger than the experimental values. This suggests that the rms radius measured from the total interaction cross section is smaller than that deduced from the fragment momentum widths from the breakup of ^{11}Li.

Very recent calculations by Thompson and Zhukov [Thom 93b, Thom 93a] have included a $2s\frac{1}{2}$ state as well as a $1p\frac{1}{2}$ state in the n–^{9}Li interaction. The three–body Fadeev wavefunctions thus contain admixtures of these two neutron configurations. The predicted ^{11}Li binding energy is shown as a function of $2s\frac{1}{2}$ and $1p\frac{1}{2}$ resonance energies in Figure 5.1. The current ^{11}Li mass is indicated in the figure by horizontal lines, and, although the ^{10}Li p–wave resonance reported here is off the scale in the figure, the vertical line indicates the lower limit in the uncertainty in this value. To meet these limits, Thompson and Zhukov's calculations would require that the s–wave ^{10}Li ground state be unbound by less than 10 keV, a result that is also in agreement with the data presented here. Their results further indicate that at lower s–wave energies, the n–^{9}Li and n–n admixtures become increasingly dominated by the $2s\frac{1}{2}$ and $^1S_0$ state, respectively. For a 10 keV s–wave, the lowest reported in [Thom 93b], these admixtures are 64% and 67%. This has several profound effects. Because s–

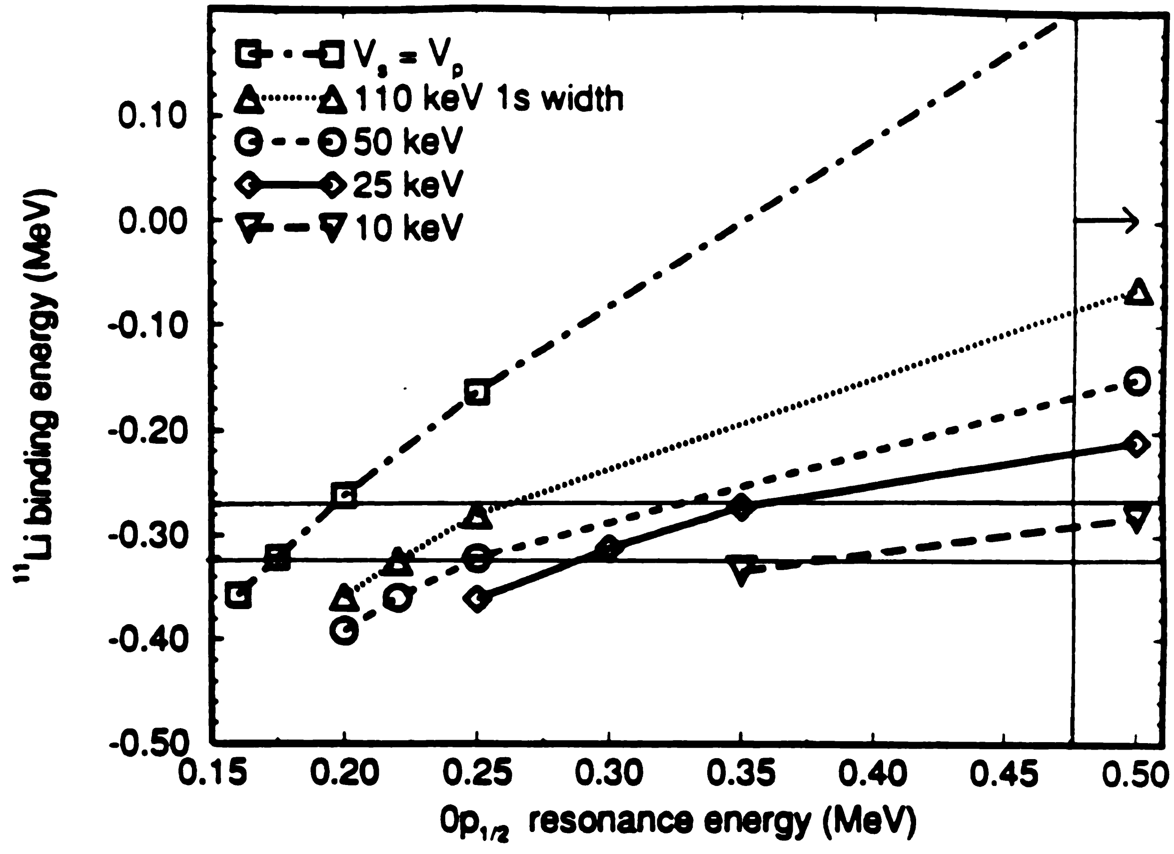

Figure 5.1: [Thom 93b] Comparison of present data with calculations by Thompson and Zhukov. This figure is identical to Figure 2.6 with the experimental results reported in this work indicated for comparison. The current ^{11}Li two–neutron separation energy (295 ± 26 keV) is indicated in the figure by horizontal lines. The value for the ^{10}Li p–wave resonance reported here (538 ± 62 keV) is off the scale in the figure, however, the vertical line indicates the lower limit in the uncertainty in this value. To meet these limits, Thompson and Zhukov's calculations would require that the s–wave ^{10}Li ground state be unbound by less than 10 keV, a result that is also in agreement with the data presented here.

wave neutron states have no centrifugal barrier, the large $2s\frac{1}{2}$ admixture in the n–^{9}Li motion leads to a ^{11}Li wavefunction with a very large rms radius (3.73 fm for the 10 keV s–wave). However, such a large matter radius corresponds to a narrow ^{9}Li fragment momentum distribution with a width σ of approximately 24 MeV/c, in good agreement with the data.

Although the ^{11}Li mass is now well known, and it seems likely that the ^{10}Li ground state is only barely unbound, the exact nature of the ^{10}Li ground state, and hence the structure of ^{11}Li, is still unknown. Theoretical models, too, have yet to reach a consensus on the details of ^{11}Li structure and are still struggling to reproduce all of the mounting experimental data regarding this puzzling nucleus. However, two main courses of action seem clear. It appears that the possibility of an s–wave ^{10}Li ground state is not a remote one, and that more realistic calculations that take this possibility into account are needed. Also, the experimental data on the low–lying structure of ^{10}Li are plagued by poor statistics and poor resolution. This situation can only be remedied by more experimental effort. By repeating experiments such as the ones presented here on other spectrometers with high resolution and large acceptance such as the S800 being constructed at the NSCL, the existence of a low–lying ^{10}Li state could be confirmed with high statistical accuracy and its spectroscopic nature could be determined from its measured width. Nevertheless, the picture of ^{11}Li which is based on the data presented in this dissertation is a considerable improvement over previous interpretations, and therefore continued progress is being made on the understanding of the new phenomenon of halo nuclei.

Appendix A

RELMASS

Analysis of mass–measurement data from a magnetic spectrometer can be divided into two major steps: calibration of the spectrometer, and measurement of the Q–value of the production reaction. For each calibration reaction, the beam energy, reaction Q–value, and ejectile angle, all of which are known, determine the kinetic energy of the ejectile. This information, when combined with the magnetic field of the spectrometer and the charge state of the ejectile, will determine the bend radius ρ of the particle through the spectrometer. This process, illustrated in the flowchart in Figure A.1, yields a series of (ρ,x) values to which a functional form, typically a first or second order polynomial, is fit. The Q–value of the production reaction is then found by reversing the process, as illustrated in Figure A.2. Whereas in the calibration process, the known Q–value of the calibration reaction is used to relate the measured ejectile position to the bend radius, the Q–value is here determined from the ejectile position.

The above processes, while relatively simple conceptually, involve a great deal of numerical calculation and are prone to error if done by hand. To facilitate analysis of experiments of this type, Toshiyuki Kubo, with suggestions from Ed Kashy, has written a computer code, RELMASS, which automates both of the above steps. When executed, the program searches the current directory for the input file `RELMASS.INP`.

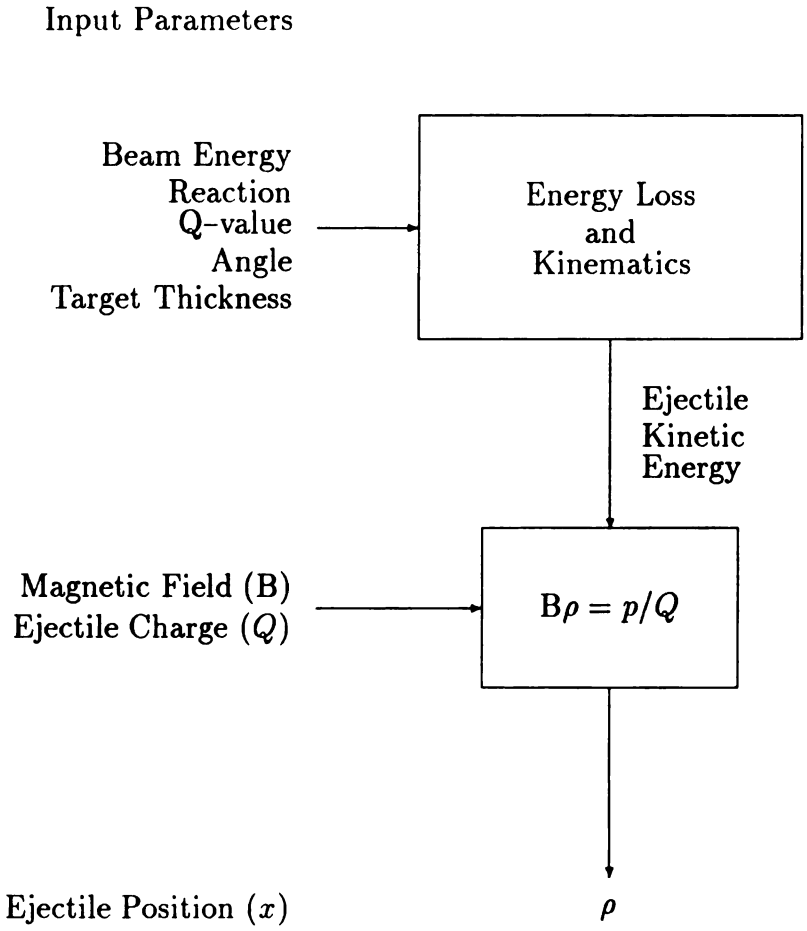

Figure A.1: Flowchart of magnetic spectrometer calibration procedures. The input parameters are all experimentally measured or calculated quantities. Each calibration reaction yields one or more sets of (ρ,x) values.

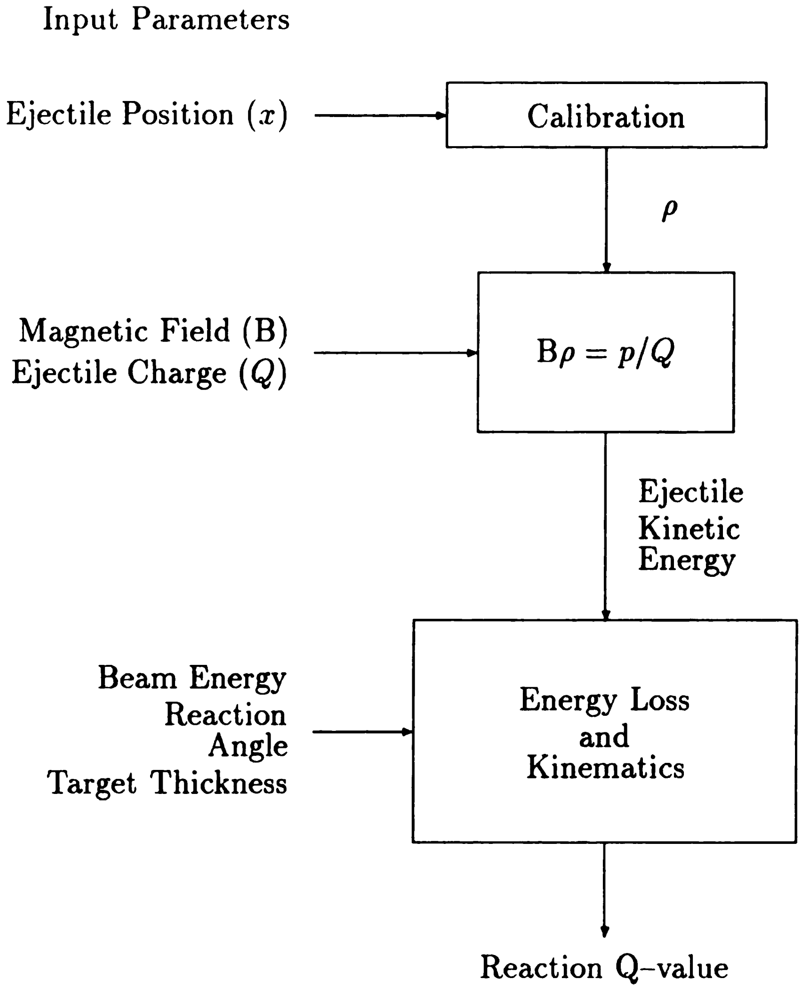

Figure A.2: Flowchart of Q–value measurement procedures with a calibrated magnetic spectrometer. As in the previous figure, the input parameters are all experimentally measured or calculated quantities. The reaction Q–value is determined from the measured ejectile position x.

Both the code and a sample input file are located in the directory

`NSCL_LIBRARY:[RELMASS]`

on the NSCL VAX cluster. Upon completion, the program creates two files, the names of which are requested from the user. The first file, given the extension `.OUT`, contains numerical details of each step of the calibration and measurement processes. The second file is a TOPDRAWER file which depicts the ρ vs x calibration curve with the calibration and measurement points. The most straightforward discussion of the operation of the program is provided by examining the input and output files, examples of which are included in Table A.1 at the end of this appendix.

Input file: `RELMASS.INP`

The input file provides the program with the parameters necessary to calibrate the spectrometer and then to measure the Q–value of a series of production reactions. The first four lines allow the user to title and comment the input file. The information in these lines has no bearing on the program operation; they are merely repeated in the output file. Following the comment lines are groups of calibration data, one group for each peak in the calibration momentum spectra. Each group of calibration data begins with the tag–string `CALIB_REACTION` followed by a label number. The label numbers are arbitrary and facilitate bookkeeping for the user. The lines following the tag–string allow the user to add a comment for that particular set of data and to specify kinematic and experimental parameters such as the reaction, beam energy, spectrometer field, target thickness, and excitation energies for the calibration peak. In addition to the target, it is possible to specify two absorber materials, one before the target and one after, through which the beam and ejectile, respectively, lose energy. Finally, for each group of calibration data, the user may define a weighting factor for use in external mode of the least-squares fitting of the calibration curve to the data, as described below. The user may also instruct the program to ignore any set of calibration data by placing the characters `//` before the tag-string, as is done for Calibration Reaction 2 in the example file given.

Following the calibration data are sets of data for Q-value measurements. Each dataset is preceded by the tag-string `MASS_MEASUREMENT` followed by an arbitrary label number. The first sixteen lines of each measurement dataset are identical to those of a calibration dataset. The next three lines pertain to the searching technique used by the program to find the measured Q-value. When RELMASS processes a dataset from a production reaction, it consults the MASSPACK table of atomic masses to obtain an initial estimate of the Q-value. This estimated Q-value, combined with the rest of the information in the dataset, specifies a point on the (ρ–x) plane, which may or may not lie on the calibration curve. The program then iteratively varies the mass of either the ejectile or residue particle, the choice specified by the user, to place the point on the calibration curve. These three lines specify the maximum number of iterations, the variational step size, and the desired absolute accuracy of the mass search. The next line allows the user to specify which mass, ejectile or residual, should be varied. The next six lines pertain to various routines in the program that estimate uncertainties. As of this writing (November 1993), these routines are not implemented and the parameters in these lines are ignored. As with calibration datasets, the user may instruct the program to ignore any measurement dataset by placing the characters `//` before its tag-string.

The last set of data is preceded by the tag-string `LEAST_SQUARE` and determines various aspects of the least-squares fitting of the calibration curve. There are three possible modes for weighting the calibration data in the fit. The first, equal mode, gives each data point an equal weight. Internal mode weights each data point by the uncertainties in its peak position. External mode weights each data point by the factor specified with its dataset.

Output file

The output file is named by the user and contains numerical details of each step of the calibration and measurement processes. The first and second pages list the input data for the calibration reactions and the control parameters for the least-squares fitting of the calibration points. The third page lists the input data for the measurement reactions and the control parameters for the mass search. The fourth page specifies the atomic and nuclear (i.e. sans electrons) masses of each participant in the calibration reactions as well as the ground-state Q-values. The kinetic energy of the calibration reaction ejectiles is given on the fifth page. The program includes energy-loss effects in the target and calculates the ejectile energy as the average of the values obtained by assuming the reaction takes place at the front and back surfaces of the target. The sixth page presents all of the calibration points (ρ,x) and lists the polynomial coefficients that provided the best fit to these points. The polynomial listed here is then used in subsequent steps to measure reaction Q-values. The seventh page presents the first guesses, based on the MASSPACK table, of the kinematic parameters for the measurement reaction. Also listed on this page is the (ρ,x) point that is taken as the initial guess in the iterative mass search, the steps of which are detailed on the eighth page. Finally, the ninth page lists the ejectile mass and reaction Q-value as obtained from the MASSPACK table and as obtained from the measurement. Also given on the ninth page is a table of uncertainty estimates. However, since the relevant subroutines are not fully implemented, these values should not be used.

Table A.1: An example of the RELMASS input file, **RELMASS.INP**, is listed on the two following pages. An example RELMASS output file is listed on the nine pages following the listing of **RELMASS.INP**. The contents of both files are discussed in the text.

```
filename: RELMASS_THESIS.INP
Input data for an analysis of mass measurement
COMMENT_DATA   (A80)
  Example file : Two calibration points and one mass measurement.

CALIB_REACTION 1.1   Read format (T46,A40/T46,A26,15(/T46,F15.0))
  Comment                                   : 10Be3+ (5.3)
  Reaction, a + A -> b + B, A(a,b)B         : 14C(11B,10Be)15N
  Projectile energy, pos[MeV],neg[MeV/A]    : -32.1365
  Scattering angle of ejectile[degrees]     :  0.0
  Excitation energy of ejectile[MeV]        :  0.0
  Excitation energy of residual[MeV]        :  5.2845
  Charge of ejectile                        :  3.0
  Magnetic fields of spectrograph[Tesla]    :  0.921608
  Thickness[mg/cm2] of absorber-1           :  0.0
  Atomic number (Z) of absorber-1           :  0.0
  Thickness[mg/cm2] of target               :  0.450
  Atomic number (Z) of target               :  6.0
  Thickness[mg/cm2] of absorber-2           :  0.0
  Atomic number (Z) of absorber-2           :  0.0
  Focal plane position of ejectile[channel] :  60.136
  Error(one-sigma) of position[channel]     :  0.020
  Weight factor(0 to 1, if zero, ignored)   :  1.0

CALIB_REACTION 1.2
  Comment                                   : 10Be3+ (g.s.)
  Reaction, a + A -> b + B, A(a,b)B         : 14C(11B,10Be)15N
  Projectile energy, pos[MeV],neg[MeV/A]    : -32.1365
  Scattering angle of ejectile[degrees]     :  0.0
  Excitation energy of ejectile[MeV]        :  0.0
  Excitation energy of residual[MeV]        :  0.0
  Charge of ejectile                        :  3.0
  Magnetic fields of spectrograph[Tesla]    :  0.921608
  Thickness[mg/cm2] of absorber-1           :  0.0
  Atomic number (Z) of absorber-1           :  0.0
  Thickness[mg/cm2] of target               :  0.450
  Atomic number (Z) of target               :  6.0
  Thickness[mg/cm2] of absorber-2           :  0.0
  Atomic number (Z) of absorber-2           :  0.0
  Focal plane position of ejectile[channel] :  140.345
  Error(one-sigma) of position[channel]     :  0.069
  Weight factor(0 to 1, if zero, ignored)   :  1.0

//CALIB_REACTION 2
  Comment                                   : This reaction is commented out
  Reaction, a + A -> b + B, A(a,b)B         : 14C(11B,9Li)16O
  Projectile energy, pos[MeV],neg[MeV/A]    : -32.1365
  Scattering angle of ejectile[degrees]     :  0.0
  Excitation energy of ejectile[MeV]        :  0.0
  Excitation energy of residual[MeV]        :  0.0
  Charge of ejectile                        :  3.0
  Magnetic fields of spectrograph[Tesla]    :  0.866737
  Thickness[mg/cm2] of absorber-1           :  0.0
  Atomic number (Z) of absorber-1           :  0.0
  Thickness[mg/cm2] of target               :  0.450
  Atomic number (Z) of target               :  6.0
  Thickness[mg/cm2] of absorber-2           :  0.0
  Atomic number (Z) of absorber-2           :  0.0
  Focal plane position of ejectile[channel] :  101.806
  Error(one-sigma) of position[channel]     :  0.074
  Weight factor(0 to 1, if zero, ignored)   :  0.0

MASS_MEASUREMENT 1
  Comment                                   : 9Li mass meas
  Reaction, a + A -> b + B, A(a,b)B         : 14C(11B, 9Li)16O
  Projectile energy, pos[MeV],neg[MeV/A]    : -32.1365
```

```
  Scattering angle of ejectile[degrees]      :   0.0
  Excitation energy of ejectile[MeV]         :   0.0
  Excitation energy of residual[MeV]         :   0.0
  Charge of ejectile                         :   3.0
  Magnetic fields of spectrograph[Tesla]     :   0.863664
  Thickness[mg/cm2] of absorber-1            :   0.0
  Atomic number (Z) of absorber-1            :   0.0
  Thickness[mg/cm2] of target                :   0.450
  Atomic number (Z) of target                :   6.0
  Thickness[mg/cm2] of absorber-2            :   0.0
  Atomic number (Z) of absorber-2            :   0.0
  Focal plane position of ejectile[channel] :   137.588
  Error(one-sigma) of position[channel]      :   0.211
  Maximum number of iteration in mass search:   100.
  Energy step in the iteration[MeV]          :   5.0D-2
  Goal of position difference in search[ch] :   1.0D-3
  Ejectile mass(0.) or residue mass(1.) ?    :   0.0
  dQ/d(Eproj), d(Eproj) = X*Eproj, X[%] =    :   0.1
  dQ/d(Theta), d(Theta) [deg.] =             :   1.0
  dQ/d(position), d(position) [channel] =    :   1.0
  dQ/d(Thick,abs1),d(Thick)=X*Thick, X[%] = :   0.0
  dQ/d(Thick,targ),                  X[%] = :   1.0
  dQ/d(Thick,abs2),                  X[%] = :   0.0

LEAST_SQUARE
  Do you make fitting ?  Yes(0.0), No(1.0)  :   0.0
  Order of fitting function(up to 3rd-order):   1.0
  Weight mode(1;equal,2;internal,3;external):   1.0

END_OF_DATA
```

```
RELMASS ver.1.0 :   Example file : Two calibration points and one mass measurement.                 << INPUT DATA >>

Input data file : RELMASS.INP

**** Data of calibration runs (max. 30) ****

------------------------------------------------------------------------------------------------------------------------
              Reaction            Energy*     Angle    Ex(proj.)   Ex(res.)   Q/e    Mag. field  Position (1s-error)  Weight**
 #            T(P,E)R           [MeV,MeV/A]  [deg.]      [MeV]       [MeV]   (ejec.)   [Tesla]        [channel]
------------------------------------------------------------------------------------------------------------------------
 1    14C(11B,10Be)15N             -32.1365    0.000     0.0000      5.2845    3.      0.921608    60.136 (  0.0200)   1.000
 2    14C(11B,10Be)15N             -32.1365    0.000     0.0000      0.0000    3.      0.921608   140.345 (  0.0690)   1.000
------------------------------------------------------------------------------------------------------------------------
*  Projectile energy is given in MeV/nucleon, if it has a negative value.
** External weight factor for least-square fit.


--------------------------------------------------------
      Absorber-1*        Target*          Absorber-2*
    Thickness   Z   Thickness   Z   Thickness   Z
 #   [mg/cm2]        [mg/cm2]         [mg/cm2]
--------------------------------------------------------
 1      0.0000   0.      0.4500   6.      0.0000   0.
 2      0.0000   0.      0.4500   6.      0.0000   0.
--------------------------------------------------------
* Target is supposed to consist of these three layers.
  Absorber thickness should be zero if it does not exist.
```

```
RELMASS ver.1.0 :   Example file : Two calibration points and one mass measurement.                    << INPUT DATA >>

Input data file : RELMASS.INP


**** Control parameters for least-square fit. ****

----------------------------------------------------------------------
Order of fitting function = 1.
   Position[ch] = a(1) + a(2)*rho[m] + a(3)*rho[m]**2 + a(4)*rho[m]**3
----------------------------------------------------------------------
Weight factors in fitting are based on Mode 1.
   Mode 1 : equal weights for all data.
        2 : weights are given from error of position.
        3 : weights are given externally.
----------------------------------------------------------------------
```

```
RELMASS ver.1.0 :   Example file : Two calibration points and one mass measurement.                << INPUT DATA >>

Input data file : RELMASS.INP

**** Data of mass measurement runs (max. 5) ****

------------------------------------------------------------------------------------------------------------------
          Reaction                Energy*   Angle   Ex(proj.)   Ex(res.)   Q/e   Mag. field  Position (1s-error)
#          T(P,E)R               [MeV,MeV/A] [deg.]   [MeV]      [MeV]   (ejec.)  [Tesla]        [channel]
------------------------------------------------------------------------------------------------------------------
1    14C(11B, 9Li)16O              -32.1365   0.000    0.0000     0.0000    3.     0.863664  137.588 (  0.2110)
------------------------------------------------------------------------------------------------------------------
* Projectile energy is given in MeV/nucleon, if it has a negative value.


------------------------------------------------------
     Absorber-1*      Target*        Absorber-2*
   Thickness   Z  Thickness   Z  Thickness   Z
#   [mg/cm2]       [mg/cm2]        [mg/cm2]
------------------------------------------------------
1     0.0000   0.     0.4500   6.     0.0000   0.
------------------------------------------------------
* Target is supposed to consist of these three layers.
  Absorber thickness should be zero if it does not exist.


**** Control parameters in searching for mass value. ****

----------------------------------------------------------
     Mode   Max. number    Energy delta   channel diff.
#           of iteration      [MeV]         [channel]
----------------------------------------------------------
1   ejec       100.          0.0500        0.100E-02
----------------------------------------------------------
   Excitation energy of ejectile or residue is searched for
by the iteration based on Newton method. The search is made
such that calculation reproduces the measured position.

Mode: ejec (ejectile) or res (residual nucleus).
Energy delta:  small energy increments used in calculating
               derivative.
Channel diff.: iteration stops if the position difference
               is smaller than this value.
```

```
RELMASS ver.1.0 :   Example file : Two calibration points and one mass measurement.                <<  OUTPUT DATA >>

Output data file : relmass.out

**** Atomic masses of reaction elements for calibration runs ****

-------------------------------------------------------------------------------------------------------------------
           Reaction         Mass(T)*     Mass(P)*     Mass(E)*     Mass(R)*     Q value**    EXejec      EXres
 #          T(P,E)R         [a.m.u.]     [a.m.u.]     [a.m.u.]     [a.m.u.]       [MeV]       [MeV]      [MeV]
-------------------------------------------------------------------------------------------------------------------
 1    14C ( 11B , 10BE) 15N   14.003242    11.009306    10.013534    15.000109     -1.02049     0.0000     5.2845
                            13.999950    11.006563    10.011340    14.996269
 2    14C ( 11B , 10BE) 15N   14.003242    11.009306    10.013534    15.000109     -1.02049     0.0000     0.0000
                            13.999950    11.006563    10.011340    14.996269
-------------------------------------------------------------------------------------------------------------------
*  These are atomic masses which are taken from the 1986 compilation of mass measurements and predictions (1986 MASSPACK).
   The upper raw gives atomic masses and the lower raw nuclear masses which are obtained by subtracting masses of electrons.
   1 a.m.u. = 931.5016 MeV.  Electron mass = 0.5110034 MeV
** Ground-state Q value
```

```
RELMASS ver.1.0 :   Example file : Two calibration points and one mass measurement.                  << OUTPUT DATA >>

Output data file : relmass.out

**** Two-body kinematics calculation for calibration runs ****

-------------------------------------------------------------------------------------------------------------------------
             Reaction                Eproj      Angle      Eejec0*      Eejec1*      Eejec2*      Eejec**     DEejec**
#            T(P,E)R                 [MeV]     [deg.]       [MeV]        [MeV]        [MeV]        [MeV]       [MeV]
-------------------------------------------------------------------------------------------------------------------------
1   14C ( 11B , 10BE) 15N          353.5015     0.000     346.3896     346.2822     346.2118     346.2470   0.7037E-01
2   14C ( 11B , 10BE) 15N          353.5015     0.000     351.8803     351.7742     351.7025     351.7384   0.7170E-01
-------------------------------------------------------------------------------------------------------------------------
*  Eejec0: ejectile energy calculated by ignoring energy-loss effects.
   Eejec1: ejectile energy considering energy-loss effects, assuming that the reaction occures at the target entrance.
   Eejec2: ejectile energy considering energy-loss effects, assuming that the reaction occures at the target exit.
** Eejec = (Eejec1 + Eejec2)/2 : mean ejectile energy,  DEejec = |Eejec1 - Eejec2| : energy spread.
```

```
RELMASS ver.1.0 :   Example file : Two calibration points and one mass measurement.                  << OUTPUT DATA >>

Output data file : relmass.out

**** Least-square fit for calibration runs ****

(Calibration curve)

      Position[channel] = a(0) + a(1)*rho[m]

(Coefficients & their errors)

      a(0) = -.991077E+04 (0.176512E+03)
      a(1) = 0.322234E+04 (0.568150E+02)

      Chi-square = 0.0000E+00

**********************************************


**** Data used in least-square fitting (calibration runs) ****

---------------------------------------------------------------------------------------------------------------------------
            Reaction            Eejec     Momentum   Charge   Brho      Bfield      rho     Meas.position (err) | Lsqf.position*
#                               [MeV]     [MeV/c]             [Tm]      [Tesla]   [meter]      [channel]        |   [channel]
---------------------------------------------------------------------------------------------------------------------------
1  14C ( 11B , 10BE) 15N      346.2470   2564.790    3.    2.851740  0.921608  3.094309   60.136 (  0.0000) |    60.136
2  14C ( 11B , 10BE) 15N      351.7384   2585.422    3.    2.874680  0.921608  3.119200  140.345 (  0.0000) |   140.345
---------------------------------------------------------------------------------------------------------------------------
* Position calculated using the calibration curve obtained from least-square fit.
```

```
RELMASS ver.1.0 :   Example file : Two calibration points and one mass measurement.            << OUTPUT DATA >>

Output data file : relmass.out

**** Kinematics calculation using 1986 MASSPACK for mass measurement runs ****

---------------------------------------------------------------------------------------------------------------------
            Reaction           Mass(T)*    Mass(P)*    Mass(E)*    Mass(R)*     Q value**    EXejec      EXres
#           T(P,E)R            [a.m.u.]    [a.m.u.]    [a.m.u.]    [a.m.u.]     [MeV]        [MeV]       [MeV]
---------------------------------------------------------------------------------------------------------------------
1    14C ( 11B ,  9LI) 16O     14.003242   11.009306    9.026789   15.994915    -8.52896     0.0000      0.0000
                               13.999950   11.006563    9.025143   15.990526
---------------------------------------------------------------------------------------------------------------------
*  These are atomic masses which are taken from the 1986 compilation of mass measurements and predictions (1986 MASSPACK).
   The upper raw gives atomic masses and the lower raw nuclear masses which are obtained by subtracting masses of electrons.
   1 a.m.u. = 931.5016 MeV.  Electron mass = 0.5110034 MeV ** Ground-state Q value


---------------------------------------------------------------------------------------------------------------------
            Reaction             Eproj      Angle      Eejec0*     Eejec1*     Eejec2*     Eejec**    DEejec**
#           T(P,E)R              [MeV]      [deg.]     [MeV]       [MeV]       [MeV]       [MeV]      [MeV]
---------------------------------------------------------------------------------------------------------------------
1    14C ( 11B ,  9LI) 16O     353.5015     0.000     342.0941    342.0380    341.9172    341.9776   0.1208E+00
---------------------------------------------------------------------------------------------------------------------
*  Eejec0: ejectile energy calculated by ignoring energy-loss effects.
   Eejec1: ejectile energy considering energy-loss effects, assuming that the reaction occures at the target entrance.
   Eejec2: ejectile energy considering energy-loss effects, assuming that the reaction occures at the target exit.
** Eejec = (Eejec1 + Eejec2)/2 : mean ejectile energy,  DEejec = |Eejec1 - Eejec2| : energy spread.


------------------------------------------------------------------------------------------------------------------------------
           Reaction            Eejec    Momentum   Charge   Brho      Bfield      rho      Meas.position (err) | Lsqf.position*
#                              [MeV]    [MeV/c]             [Tm]      [Tesla]   [meter]        [channel]       |   [channel]
------------------------------------------------------------------------------------------------------------------------------
1   14C ( 11B ,  9LI) 16O    341.9776   2422.172     3.   2.693165  0.863664  3.118302  137.588 (  0.2110) |     137.450
------------------------------------------------------------------------------------------------------------------------------
* Position calculated using the calibration curve obtained from least-square fit.
```

```
RELMASS ver.1.0 :   Example file : Two calibration points and one mass measurement.              << OUTPUT DATA >>

Output data file : relmass.out

**** Search for excitation energy of ejectile or residue by iteration based on Newton method ****

Reaction #1 :  14C ( 11B ,  9LI) 16O      --- Excitation energy of ejectile   9LI is searched. ---

                Energy increments = 0.5000E-01 MeV     Channel difference limit = 0.1000E-02 ch.

Iter.#  0  EXejec[MeV] =  0.0000    EXres[MeV] =  0.0000
           Eejec1[MeV] =  342.038   Eejec2[MeV] =  341.917   Eejec[MeV] =  341.978
           P[MeV/c] =  2422.172     Brho[Tm] = 2.693165      rho[m] = 3.118302
           Channel(search) = 137.450   Channel(meas.) = 137.588   Channel diff. = -.1381E+00

Iter.#  1  EXejec[MeV] = -0.0086    EXres[MeV] =  0.0000
           Eejec1[MeV] =  342.047   Eejec2[MeV] =  341.926   Eejec[MeV] =  341.987
           P[MeV/c] =  2422.205     Brho[Tm] = 2.693202      rho[m] = 3.118345
           Channel(search) = 137.588   Channel(meas.) = 137.588   Channel diff. = -.1027E-04

--------------------------------------------------------------------------------------------------------------
    Isotope  EX energy   Eejec      Momentum     Brho       Bfield      rho     Position(sear.)   Poition(measr.)
 #             [MeV]     [MeV]      [MeV/c]      [Tm]       [Tesla]    [meter]    [channel]         [channel]
--------------------------------------------------------------------------------------------------------------
 1    9LI     -0.0086   341.9868   2422.205   2.693202   0.863664   3.118345    137.588           137.588
--------------------------------------------------------------------------------------------------------------
```

```
RELMASS ver.1.0 :   Example file : Two calibration points and one mass measurement.               << OUTPUT DATA >>

Output data file : relmass.out

**** Results of Q-value search ****

----------------------------------------------------------------------------------------------------------------------
                                     | Excitation energy |            1986 MASSPACK*            |         Present results*
                                     |                   |                                      |
 #          Reaction         Isotope |  Initial Searched |    Mass    Mass excess   Q-value     |   Mass    Mass excess  Q-value
                            searched |   [MeV]    [MeV]  | [a.m.u.]     [MeV]       [MeV]      | [a.m.u.]     [MeV]      [MeV]
----------------------------------------------------------------------------------------------------------------------
 1  14C ( 11B ,  9LI) 16O      9LI   |  0.0000   -0.0086 |  9.026789   24.95410    -8.52896    |  9.026780   24.94552   -8.52037
----------------------------------------------------------------------------------------------------------------------
* Values are shown for ground state.


*** Error analysis tools ****

----------------------------------------------------------------------------------------------------------------------
 #          Reaction         Isotope |    dQ/dEproj     dQ/dAngle    dQ/dChannel    dQ/dThick1    dQ/dThick2    dQ/dThick3
                            searched |    [MeV/MeV]    [MeV/deg.]     [MeV/ch.]   [MeV/mg/cm2]  [MeV/mg/cm2]  [MeV/mg/cm2]
----------------------------------------------------------------------------------------------------------------------
 1  14C ( 11B ,  9LI) 16O      9LI   |   0.9258E+00   -.8963E-01    -.6216E-01    0.0000E+00    -.2411E+00    0.0000E+00
                                     |   (-.11E-06)   (-.30E-03)    (-.17E-03)    (0.00E+00)    (-.12E-04)    (0.00E+00)
                                     |   0.9261E+00   0.8963E-01    -.6216E-01    0.0000E+00    -.2411E+00    0.0000E+00
                                     |   (-.17E-06)   (-.30E-03)    (-.39E-05)    (0.00E+00)    (-.88E-05)    (0.00E+00)
----------------------------------------------------------------------------------------------------------------------

# 1  d(Eproj) -  0.1000E+00 %  d(Angle) -  0.1000E+01 deg.  d(channel) - 0.1000E+01 ch.
     d(Thick1) - 0.0000E+00 %  d(Thick2) - 0.1000E+01 %     d(Thick3) -  0.0000E+00 %
```

Appendix B

Calculations of Neutron Resonance Line Shapes

To analyze the data from the $^{11}B(^{7}Li,^{8}B)^{10}Li$ reaction, resonance scattering calculations were performed to estimate the widths and line shapes of the n–^{9}Li resonances. The Schrödinger equation was solved numerically for a single neutron moving in the potential created by a ^{9}Li nucleus. The potential consisted of, in addition to Coulomb and centrifugal terms, a Woods–Saxon term

$$V_{\mathrm{WS}}(r) = \frac{-V_0}{1 + exp(r - r_0 A^{1/3})/a} = -V_0 f(r) \tag{B.1}$$

and a Thomas spin–orbit term

$$V_{\mathrm{SO}}(r) = W_0 \sigma \cdot \ell \frac{1}{r}\frac{df}{dr}. \tag{B.2}$$

The parameters r_0, a, and W_0 were taken to be 1.25 fm, 0.65 fm and 15.64 MeV fm^2 respectively [Brow 92]. The results of the line shape calculations were insensitive to small variations of these parameters. Holding V_0 constant, the wavefunction $\Psi_{\mathrm{E}}(r)$ was found for the neutron at a given kinetic energy E. To estimate the line shapes for the neutron decay of ^{10}Li, the wavefunction was normalized inside the nucleus [Sher 85]

$$S(E) = \int_0^{\infty} \Psi_{\mathrm{E}}^2(r) \frac{dV_{\mathrm{WS}}}{dr} r^2 dr. \tag{B.3}$$

The behavior of S as a function of the neutron kinetic energy E provided the single–particle resonance line shape. The energy at which S reached a maximum, that is, the resonance energy, varied with the value chosen for V_0. By mapping $S(E)$ for different values of V_0 it was possible to explore the behavior of the line shapes, and in particular the widths, as a function of resonance energy for $2s\frac{1}{2}$ and $1p\frac{1}{2}$ neutrons.

$2s\frac{1}{2}$ line shapes

The function $S(E)$ for several $2s\frac{1}{2}$ neutron states is shown in the top part of Figure B.1. Depicted are states with peak energies at 0, 30, 150, and 300 keV. The widths of these states increases rapidly with peak energy. For states with energy above 100 keV, the width is so large that the state could not be detected above background. For states below 100 keV, the line shapes are narrow enough to be dominated by the resolution of the spectrometer, and were approximated in the fitting procedures by a Lorentzian with Γ = 230 keV.

$1p\frac{1}{2}$ line shapes

The line shapes for several $1p\frac{1}{2}$ neutron states are shown in the bottom part of FIgure B.1. Shown here are states with peak energies at 100, 200, 500, and 700 keV. Although the widths of these states also increases with peak energy, the effect is much less dramatic than that described above. For p–waves below 100 keV peak energy, the line shape was also approximated by a Lorentzian in the fitting procedures. For p–waves with peak energy above 100 keV, the line shapes were parametrized for inclusion in the fitting procedures. The parametrization was found by trial–and–error by examining the shape of the function $S(E)$. On the low–energy side of the peak, $S(E)$ exhibits the rapid decay of a Gaussian curve. On the high–energy side of the peak, the function appears to have two decay components: a Lorentzian–like decay

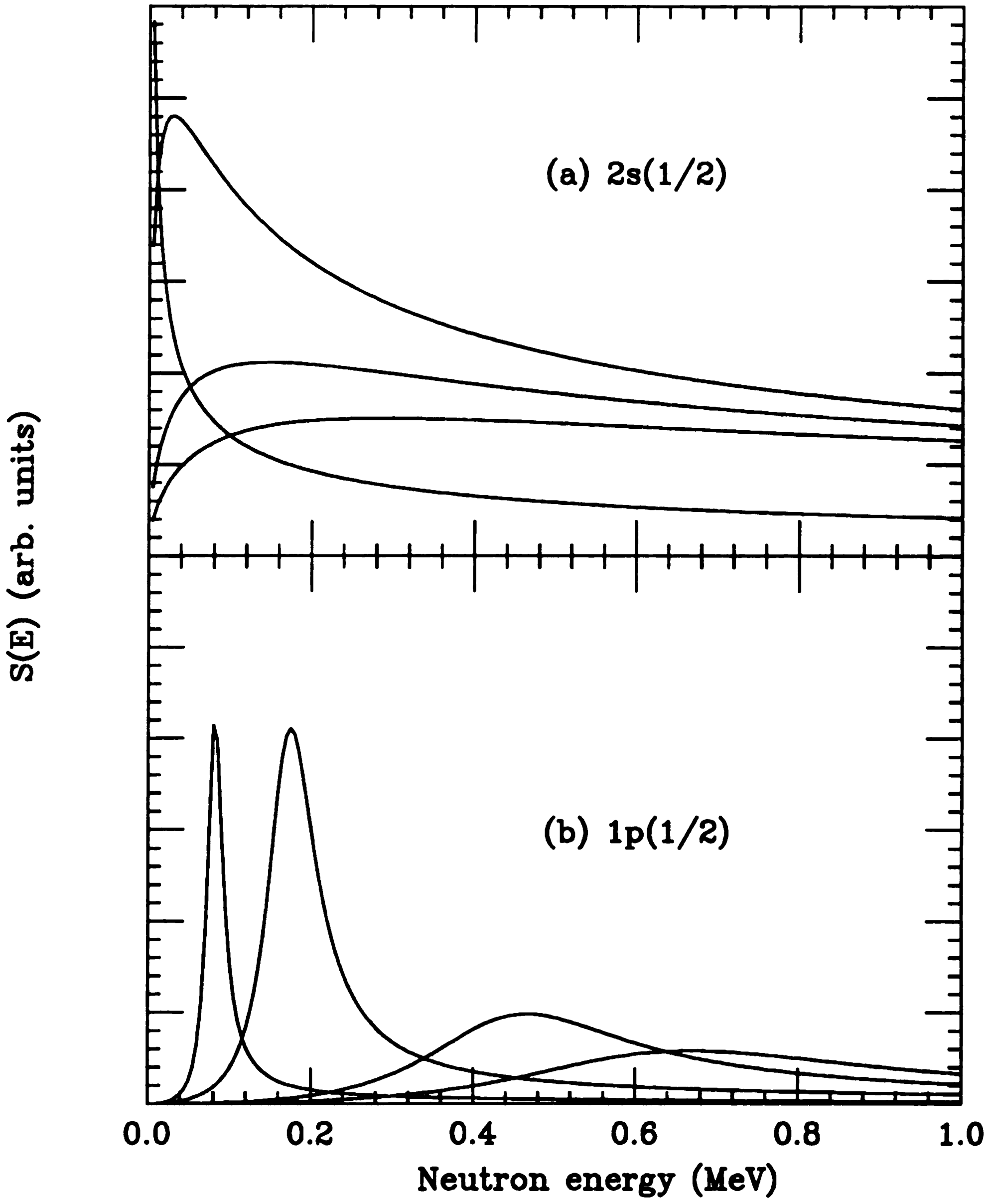

Figure B.1: Calculated line shapes for $2s\frac{1}{2}$ and $1p\frac{1}{2}$ n–^{9}Li states at several energies. The top part of the figure contains line shapes for $2s\frac{1}{2}$ states with peak energies of 0, 30, 150, and 300 keV. The bottom part of the figure contains line shapes for $1p\frac{1}{2}$ states with peak energies of 100, 200, 500, and 700 keV. In both frames, the line shape for the lowest energy state was reduced by approximately 75% to fit on the same scale as the other states.

and a very long, almost constant, tail. With these considerations in mind, the final parametrization used for $1p\frac{1}{2}$ states above 100 keV peak energy was

$$S(E) = \begin{cases} N \exp\left[-\frac{(E-E_{\text{res}})^2}{2\Gamma_{\text{low}}^2}\right] & \text{if } E < E_{\text{res}} \\ N\left[R + (1-R)\frac{\Gamma_{\text{high}}^2}{A(E-E_{\text{res}})^2+\Gamma_{\text{high}}^2}\right] & \text{if } E > E_{\text{res}}. \end{cases} \tag{B.4}$$

This model was fitted to the calculated line shapes at several resonance energies and in this way, the four parameters Γ_{low}, Γ_{high}, R, and A were determined as functions of the resonance energy E_{res}. An example of this model fitted to a 500 keV resonance is shown in Figure B.2. The resolution of the S320, a Lorentzian with a full-width of 230 keV, was incorporated in the model by adding the S320 half-width in quadrature with the model widths, Γ_{low} and Γ_{high}. The final parametrization that was used in the fitting procedure had two free parameters, the resonance energy E_{res} and the total amplitude N.

The computer code RESCALC

The resonance calculations described above involved the numerical solution to the Schrödinger equation for a particle in a potential well. The computer code RESCALC, the C source code for which is listed in Table B.1 at the end of this appendix, was written, with helpful suggestions from Alex Brown and George Bertsch, to accomplish this. Instructions for compiling and linking the code at the NSCL are given in the program comments at the beginning of the listing.

The user is first asked to choose between a Woods–Saxon or a Gaussian form for the nuclear potential, and to specify the appropriate parameters (e.g. depth and width/diffuseness) for the chosen well. The user is then prompted for the depth of a Thomas spin–orbit term, the form for which is given above. Next, the user is asked for the spin, orbital, and total angular momenta for the system and the masses and

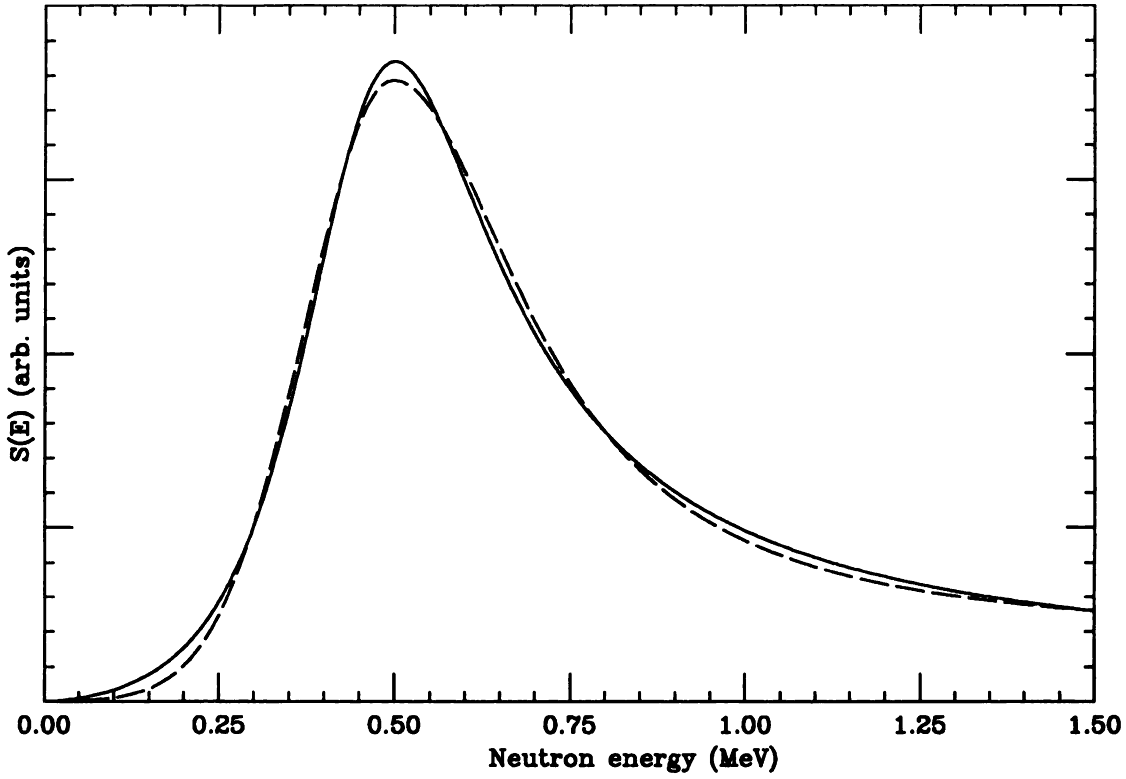

Figure B.2: Six-parameter model fitted to calculated line shape for a $1p\frac{1}{2}$ neutron state at 500 keV resonance energy. Similar fits were made to line shapes at other energies; four of the six parameters were thus determined as functions of the resonance energy.

Table B.1: The listing of the RESCALC C source code is given on the nine pages at the end of this appendix. The operation of the program is discussed in the text as well as in the program comments.

charges of the target and projectile. The program then calculates several observables over a range of projectile energies, specified by the user, and writes the calculated data to the file `RESONANC.OUT`.

At each projectile energy, the Schrödinger equation is solved, using the Numerov algorithm [Koon 86], to yield the wavefunction $\Psi_{\mathrm{E}}(r)$, from which the function $S(E)$ is calculated. The scattering phase shift δ is found by solving for the wavefunction without the nuclear and spin–orbit terms in the potential and comparing the phases of the wavefunctions at large radii. The values then written to the output file are the scattering energy E, the cross–section–related quantities $\sin^2(\delta)$ and $\frac{\sin^2(\delta)}{E}$, and the function $S(E)$. The code is very thoroughly commented and is easily modified to calculate other observables from the wavefunction, potentials, and local wave number, all of which are stored in global arrays in the program.

```
/**************************************************************************
***************************************************************************
***************************************************************************

TO COMPILE/LINK THIS PROGRAM ON A VAX AT NSCL:
   cc rescalc.c
   link rescalc,sys$library:crtlib/opt


This program solves the radial Schrodinger equation:

        d2u     ( V(r) - E )
        ---  =  ------------ * u(r)  =  k2(r) * u(r)
        dx2       hbar2/2M

where
                      |-                -|
        V(r)  =   C * |  Vws(r) + Vso(r)  | + Vcentrif + Vcoul
                      |-                -|

The main engine of the program consists of the functions arranged in
the hierarchy diagrammed below:

        Calc_Observbls _____ Make_Well
                         |__ Solve_Schrodinger _____ Diff_eq

Calc_Observbls calls Make_Well which packs an array with V(r) using several
global parameters for the either the Woods-Saxon form or a Gaussian form
for the nuclear potential.  It then Calls Solve_Schrodinger
which uses V(r) to find the radial wavefunction u(r).  Solve_Schrodinger
uses the function Diff_eq to do the mathematical nitty-gritty of solving
the differential equation.  Once u(r) is found, Solve_Schrodinger performs
the appropriate normalization, and looks for bound states if applicable.
Calc_Observbls, if necessary, calls Make_Well with free space parameters
and calls Solve_Schrodinger with the new well.  This is so Calc_Observbls
can find the scattering phase shift.

***************************************************************************
***************************************************************************
***************************************************************************

  INCLUDE FUNCTIONS BELOW

***************************************************************************
***************************************************************************
**************************************************************************/

#include <math.h>
#include "sys$admin:[young.cstuff.my_std]bmymath.h"

/**************************************************************************
***************************************************************************
***************************************************************************

  GLOBAL VARIABLES AND PERTINENT DEFINES BELOW

***************************************************************************
***************************************************************************
**************************************************************************/

#define MAX_ARRAY_SIZE 2010

RealType s_proj2,l,j2;          /* 2*s,l, 2*j for incoming particle */
RealType at,zt,ap,zp;           /* mass and charge of targ and projectile */
RealType Vnorm, adiff, R0;      /* Nuclear potential parameters */
RealType Vspino;                /* Spin orbit parameter  */
```

```
int      potential_type;      /* nuke potential selector */
RealType *u;                  /* radial wavefunction */
RealType *V;                  /* Total radial potential */
RealType *dVws;               /* Radial derivative of nulear potential */
RealType *K2;                 /* Local wave number squared */
RealType *EB;                 /* Array of bound state energies */

int NMax;                  /* Number of radial steps in mesh and */
RealType delr;           /* the size of each step.            */

RealType hbsd2m;         /* h-bar squared divided by 2 * reduced mass */

/***************************************************************************
****************************************************************************
****************************************************************************

  FUNCTION DECLARATIONS BELOW

****************************************************************************
****************************************************************************
****************************************************************************/

void Initialize_Global_Variables( void );

void Calc_Observbls( RealType E, RealType *dphi,
                     int *nodes, RealType *SurfParam );

void Make_Well( RealType nuclear_pot_const );

void Solve_Schrodinger(  RealType E, int nsep, RealType *phi );

void Diff_eq(  int nfrom,  int nto,  int nstep,
               RealType *uu,   RealType *duu,  RealType *intu2 );

void Kill_Global_Variables( void );

/***************************************************************************
****************************************************************************
****************************************************************************

  FUNCTION DEFINITIONS BELOW

****************************************************************************
****************************************************************************
***************************************************************************/
#include "sys$admin:[young.cstuff.my_std]bmymath.i"

int main( void )
{
   RealType E,dphi,surf;
   int nodes;
   RealType Estart,Estop,delE;
   FILE *outfile;

   Initialize_Global_Variables();
/*

The lines contained in this comment are for the original version of the
program, which asks for a single energy and writes the observables to
the screen.

  Start:
             EB[0] = 0.0000;
             puts("\nEnter E (E < 0 quits program).");
             scanf("%lf",&E);
          if (E < 0.0000) goto End;
```

```
          Calc_Observbls(E,&dphi,&nodes,&surf);
     printf("sin^2(d)   = %lf\n",sin(dphi)*sin(dphi));
     printf("sin^2(d)/E = %lf\n",sin(dphi)*sin(dphi)/E);
     printf("S          = %lf\n",surf);
          goto Start;
  End:

The lines below are for the "eloop" version of the program, which
asks for a max,min,delta values for E and then loops over the
energy values, writing the ovservables out to a file.

*/
   if((outfile=fopen("resonanc.out","w"))==NULL)
   {
      fprintf(stderr,"Cannot open output file.\n");
      exit(1);
   }
   puts("Enter Estart, Estop, delE -- (MeV) separated by commas please.");
   scanf( "%lf, %lf, %lf", &Estart, &Estop, &delE);
   for ( E = Estart; E <= Estop; E += delE )
   {
      Calc_Observbls(E,&dphi,&nodes,&surf);
      fprintf( outfile, "%lf  %lf  %lf  %lf\n",  E,
                                                 sin(dphi)*sin(dphi),
                                                 sin(dphi)*sin(dphi)/E,
                                                 surf );
   }
   fclose( outfile );

   Kill_Global_Variables();
   return 0;
}
/*%%%%%%%%%%%%%%%%%%%%*/
/*%%%%%%%%%%%%%%%%%%%%*/
void Initialize_Global_Variables( void )
{
   RealType red_mass;

   u = vector(0,MAX_ARRAY_SIZE);
   V = vector(0,MAX_ARRAY_SIZE);
   dVws = vector(0,MAX_ARRAY_SIZE);
   K2 = vector(0,MAX_ARRAY_SIZE);
   EB = vector(0,MAX_ARRAY_SIZE);

   puts("\n");
   puts("\n");
   puts("\n");
   puts("\n");
   puts("\n");
NFG_Pot_Type:
   puts("\nSelect nuclear potential type:");
   puts("Enter 1 for Gaussian well, 2 for Woods-Saxon well.");
   scanf( "%d", &potential_type );
   if( potential_type == 1 )
   {
      puts("\nGaussian nuclear potential." );
      puts("\n  Vnuke = -V0 * exp( -(r/a)^2 )" );
      puts("\n  R = R0 * atarg^0.33" );
   }
   else if ( potential_type == 2 )
   {
      puts("\nWoods-Saxon nuclear potential.");
      puts("\n  Vnuke = -V0 * exp( (r - R)/a )" );
      puts("\n  R = R0 * atarg^0.33" );
   }
   else
```

```
   {
      goto NFG_Pot_Type;
   }
   puts("\nNuclear potential parameters:");
   puts("Enter V0, a, R0 -- (MeV, fm, fm) separated by commas please.");
   scanf( "%lf, %lf, %lf", &Vnorm, &adiff, &R0);
   puts("\nSpin-orbit potential parameter:");
   puts("\n  Vnuke = -V0 * f(r)" );
   puts("\n  Vso   =  W0 * (df/dr)*(1/r)*(L.S) " );
   puts("\nEnter W0 (MeV).");
   scanf( "%lf", &Vspino );
   puts("\nV0, a, R0, W0 = ");
   printf( "%lf %lf %lf %lf\n", Vnorm, adiff, R0, Vspino );
   puts("\n");
   puts("Angular momentum parameters:");
   puts("NOTE: I dont check for legal combinations of s,l,j.");
   puts("      Thats up to you.");
   puts("Enter 2s_projectile, l, 2j -- separated by commas please.");
   scanf( "%lf, %lf, %lf", &s_proj2, &l, &j2 );
   puts("\n2s_projectile, l, 2j = ");
   printf( "%lf %lf %lf\n", s_proj2, l, j2 );
   puts("\n");
   puts("Enter at, zt, ap, zp -- separated by commas please.");
   scanf( "%lf, %lf, %lf, %lf", &at, &zt, &ap, &zp );
   puts("\nat, zt, ap, zp  = ");
   printf( "%lf %lf %lf %lf\n", at, zt, ap, zp );
   puts("\n");
   puts("\n");

   delr = 0.1;

   red_mass = 931.49432 * at * ap / ( at + ap );
   hbsd2m = (197.33) * (197.33) / ( 2.000 * red_mass );

   return;
}
/*%%%%%%%%%%%%%%%%%%%%*/
/*%%%%%%%%%%%%%%%%%%%%*/
void Kill_Global_Variables( void )
{
   free_vector(u,0,MAX_ARRAY_SIZE);
   free_vector(V,0,MAX_ARRAY_SIZE);
   free_vector(dVws,0,MAX_ARRAY_SIZE);
   free_vector(K2,0,MAX_ARRAY_SIZE);
   free_vector(EB,0,MAX_ARRAY_SIZE);

   return;
}
/*%%%%%%%%%%%%%%%%%%%%*/
/*%%%%%%%%%%%%%%%%%%%%*/
void Calc_Observbls( RealType E, RealType *dphi,
                     int *nodes, RealType *SurfParam )
/*
Input parameters:   E  ---  Kinetic energy of projectile

Output parameters:  dphi --- Phase shift of wavefunction at max r
                             with nuclear potential with respect to
                             wavefunction without nuclear potential.
                    nodes -  Number of nodes in wavefunction.
                    SurfParam - Surface parameter defined as

                                      |   r=OO           |2
                                      |  /       dV      |
                                  S = |  |  u(r) -- dr   |
                                      |  /       dr      |
                                      |   r=0            |
```

```
                                see R.Sherr and G.Bertsch
                                    Phys Rev C 32 1809 (1985)
                                equation 2.
Notes:

This function accepts the incident energy E, sets up (with Make_Well) and
solves (with Solve_Schrodinger) the Schrodinger equation and then calcul-
ates some observables with the results of this solution.
*/
{
   RealType phi_with_pot, phi_without_pot;
   int nsep,i;
   FILE *outfile;

   NMax = 2000;                     /* Default: resonance, need lotta    */
   nsep = NMax;                     /* mesh points                       */

   Make_Well( 1.000 );              /* Set up well with nuke potential   */

   if( E < V[NMax])                 /* If bound state, we dont need many */
   {                                /* mesh points.  See notes on Solve_ */
      NMax = 200;                   /* Schrodinger for info on nsep      */
      nsep = ( R0/delr ) * pow(at,0.33333333);
   }

   Solve_Schrodinger( E, nsep, &phi_with_pot );

   *nodes = 0;                      /* Calculate nodes and surface param */
   *SurfParam = 0.0;
   for( i=1; i<=100; i++ )
   {
      if( u[i]*u[i+1] < 0.000 )  (*nodes)++;
      *SurfParam += u[i]*u[i]*dVws[i];
   }

/* BMYoung 11/24/92 Write potential and wavefunc to file
         if(!(outfile=fopen("resout.dat","w")))
         {
            printf("cannot open output file.\n");
            exit(1);
         }
         for(i=0;i<=NMax;i++)
         {
            fprintf(outfile,"%lf  %lf  %lf\n",(i*delr),V[i],u[i]);
         }
         fclose(outfile);
BMYoung 11/24/92 */


   *dphi = 0.000;
   if( E >= V[NMax] )               /* If resonance, we need wavefunc    */
   {                                /* with no nuke potential.           */
      Make_Well( 0.000 );
      Solve_Schrodinger( E, nsep, &phi_without_pot );
      *dphi = phi_with_pot - phi_without_pot;
   }

/*  PUT IN SOME KIND OF WARNING ABOUT IF E>0 AND E<V[NMAX] INCREASE NMAX */
   return;
}
/*%%%%%%%%%%%%%%%%%%%%%*/
/*%%%%%%%%%%%%%%%%%%%%%*/
void Make_Well( RealType nuclear_pot_const )
/*
Packs the array V[] with the total radial potential.
Packs the array dVws[] with the derivative of the nuclear potential.
```

```
*/
{
   RealType ZZ, Rws, V0ws, r, Vcentrif, Vcoul, y, ey, fws, Vws;
   RealType l_factor,Vso;
   int i;

   ZZ = zt*zp;
   Rws = R0 * pow(at,0.33333333);

   for( i=1; i<=NMax; i++ )
   {
      r = delr * i;

      Vcentrif = l*(l+1.0)*hbsd2m/(r*r);


      if( r < Rws )
      {
         Vcoul = ZZ*1.44*(1.5-0.5*r*r/(Rws*Rws))/Rws;
      }
      else
      {
         Vcoul = ZZ*1.44/r;
      }


/*      if( j2 > (2.0*l) )
      {
         l_factor = l;
      }
      else if ( j2 == (2.0*l) )
      {
         l_factor = 0.000;
      }
      else
      {
         l_factor = -(l+1.000);
      }
*/
/*  L.S = 0.5 * ( j(j+1) - l(l+1) - s(s+1) ) */

      l_factor = 0.5 * (  j2*(j2+2.0)/4.0
                        - l*(l+1)
                        - s_proj2*(s_proj2+2.0)/4.0   );

      if ( potential_type == 1 )                /* Gaussian well */
      {
         y   = r/adiff;
         ey  = exp(-y*y);
         Vws = -Vnorm*ey;

         Vso = -(Vspino*2.0/(adiff*adiff))*l_factor*ey;

         dVws[i] = 2.0*Vnorm*r*ey/(adiff*adiff);
      }
      else if ( potential_type == 2 )           /* WS well       */
      {
         y = (r-Rws)/adiff;
         if( y < 13.82 )      /* ie if exp(y) < 1e6 */
         {
            ey  = exp(y);
                fws = 1.0 / ( 1.0 + ey );
         }
         else
         {
            ey  = 999999.;
```

```
                fws = 0.000000;
            }
            Vws = -Vnorm*fws;

            Vso = -Vspino*fws*fws*ey*l_factor/(r*adiff);

            dVws[i] = Vnorm*fws*fws*ey/adiff;
        }

        V[i] = nuclear_pot_const*(Vws + Vso) + Vcentrif + Vcoul;
    }
    return;
}
/*%%%%%%%%%%%%%%%%%%%%*/
/*%%%%%%%%%%%%%%%%%%%%*/
void Solve_Schrodinger(  RealType E, int nsep, RealType *phi )
/*
Input parameters:   E  ---  Kinetic energy of projectile
                    nsep -  see explanation below in Notes

Output parameters:  phi --- Phase of wavefunction at max r

Notes:

Solves the Schrodinger equation using two different methods.
If the energy E is greater than the potential (global array V[]) at
NMax, then Solve_Schrodinger calls Diff_eq to find the wavefunction from
r=delr to r=delr*NMax.  The phase of the wavefunction is determined and
the wavefunction is normalized.
If the energy E is less than the potential at NMax, Solve_Schrodinger looks
for a bound state near the given energy.  First of all, we cant start at
r~0 and work our way out.  The wave function must go to 0 at r=0 AND at
r=infinity.  So, the routine defines the wavefunction at both extremes
and works its way out from r~0 and in from r~infinity towards nsep which
is arbitrarily defined outside the routine.  Once this is done, the
wavefunctions are compared at nsep and a better guess is made on a bound state.
This calculation is repeated until
1) the energy goes above 0, 2) the matchup of the wavefunctions agrees to
within a specified tolerance, 3) more than 20 tries are made.
*/
{
   RealType ul,dul,inul,u2,du2,inu2;
   RealType k,t,x,sum;
   int i,num_bound_guesses, searched_for_resonance;

   num_bound_guesses = 0;                /* Initialize a few things */
   x = 0.000000;
   searched_for_resonance = 0;

   do
   {
      for( i=1; i<=NMax; i++ )           /* Pack K2[] for the current E */
      {
         K2[i] = (-E + V[i] )*delr*delr/hbsd2m;
      }
      u[1] = 0.00001;                    /* Define u[] near the origin  */
      u[2] = u[1] * pow( 2.0, (l+1.0) );

      if( E > V[ NMax ] )                /* If resonance...             */
      {
         Diff_eq( 1, NMax, 1, &ul, &dul, &inul );              /* Get u[]  */
         k = sqrt( -K2[ NMax ] );                   /* Get wavenumber, phi, */
         *phi = atan( ul * k / dul );               /* and normalization    */
         t = sqrt( ul*ul + (dul*dul)/(k*k) ) * sqrt( k/delr );
         searched_for_resonance = 1;
      }
```

```
      else                                     /* If bound state...           */
      {
         Diff_eq( 1, nsep, 1, &u1, &du1, &inu1 );  /* Get u[] -- 0 to nsep */
         u[ NMax ] = 0.000000;                    /* Get u[] -- 00 to nsqp */
         u[ NMax - 1 ] = 0.00001;
         Diff_eq( NMax, nsep, -1, &u2, &du2, &inu2 );
/*
Match up the two wavefunctions u[], as per G. Bertsch's suggestion, and
guess the bound state energy.
*/
         x = u1*u2*(du1*u2-du2*u1)/(delr*delr*(inu1*u2*u2+inu2*u1*u1));
         E += x*hbsd2m;
         EB[0] = E;                         /*   The latest b.s. energy guess   */
                                            /*   is stored in EB[0]             */
         for( i=1; i<=(nsep-1); i++ )
         {
            u[i] = u[i] * u2;
         }
         for( i=nsep; i<=NMax; i++ )
         {
            u[i] = u[i] * u1;
         }
         sum = 0.000000;
         for( i=1; i<=NMax; i++ )
         {
            sum += u[i] * u[i];
         }
         t = sqrt( sum * delr );            /* Find the normalization */
         num_bound_guesses++;
      }
   }while(     ( (fabs(x) > 0.00001) || (num_bound_guesses <= 20) )
           && (!searched_for_resonance)                              );

   for( i=1; i<=NMax; i++ )                 /* Normalize the wavefunciton */
   {
      u[i] = u[i] / t;
   }
   return;
}
/*%%%%%%%%%%%%%%%%%%%%%%*/
/*%%%%%%%%%%%%%%%%%%%%%%*/
void Diff_eq(  int nfrom,   int nto,   int nstep,
               RealType *uu,   RealType *duu,   RealType *intu2 )
/*
Input parameters:  nfrom,nto,nstep --- array index limits and step size
                                       over which to solve the differential
                                       equation.
Output parameters:   uu        ---     value of wavefunction u at array
                                       index nto
                     duu       ---     value of du/dr at array index nto
                     intu2     ---     integral of u*u from nfrom to nto

Notes:

Uses the global arrays u[] and K2[] and solves the differential equation

   d2u/dr2 = u * k2

from array elements nfrom to nto stepwise in steps nstep.  This function
also calculates the integral of u*u over the requested interval and returns
it as *intu2.  Also, the values of u and du/dr at location nto are returned
as *uu and *duu respectively.  A brief mathematical note is in order here.
The algorithm used to solve the differential equation is the Numerov algorithm.
A full-blown description is given in S. E. Koonin, Computational Physics,
Addison-Wesley 1986, p50ff.  The formula used is presented below.
```

```
NUMEROV ALGORITHM

   d2u/dr2 = u * k2 --- let h be the width of one mesh point.  The formula
                        used is

   u(r+2h) - 2u(r+h) + u(r)      5
   ------------------------  =  -- * u(r+2h) * K2(r+2h) +
             h*h                60

                                 5
                                 - * u(r+h) * K2(r+h) +
                                 6

                                 5
                                -- * u(r) * K2(r)
                                60

   This is solved for u(r+2h), and since we know K2() everywhere, we can use
   u(r) and u(r+h) to step our way over r.

ALSO USED

   du |         4 * ( u(r+h) - u(r) ) - ( u(r+h) - u(r-h) )
   -- |     =   -------------------------------------------
   dr |r+h                         2h

*/
{
   RealType u1,u2,k2_1,k2_2,k2_3;
   int n;

   *intu2 = 0.0;              /* Zero the integral */
   u1 = u[nfrom];             /* Get u(r) and K2(r) */
   k2_1 = K2[nfrom];

   n = nfrom + nstep;         /* Get u(r+h) and K2(r+h) */
   u2 = u[n];
   k2_2 = K2[n];

   n += nstep;

   while( n <= nto )
   {                          /* Get K2(r+2h) and find u(r+2h) */
      k2_3 = K2[n];
      u[n] = ( 2.0*u2 - u1 + 0.83333333*u2*k2_2 + 0.083333333*u1*k2_1 ) /
             ( 1.0 - 0.083333333*k2_3 );

      u1 = u2;                /* Get ready to increment u and k2 by h */
      k2_1 = k2_2;            /* and update the integral sum.         */
      u2 = u[n];
      k2_2 = k2_3;
      *intu2 += u2*u2;
      n += nstep;
   }
                             /* We are at the end of the interval, find */
   n -= (3.0 * nstep);       /* du/dr and return it and u.              */
   *duu = ( 4.0*(u2-u1) - (u2-u[n]) ) / ( 2.0*nstep );
   *uu = u2;
   return;
}
/*%%%%%%%%%%%%%%%%%%%%%*/
```

Appendix C

Maximum Likelihood Fitting Procedure

To determine quantitative details of the low–lying structure of ^{10}Li from the data collected from the ^{11}B(^{7}Li,^{8}B)^{10}Li reaction, a parametrized theoretical model, described in Chapter 4 and Appendix B, was fitted to the data. However, since the statistics in the collected spectrum are low, the standard least–squares fitting technique was inapplicable. This is due to the fact that the least–squares technique relies on the assumption that the measured number of events in a given channel has a Gaussian distribution about some "true" value (hopefully the value of the parametrized model) determined by nature. In actuality, the measured number of counting events in a given channel has a Poisson distribution about the "true" value. Only for a large number of events per channel (i.e. more than 20), where the Poisson distribution approaches the Gaussian distribution, is the least–squares technique valid.

A general maximum-likelihood fitting technique, a familiar example of which is the least–squares method, seeks to fit a model function $f(x, a)$ to the data x by adjusting the model parameters a to maximize the probability of obtaining the given data set. Typically, a figure of merit is defined as the negative natural logarithm of this probability. More convenient than (but equivalent to) maximizing the probability is minimizing the figure of merit. In the example of the least-squares method, the figure of merit is the χ^2 statistic [Pres 92]. With this prescription, if the data in a given channel, (x_i, y_i), have a Poisson distribution about a model $f(x_i, a)$ with parameters a, then the total probability of obtaining the measured data set is

$$P = \prod_i \frac{\{f(x_i, a)\}^{y_i}}{y_i!} e^{-f(x_i,a)}, \tag{C.1}$$

and figure of merit is

$$\mathcal{L} = -\ln P = \sum_i \{f(x_i, a) + \ln y_i! - y_i \ln f(x_i, a)\}. \tag{C.2}$$

The $\mathcal{L}$ statistic is similar to χ^2 in that it is a measure of the goodness-of-fit, and that its minimization over the space of model parameters is the objective of the fitting procedure. However, its analytical behavior is not as well known as that of the chi-squared statistic. More specifically, using $\mathcal{L}$ it is possible to compare fits with two different models and to determine whether one fit is better than the other; but it is not possible to assign to a given value of $\mathcal{L}$ a probability analogous to the chi-square distribution as described in [Pres 92]. The statistical uncertainties on the model parameters can be determined, as described in Bevington [Bevi 69], from

$$\sigma_{a_i}^2 = \frac{2}{\partial^2 \mathcal{L} / \partial a_i^2}. \tag{C.3}$$

The computer code FIT_SPEC

The above maximum likelihood technique is carried out with the program FIT_SPEC, the FORTRAN source code for which is listed in Table C.1 at the end of this appendix. The program will fit an arbitrary function, specified in the user-modifiable function `FITFUNC`, to a set of data points read in from a file, either in (x,y) or (x,y,σ_y) format. The program will perform a maximum-likelihood fit assuming one of four statistical distributions of the data about the functional form: a Poisson distribution, or a Gaussian distribution with the uncertainty σ_y in each data point assumed to be unity, $\sqrt{y}$, or the value of σ_y read in from the file. In each case, the fitting is performed by numerically minimizing a figure of merit over the space of model parameters utilizing the subroutine **AMOEBA** from [Pres 86]. **AMOEBA** iteratively searches over the space of model parameters until either a maximum number (500) of iterations is reached or until successive changes in the figure of merit become smaller than a specified tolerance.

The program is designed to be user-modifiable; detailed instructions for such modification are given in the program comments at the beginning of the code listing. The chief modifications involve changing the function which is fitted to the data. This function **FITFUNC** can be easily located in the code by searching for the character string **BMYFITFUNC**. The function accepts as input the value at which the function is to be evaluated, and a one–dimensional array containing the values of the model parameters. It is important that the user remember the order in which the parameters are stored in the array, as the user is prompted, during operation, for initial guesses at their values. In addition to changing the function, the user must also specify the number of model parameters in the function. This is accomplished by changing the value of the parameter **NPARAMS**. The declarations for this parameter can be located in the code by searching for the character string **BMYNPARAMS**. Other parameters which the user might wish to modify are **MAXDATCHAN**, which specifies the maximum number of data points allowable, and **TOL**, which specifies the relative tolerance on successive evaluations of the figure of merit necessary for **AMOEBA** to terminate.

Upon running the program, the user is first prompted for format ((x,y) or (x,y,σ_y)) and name of the data file. If the file is successfully read, the program displays the filename, number of data points (channels), and the sum of y values in the file.

The user is prompted for the minimum and maximum x values over which the fit should be made, and the assumed statistical distribution (Poisson distribution or one of three Gaussian forms) of the data points about the model. The minimization routine requires a set of initial guesses at the model parameters. More specifically, if the model has n parameters, a given set of parameter values represents a vector in the n-dimensional space of model parameters; initially, the routine requires $n + 1$ such vectors. The program allows for two ways for the total $n(n + 1)$ initial values to be supplied. They can all be explicitly specified, or the user can specify one initial guess and a percent range over which the program will randomly pick other guesses. The latter option, in addition to being less time consuming, allows the user to hold any parameter constant for the fitting by specifying a 0% range. Once the initial guesses are supplied, the program displays a list of values of the figure of merit corresponding to each of the $n+1$ initial vectors, and enters the minimization routine. Depending on such factors as the number of parameters, complexity of the model, and required convergence tolerance for **AMOEBA**, minimization typically requires less than 30 seconds. Once convergence is reached, the program has in memory a group of $n+1$ parameter sets, the figures of merit for which all lie within the specified tolerance of each other. The user is asked for the name of an output file and a comment string to go in the output file. This file contains the results of the fitting procedure: the number of iterations **AMOEBA** required for convergence, the $n + 1$ final values of each parameter as well as their averages and uncertainties, and the value of the figure of merit evaluated at the average parameter values. Finally, the user can instruct the program to write a file containing, in (x,y) format, the optimized model over a specified range of x values.

Table C.1: The listing of the FIT_SPEC FORTRAN source code is given on the fifteen pages at the end of this appendix. The operation of the program is discussed in the text as well as in the program comments.

```
C
      PROGRAM FIT_SPEC
C
C   This program reads a SARA file and fits an arbitrary function to the
C   data over a specified region of channels.  The fit uses a maximum likelihood
C   technique that assumes the data have a Poisson distribution about the
C   "true" functional form.
C
CCCCCCCC -- Subroutines:
C
C   READ_SPECTRUM -- Reads in a file of two types: (X,Y) or (X,Y,DY)
C                    The data are stuffed into the arrays DATA and DDATA.
C   GET_PARAMETERS - Allows the user to specify initial guesses for the para-
C                    meters of the fit.  There are two options:
C                       1) Specify one initial guess and a percent range over
C                       which the computer will generate random points to jump
C                       start the fit.
C                       2) Specify all initial guesses to jump start the fit.
C                    The initial guesses are packed into the 2d array P and the
C                    1d array Y contains the values of the probability funcition
C                    for each set of initial guesses.
C   AMOEBA --------- Perfoms a simplex minimization.  This is a Numerical
C                    Recipes function.  It takes P and Y and, by calling
C                    the probability function returns the 2d array P with
C                    values of the function parameters that are within a
C                    specified tolerance of each other.
C   ZLNPROB -------- Probability function.  Actually this is the negative
C                    natural log of the true probability function assuming
C                    the data have one of several distributions about the
C                    functional form (see below for more on this).  This
C                    function accepts
C                    a 1d array X, which contains the parameters to be used
C                    in evaluating the fit function.  The fit function is
C                    evaluated many times in a sum over the specified data
C                    points.
C                    The possible distributions of the data about the
C                    functional form are (as specified by STATMODE):
C
C                       1)  Poisson distribution
C                       2)  Gaussian distribution with sigma = 1
C                       3)  Gaussian distribution with sigma = (data)**1/2
C                       4)  Gaussian distribution with sigma = dy from file
C
C
C   FITFUNC -------- The actual function to be fit to the data.  This function
C                    accepts the 1d array X, which contains the parameters of
C                    the fit, and the data ordinate datax at which the function
C                    is to be evaluated.
C   WRITE_IT_OUT --- Writes the parameters and their averages to the screen.
C                    Will also, if specified,  write a file containing the fit
C                    function in (x,y) format.
C   GET_ERRORS ----- Finds errors on each parameter in the following manner.
C                    For each parameter we have found, using AMOEBA, several
C                    values all within a specified tolerance of each other.
C                    We take an average of the values AVG and define
C                    DEL = 0.01*AVG.  Bevington defines
C
C                  sigma**2 = 2/(d**2(lnprob)/d**2x)
C
CCCCCCCC -- A mathematical description:
C
C
C               If we have data points, labelled by i, called (xi, yi), and
C               we assume the data to have a Poisson distribution about some
C               functional form f(xi).  The probability of obtaining the
C               data set (xi,yi) is:
```

```
C
C                                             |¯        yi                ¯|
C                                             |  [f(xi)]                   |
C               Prob Func = L =  Product over | -----------  exp[ -f(xi) ] |
C                                     i       |    (yi)!                   |
C                                             |_                          _|
C
C
C                                 |¯                                    ¯|
C               -ln(L) = Sum over | f(xi) + ln[ (yi)! ] - yi*ln[ f(xi) ] |
C                            i    |_                                    _|
C
C
C               For more info see
C                     --Leo, Techniques for Nuclear and Particle Physics Experi-
C                       ments. Chapter 4.
C                     --P. R. Bevington, Data Reduction and Error Analysis for
C                       the Physical Sciences. Section 3-2.
C                     --W. H. Press, B. P. Flannery, S. A. Teukolsky, W. T.
C                       Vetterling, Numerical Recipes (FORTRAN edition).
C                       Section 10.4 and Chapter 14
C
CCCCCCCC -- A note about changing the fitting function and other important
C           parameters:
C
C   First of all, the function FITFUNC must be changed to accomodate the
C   necessary model.  This function can be quickly found by searching for
C   the character string BMYFITFUNC.
C
C   Also there are two PARAMETERS that may be changed.
C
C   1) MAXDATCHAN  This gives the largest size allowable for the data array.
C                  This PARAMETER appears at the beginning of the main function,
C                  in the subroutine READ_SPECTRUM, and in the function ZLNPROB.
C                  These declarations can be quickly found by searching for
C                  the character string BMYMAXDATCHAN.
C   2) NPARAMS     This gives the number of parameters in the fit.  This
C                  PARAMETER appears at the beginning of the main function,
C                  in the subroutines WRITE_IT_OUT, GET_ERRORS and
C                  GET_PARAMETERS.  These declarations can quickly be found
C                  by searching for the character string BMYNPARAMS.
C
C   Also, there is a parameter TOL which specifies the tolerance necessary for
C   the simplex routine AMOEBA to boot out.  The declaration for TOL appears
C   in the main function just below the NPARAMS declaration.
C
C
CCCCCCCCCCCCCCCCCCCCCCCCCCCCCCCCCCCCCCCCCCCCCCCCCCCCCCCCCCCCCCCCCCCCC
CCCCCCCCCCCCCCCCCCCCCCCCCCCCCCCCCCCCCCCCCCCCCCCCCCCCCCCCCCCCCCCCCCCCC
CCCCCCCC -- Main program begins here!!! CCCCCCCCCCCCCCCCCCCCCCCCCCCCCC
C
      INTEGER MAXDATCHAN,NCHAN,MINCHAN,MAXCHAN,STATMODE,FILEMODE
CBMYMAXDATCHAN
      PARAMETER( MAXDATCHAN = 4096 )
      COMMON /DATA_STUFF/ XDATA,DATA, DDATA, NCHAN, MINCHAN, MAXCHAN
      COMMON /STAT_MODE/ STATMODE
      COMMON /FILE_MODE/ FILEMODE
      REAL*8 XDATA( 0 : MAXDATCHAN-1 )
      REAL*8  DATA( 0 : MAXDATCHAN-1 )
      REAL*8 DDATA( 0 : MAXDATCHAN-1 )
C
C
      INTEGER NPARAMS, ITER
CBMYNPARAMS
      PARAMETER( NPARAMS = 7 )
      REAL P( (NPARAMS+1), NPARAMS ), Y( NPARAMS+1 ), TOL
```

```
      REAL ERR( NPARAMS )
      PARAMETER( TOL = 0.000001 )

      EXTERNAL ZLNPROB

      PRINT *,' '
      PRINT *,'03/19/93 == fit_spec version.  NOW READS ONLY X,Y FILES'
      PRINT *,' '

 5    PRINT *,' '
      PRINT *,'Whats the format of the input file?'
      PRINT *,' '
      PRINT *,'  1)  (X,Y)'
      PRINT *,'  2)  (X,Y,DY)'
      READ *,FILEMODE
      PRINT *,' '
      IF((FILEMODE.LT.1).OR.(FILEMODE.GT.2)) GOTO 5

      CALL READ_SPECTRUM
      IF ( NCHAN .LT. 0) GOTO 9999

      IF(FILEMODE.EQ.1) THEN
 10        PRINT *,' '
           PRINT *,'Do you want 1) Poisson distribution'
           PRINT *,'            2) Gaussian distribution: sigma=1'
           PRINT *,'            3) Gaussian distribution: sigma=sqrt(y)'
           PRINT *,'of data about model?'
           READ *,STATMODE
           PRINT *,' '
           IF((STATMODE.LT.1).OR.(STATMODE.GT.3)) GOTO 10
      ENDIF

      IF(FILEMODE.EQ.2) THEN
 15      PRINT *,' '
         PRINT *,'Do you want 1) Poisson distribution'
         PRINT *,'            2) Gaussian distribution: sigma=1'
         PRINT *,'            3) Gaussian distribution: sigma=sqrt(y)'
         PRINT *,
     + '            4) Gaussian distribution: sigma=dy from file'
         PRINT *,'of data about model?'
         READ *,STATMODE
         PRINT *,' '
         IF((STATMODE.LT.1).OR.(STATMODE.GT.4)) GOTO 15
      ENDIF

      CALL GET_PARAMETERS( P, Y )
      CALL AMOEBA(P,Y,(NPARAMS+1),NPARAMS,NPARAMS,TOL,ZLNPROB,ITER)
      CALL GET_ERRORS( P, ERR )
      CALL WRITE_IT_OUT( P, NCHAN, ITER, ERR )

 9999 END
C
CCCCCCCC -- Main program ends here!!! CCCCCCCCCCCCCCCCCCCCCCCCCCCCCCC
CCCCCCCCCCCCCCCCCCCCCCCCCCCCCCCCCCCCCCCCCCCCCCCCCCCCCCCCCCCCCCCCCCCCC
CCCCCCCCCCCCCCCCCCCCCCCCCCCCCCCCCCCCCCCCCCCCCCCCCCCCCCCCCCCCCCCCCCCCC
C
      SUBROUTINE READ_SPECTRUM
C
CCCCCCCCCCCCCCCCCCCCCCCCCCCCCCCCCCCCCCCCCCCCCCCCCCCCCCCCCCCCCCCCCCCCC
C
CCCCCCC -- Input:
C
C             None
C
CCCCCCC -- Output:  Both output arguments are contained in the common
C                   block DATA_STUFF.
```

```
C
C   DATA -- 1d array of size MAXDATCHAN into which the SARA fil is to be
C           read.
C
C   NCHAN - Number of data channels actually stuffed, if read is successfull.
C           If there is an error reading the file, NCHAN is assigned a value
C           of -1 and is trapped in the main program.
C
      INTEGER MAXDATCHAN,NCHAN,MINCHAN,MAXCHAN,FILEMODE
CBMYMAXDATCHAN
      PARAMETER( MAXDATCHAN = 4096 )
      COMMON /DATA_STUFF/ XDATA,DATA, DDATA, NCHAN, MINCHAN, MAXCHAN
      COMMON /FILE_MODE/ FILEMODE
      REAL*8 DATA( 0 : MAXDATCHAN-1 ),DDATA( 0 : MAXDATCHAN-1 )
      REAL*8 XDATA( 0 : MAXDATCHAN-1 )

      INTEGER*2 DUMMY, READ_OK_FLAG
      REAL*8    TOTAL_COUNTS
      REAL*8    XMIN,XMAX
      CHARACTER * 80 FILENAME

      PRINT *, ' '
      PRINT *, ' '
      PRINT *, 'Enter the name of the input data file. '
      PRINT *, ' '
      READ(*,'(A80)') FILENAME
      PRINT *, ' '
      PRINT *, ' '

      OPEN(UNIT=1,FILE=FILENAME,STATUS='OLD')

      IF(FILEMODE.EQ.1) THEN
         TOTAL_COUNTS=0.0
         NCHAN=0
 17        READ(UNIT=1,FMT=*,END=25,ERR=20) XDATA(NCHAN),DATA(NCHAN)
           TOTAL_COUNTS = TOTAL_COUNTS + DATA(NCHAN)
           NCHAN = NCHAN + 1
         GOTO 17
 20        PRINT *,'ERROR READING SPECTRUM FILE!!'
           PRINT *, ' '
           PRINT *, ' '
           NCHAN = -1
 25      GOTO 40
      ENDIF

      IF(FILEMODE.EQ.2) THEN
         TOTAL_COUNTS=0.0
         NCHAN=0
 27        READ(UNIT=1,FMT=*,END=35,ERR=30)
     +        XDATA(NCHAN), DATA(NCHAN), DDATA(NCHAN)
           TOTAL_COUNTS = TOTAL_COUNTS + DATA(NCHAN)
           NCHAN = NCHAN + 1
         GOTO 27
 30        PRINT *,'ERROR READING SPECTRUM FILE!!'
           PRINT *, ' '
           PRINT *, ' '
           NCHAN = -1
 35      GOTO 40
      ENDIF

 40   PRINT *,'Successfully read file'
      PRINT *, FILENAME
      PRINT *,' '
      PRINT *,'Number of channels read: '
      PRINT *,NCHAN
      PRINT *,' '
```

```
      PRINT *,'Total number of counts: '
      PRINT *,TOTAL_COUNTS
      PRINT *,' '
      PRINT *,'Enter the min and max X-values for the fit.'
      READ *, XMIN,XMAX
      PRINT *,' '
      PRINT *,' '

      MINCHAN = 0
      DO WHILE ( XMIN.GT.XDATA(MINCHAN) )
        MINCHAN = MINCHAN + 1
      ENDDO

      MAXCHAN = NCHAN-1
      DO WHILE ( XMAX.LT.XDATA(MAXCHAN) )
        MAXCHAN = MAXCHAN - 1
      ENDDO

      RETURN
      END
C
CCCCCCCCCCCCCCCCCCCCCCCCCCCCCCCCCCCCCCCCCCCCCCCCCCCCCCCCCCCCCCCCCCCCCC
CCCCCCCCCCCCCCCCCCCCCCCCCCCCCCCCCCCCCCCCCCCCCCCCCCCCCCCCCCCCCCCCCCCCCC
C
      SUBROUTINE GET_PARAMETERS( P, Y )
C
CCCCCCCCCCCCCCCCCCCCCCCCCCCCCCCCCCCCCCCCCCCCCCCCCCCCCCCCCCCCCCCCCCCCCC
C
CCCCCCC -- Input:
C
C              None
C
CCCCCCC -- Output:
C
C   P --- 2d matrix of dimensions (NPARAMS+1,NPARAMS) which will
C         contain the initial guesses for the parameters.  The NPARAMS+1
C         rows of this matrix contain a set of NPARAMS parameter guesses.
C
C   Y --- 1d vector of dimension (NPARAMS+1) which will contain the values
C         of the probability function ZLNPROB at each of the sets of parameters.
C
      INTEGER NPARAMS
CBMYNPARAMS
      PARAMETER( NPARAMS = 7 )
      REAL P( (NPARAMS+1), NPARAMS ), Y( NPARAMS+1 )

      INTEGER*4 I
      INTEGER DUM, GUESSNUM, PARAMNUM
      REAL FIRSTGUESS( NPARAMS ), PERCENTRANGE( NPARAMS ), FG, PR
      REAL GUESS

      PRINT *,'Okay, there are ',NPARAMS,' parameters in this fit.'
      PRINT *,'I need ',NPARAMS+1,' guesses for these parameters.'
 5    PRINT *,' '
      PRINT *,' '
      PRINT *,'You have 2 choices. 1) Enter all guesses yourself.'
      PRINT *,'                    2) Enter a guess and a percent range'
      PRINT *,'                       and let me make random guesses.'
      PRINT *,' '
      PRINT *,'Choose!!! '
      PRINT *,' '
      READ *,DUM
      PRINT *,' '
      PRINT *,' '
      IF (DUM .EQ. 1) THEN
        DO GUESSNUM = 1,NPARAMS+1
```

```
          DO PARAMNUM = 1,NPARAMS
                  PRINT *,'   Guess #: ',GUESSNUM
                  PRINT *,'   Param #: ',PARAMNUM
                  PRINT *,'Enter guess. '
                  PRINT *,' '
                  READ *,P( GUESSNUM, PARAMNUM )
                  PRINT *,' '
                  PRINT *,' '
          ENDDO
        ENDDO
      ELSE IF (DUM .EQ. 2) THEN
        DO PARAMNUM = 1,NPARAMS
          PRINT *,'Enter first guess and percent range for param # ',PARAMNUM
          PRINT *,' '
          READ *,FG,PR
          FIRSTGUESS( PARAMNUM ) = FG
          PERCENTRANGE( PARAMNUM ) = FG * PR / 2.0
          PRINT *,' '
          PRINT *,' '
        ENDDO
        PRINT *,'Enter seed for randum number generator.'
        READ *,I
        PRINT *,' '
        PRINT *,' '
        DO PARAMNUM = 1,NPARAMS
            P( 1, PARAMNUM ) = FIRSTGUESS( PARAMNUM )
        ENDDO
        DO GUESSNUM = 2,NPARAMS+1
          DO PARAMNUM = 1,NPARAMS
            GUESS=FIRSTGUESS(PARAMNUM)+(2.0*RAN(I)-1.0)*
     + PERCENTRANGE(PARAMNUM)
            P( GUESSNUM, PARAMNUM ) = GUESS
          ENDDO
        ENDDO
      ELSE
            PRINT *,'INVALID CHOICE'
            GOTO 5
      ENDIF
      PRINT *,' '
      PRINT *,'Values of prob func.'
      DO GUESSNUM = 1,NPARAMS+1
        DO PARAMNUM = 1,NPARAMS
            FIRSTGUESS( PARAMNUM ) = P( GUESSNUM, PARAMNUM )
        ENDDO
        Y( GUESSNUM ) = ZLNPROB( FIRSTGUESS )
        PRINT *,Y( GUESSNUM )
      ENDDO
      PRINT *,' '

      END
C
CCCCCCCCCCCCCCCCCCCCCCCCCCCCCCCCCCCCCCCCCCCCCCCCCCCCCCCCCCCCCCCCCCCCCC
CCCCCCCCCCCCCCCCCCCCCCCCCCCCCCCCCCCCCCCCCCCCCCCCCCCCCCCCCCCCCCCCCCCCCC
C
      SUBROUTINE GET_ERRORS( P, ERR )
C
CCCCCCCCCCCCCCCCCCCCCCCCCCCCCCCCCCCCCCCCCCCCCCCCCCCCCCCCCCCCCCCCCCCCCC
C
CCCCCCC -- Input:
C
C   P --- 2d array of dimension (NPARAMS+1,NPARAMS) containing the
C         final values for the fit parameters.
C
CCCCCCC -- Output:
C
C   ERR - 1d array of dimension (NPARAMS) containing errors on each parameter
```

```
C           None
C
      INTEGER NPARAMS, PARAMNUM, DUM, GUESSNUM
CBMYNPARAMS
      PARAMETER( NPARAMS = 7 )
      REAL P( (NPARAMS+1), NPARAMS ), AVG( NPARAMS ), ERR( NPARAMS )
      REAL PARAMSUM,PARAMVAL,DELTA,Y0,Y_PLUS_DEL,Y_MINS_DEL
      REAL TOP,BOTTOM

      DO PARAMNUM = 1,NPARAMS
        PARAMSUM = 0.0
        DO GUESSNUM = 1,(NPARAMS+1)
            PARAMSUM = PARAMSUM + P(GUESSNUM,PARAMNUM)
        ENDDO
        AVG( PARAMNUM ) = PARAMSUM/FLOAT(NPARAMS + 1)
      ENDDO

      DO PARAMNUM = 1,NPARAMS
        PARAMVAL = AVG(PARAMNUM)
        DELTA = PARAMVAL*0.01

        AVG(PARAMNUM) = PARAMVAL-DELTA
        Y_MINS_DEL = ZLNPROB( AVG )

        AVG(PARAMNUM) = PARAMVAL+DELTA
        Y_PLUS_DEL = ZLNPROB( AVG )

        AVG(PARAMNUM) = PARAMVAL
        Y0 = ZLNPROB( AVG )

        BOTTOM = Y_PLUS_DEL- 2.0*Y0+Y_MINS_DEL
        IF (BOTTOM.LT.0.0001) THEN
            ERR(PARAMNUM) = 999999.0
        ELSE
            ERR(PARAMNUM) = SQRT( ABS( 2.0*DELTA / BOTTOM ) )
        ENDIF
      ENDDO
      RETURN
      END
C
CCCCCCCCCCCCCCCCCCCCCCCCCCCCCCCCCCCCCCCCCCCCCCCCCCCCCCCCCCCCCCCCCCCCCCC
CCCCCCCCCCCCCCCCCCCCCCCCCCCCCCCCCCCCCCCCCCCCCCCCCCCCCCCCCCCCCCCCCCCCCCC
C
      SUBROUTINE WRITE_IT_OUT( P, NCHAN, ITER, ERR )
C
CCCCCCCCCCCCCCCCCCCCCCCCCCCCCCCCCCCCCCCCCCCCCCCCCCCCCCCCCCCCCCCCCCCCCCC
C
CCCCCCC -- Input:
C
C   P --- 2d array of dimension (NPARAMS+1,NPARAMS) containing the
C         final values for the fit parameters.
C
C   NCHAN -- Number of channels in input spectrum.  This is used to
C            write out a file containing (x,y) values for the fit function.
C
C   ITER -- number of iterations needed for AMOEBA to converge.
C
C   ERR --- 1d array of dimension (NPARAMS) containing sigma for each
C           parameter.
C
CCCCCCC -- Output:
C
C           None
C
      INTEGER NPARAMS, NCHAN, ITER, GUESSNUM, PARAMNUM, DUM
CBMYNPARAMS
```

```
      PARAMETER( NPARAMS = 7 )
      REAL P( (NPARAMS+1), NPARAMS ), X( NPARAMS ), ERR( NPARAMS )
      CHARACTER * 80 FILENAME,COMMENT
      REAL PARAMSUM,Y
      REAL XMIN,XMAX,XX,DX,NUMSTEPS

      PRINT *,' '
      PRINT *,' '
      PRINT *,'Enter filename where I should write the results.'
      PRINT *,' '
      READ(*,'(A80)') FILENAME
      PRINT *,' '
      PRINT *,' '
      PRINT *,'Enter some comment about the fit.'
      PRINT *,' '
      READ(*,'(A80)') COMMENT
      PRINT *,' '
      PRINT *,' '
      OPEN(UNIT=1,FILE=FILENAME,STATUS='NEW')
      WRITE(1,*) COMMENT
      WRITE(1,*) ' '
      WRITE(1,*) 'Iterations = ',ITER
      PRINT *,'Iterations = ',ITER
      WRITE(1,*) ' '
      DO PARAMNUM = 1,NPARAMS
        WRITE(1,*) 'Parameter ',PARAMNUM,' :'
        PARAMSUM = 0.0
        DO GUESSNUM = 1,(NPARAMS+1)
            WRITE(1,*) '     ',P(GUESSNUM,PARAMNUM)
            PARAMSUM = PARAMSUM + P(GUESSNUM,PARAMNUM)
        ENDDO
        X( PARAMNUM ) = PARAMSUM/FLOAT(NPARAMS + 1)
        PRINT *,PARAMNUM,PARAMSUM/FLOAT(NPARAMS+1),ERR(PARAMNUM)
        WRITE(1,*) 'Avg. sigma = ',PARAMSUM/FLOAT(NPARAMS+1),
     +     ERR(PARAMNUM)
        WRITE(1,*) ' '
      ENDDO
      Y = ZLNPROB( X )
      PRINT *,'-ln(Prob) = ',Y
      PRINT *,' '
      WRITE(1,*) '-ln(Prob) = ',Y
      CLOSE(UNIT=1)
      PRINT *,' '
      PRINT *,'Do you want me to make a file with the fit function in '
      PRINT *,'xy format? '
      PRINT *,'1)Yes  Any other integer)No'
      PRINT *,' '
      PRINT *,'Choose!!! '
      PRINT *,' '
      READ *,DUM
      PRINT *,' '
      PRINT *,' '
      IF (DUM .EQ. 1) THEN
        PRINT *,'Enter filename where I should write the results.'
        PRINT *,' '
        READ(*,'(A80)') FILENAME
        PRINT *,' '
        PRINT *,' '
        OPEN(UNIT=1,FILE=FILENAME,STATUS='NEW')
        PRINT *,'Enter XMIN,XMAX,and number of steps.'
        PRINT *,' '
        READ *,XMIN,XMAX,NUMSTEPS
        PRINT *,' '
        PRINT *,' '
        DX = (XMAX-XMIN)/NUMSTEPS
        DO XX=XMIN,XMAX,DX
```

```
            Y = FITFUNC( X, XX )
            WRITE(1,*) XX,Y
          ENDDO
          CLOSE(UNIT=1)
      ENDIF

      RETURN
      END
C
CCCCCCCCCCCCCCCCCCCCCCCCCCCCCCCCCCCCCCCCCCCCCCCCCCCCCCCCCCCCCCCCCCCCCC
CCCCCCCCCCCCCCCCCCCCCCCCCCCCCCCCCCCCCCCCCCCCCCCCCCCCCCCCCCCCCCCCCCCCCC
C
      REAL FUNCTION ZLNPROB( X )
C
CCCCCCCCCCCCCCCCCCCCCCCCCCCCCCCCCCCCCCCCCCCCCCCCCCCCCCCCCCCCCCCCCCCCCC
C
CCCCCCC -- Input:
C
C   X -- A 1d array of dimension NPARAMS containing the parameters for
C        the fit.
C
CCCCCCC -- Output:
C
C   The returned funciton value is the value of the probability function
C   with the input parameters.
C
      REAL X(*)
      INTEGER MAXDATCHAN,NCHAN,MINCHAN,MAXCHAN,STATMODE
CBMYMAXDATCHAN
      PARAMETER( MAXDATCHAN = 4096 )
      COMMON /DATA_STUFF/ XDATA,DATA, DDATA, NCHAN, MINCHAN, MAXCHAN
      COMMON /STAT_MODE/ STATMODE
      REAL*8   DATA( 0 : MAXDATCHAN-1 )
      REAL*8 DDATA( 0 : MAXDATCHAN-1 )
      REAL*8 XDATA( 0 : MAXDATCHAN-1 )

      REAL*8 F, SUM, TEMP
      INTEGER CHAN
      REAL*8 XX, Y, DY

      SUM = 0.0
      DO CHAN = MINCHAN,MAXCHAN
        XX= XDATA( CHAN )
        Y = DATA( CHAN )
        DY= DDATA( CHAN )
        F = FITFUNC( X, XX )
C
C  If statmode = 1 then we want Poisson statistics
C
        IF (STATMODE.EQ.1) THEN
           IF (F.GT.0.0) THEN
              SUM = SUM + F - Y * LOG(F) + FACLOG(NINT(Y))
           ELSE
              PRINT *,F
           ENDIF
        ENDIF
C
C  If statmode = 2 then we want Gaussian statistics, calculate good ol'
C  fashioned chi-squared with sigma=1.
C
        IF (STATMODE.EQ.2) THEN
            TEMP = (Y - F)
            SUM = SUM + TEMP*TEMP/2.0
        ENDIF
C
C  If statmode = 3 then we want Gaussian statistics, calculate good ol'
```

```
C  fashioned chi-squared with sigma=sqrt(y).
C
        IF (STATMODE.EQ.3) THEN
            IF (Y.LE.0.0) THEN
              DY = 1.0
            ELSE
              DY = SQRT(Y)
            ENDIF
            TEMP = (Y - F)/DY
            SUM = SUM + TEMP*TEMP/2.0
        ENDIF
C
C  If statmode = 4 then we want Gaussian statistics, calculate good ol'
C  fashioned chi-squared with sigma=dy from data file
C
        IF (STATMODE.EQ.4) THEN
            TEMP = (Y - F)/DY
            SUM = SUM + TEMP*TEMP/2.0
        ENDIF

      ENDDO
      ZLNPROB = SUM

      RETURN
      END
C
cccccccccccccccccccccccccccccccccccccccccccccccccccccccccccccccccccccc
cccccccccccccccccccccccccccccccccccccccccccccccccccccccccccccccccccccc
C
      REAL FUNCTION FACLOG( N )
C
cccccccccccccccccccccccccccccccccccccccccccccccccccccccccccccccccccccc
C
CCCCCCC -- Input:
C
C   N -- Integer argument
C
CCCCCCC -- Output:
C
C   The value returned is the natural log of the factorial of the argument.
C
      INTEGER I,N

      FACLOG = 0.0
      IF (N .GT. 1 ) THEN
        DO I = 2,N
          FACLOG = FACLOG + LOG(FLOAT(I))
        ENDDO
      ENDIF

      RETURN
      END
C
cccccccccccccccccccccccccccccccccccccccccccccccccccccccccccccccccccccc
cccccccccccccccccccccccccccccccccccccccccccccccccccccccccccccccccccccc
CBMYFITFUNC
C
      REAL FUNCTION FITFUNC(X, XX)
C
cccccccccccccccccccccccccccccccccccccccccccccccccccccccccccccccccccccc
C
CCCCCCC -- Input:
C
C   X --- 1d array of dimension NPARAMS containing the fit parameters.
C
C   XX -- X value at which to evaluate the function.
```

```
C
CCCCCCC -- Output:
C
C   The returned value is fit function evaluated at the input channel number
C   with the input parameter set.
C
C   Functional form has 5 components:
C
C   ---A constant background  K
C
C   ---A 3 body phase space background
C         ZETA = ( CHAN - X0 ) / ( ENDCHAN - X0 )
C         BACK = A * SQRT( 1 - ZETA*ZETA )
C
C   ---2 p-waves
C      PWAVE = N * EXP( -(E-XR)*(E-XR)/(2*GLOW*GLOW) )
C   if chan > xr
C
C      PWAVE = N * [ R + (1-R) * GHI * GHI / (FUDGEHI*(E-XR)**2 + GHI*GHI) ]
C   if chan < xr
C
C    R   = -0.06874 + 0.38989*EN - 0.18571*EN*EN
C    GHI =  2.31417 - 6.22500*EN + 3.83333*EN*EN
C    GLOW = -0.09409 + 0.53771*EN - 0.21429*EN*EN
C    FUDGEHI = 61.96055 - 231.11300*EN + 216.0000*EN*EN
C
C    GHI**2 = GHI**2 + FUDGEHI*DEVHWHM*DEVHWHM
C    GLOW**2 = GLOW**2 + DEVHWHM*DEVHWHM/2LN2
C
C   ---A narrow s-wave at zero energy
C         SWAVE = B * 9.923 / ( (CHAN-ZEROCHAN)**2 + 9.923 )
C
C
C
C   X(1) = XR1 \
C   X(2) = N1   > p-wave parameters
C   X(3) = XR2 /
C   X(4) = N2 /
C   X(5) = B    > s-wave parameter
C   X(6) = A    > 3body background amplitude
C   X(7) = K    > constant background
C
C
C
      REAL X(*)
      REAL*8 XX
      REAL EN
      REAL DEVHWHM
      REAL RE, GLOWE, GHIE, FUDGEHIE
      REAL R,  GLOW,  GHI,  FUDGEHI
      REAL ZZ,PWAVE1,PWAVE2
      REAL SWAVE, ZEROCHAN
      REAL ENDCHAN, X0, ZETA, BACKGROUND
      REAL K
C
C First P-WAVE
C
C
C OK first convert X(1) to neutron resonance energy
C
C Use the calibration at the bottom of p116 in log, converted to a 1k
C scale.  This is only good for 0.1 < EN < 1.25.
C
      EN = 18.3621 - 0.03412*X(1)
C
C Now calculate RE,GLOWE,GHIE,FUDGEHIE
```

```
C
C NOTE: In real life DEVHWHM = 0.115MeV.  Using the above calibration
C        for a 1k scale, this corresponds to HWHM = 3.370 chan/1k
C                                                FWHM = 6.741 chan/1k
C
      DEVHWHM = 0.115
      RE   =   -0.06874 + 0.38989*EN - 0.18571*EN*EN
      FUDGEHIE = 61.96055 - 231.11300*EN + 216.0000*EN*EN
      GHIE = 2.31417-6.22500*EN+3.83333*EN*EN
      GLOWE =  -0.09409 + 0.53771*EN - 0.21429*EN*EN
C
C Now add the device HWHM
C
      GHIE = SQRT( GHIE**2 + FUDGEHIE*DEVHWHM*DEVHWHM )
      GLOWE = SQRT( GLOWE**2 + DEVHWHM*DEVHWHM/1.3863 )
C
C Now we need to convert from energies back to channels
C
C  FUDGEHIE and RE dont need to be changed
C  GHIE and GLOWE do ==>    G = GE / (dE/dx)
C
      FUDGEHI = FUDGEHIE
      R = RE
      GHI = GHIE / 0.03412
      GLOW = GLOWE / 0.03412
C
C Calculate the resonance shape
C
      ZZ = XX-X(1)
      IF (ZZ.LT.0.0) THEN
        PWAVE1 = X(2) * (R + (1.0-R)*GHI*GHI/(FUDGEHI*ZZ*ZZ+GHI*GHI))
      ELSE
        PWAVE1 = X(2)*EXP(-(ZZ*ZZ)/(2.0*GLOW*GLOW))
      ENDIF
C
C Second P-WAVE
C
C
C OK first convert X(3) to neutron resonance energy
C
C Use the calibration at the bottom of p100 in log, converted to a 1k
C scale.  This is only good for 0.1 < EN < 1.25.
C
      EN = 18.3621 - 0.03412*X(3)
C
C Now calculate RE,GLOWE,GHIE,FUDGEHIE
C
C NOTE: In real life DEVHWHM = 0.115MeV.  Using the above calibration
C        for a 1k scale, this corresponds to HWHM = 3.370 chan/1k
C                                                FWHM = 6.741 chan/1k
C
      DEVHWHM = 0.115
      RE   =   -0.06874 + 0.38989*EN - 0.18571*EN*EN
      FUDGEHIE = 61.96055 - 231.11300*EN + 216.0000*EN*EN
      GHIE = 2.31417-6.22500*EN+3.83333*EN*EN
      GLOWE =  -0.09409 + 0.53771*EN - 0.21429*EN*EN
C
C Now add the device HWHM
C
      GHIE = SQRT( GHIE**2 + FUDGEHIE*DEVHWHM*DEVHWHM )
      GLOWE = SQRT( GLOWE**2 + DEVHWHM*DEVHWHM/1.3863 )
C
C Now we need to convert from energies back to channels
C
C  FUDGEHIE and RE dont need to be changed
C  GHIE and GLOWE do ==>    G = GE / (dE/dx)
```

```
C
      FUDGEHI = FUDGEHIE
      R = RE
      GHI = GHIE / 0.03412
      GLOW = GLOWE / 0.03412
C
C Calculate the resonance shape
C
      ZZ = XX-X(3)
      IF (ZZ.LT.0.0) THEN
        PWAVE2 = X(4) * (R + (1.0-R)*GHI*GHI/(FUDGEHI*ZZ*ZZ+GHI*GHI))
      ELSE
        PWAVE2 = X(4)*EXP(-(ZZ*ZZ)/(2.0*GLOW*GLOW))
      ENDIF
C
C S-WAVE
C
C   Note -- 11.360 is 3.370 squared -- the s-wave is the width of
C           the resolution
C
C      ZEROCHAN = 538.1624   <===   0 keV
C      ZEROCHAN = 536.6970   <===  50 keV
C      ZEROCHAN = 535.2315   <=== 100 keV
C
      ZEROCHAN = 536.6970
      ZETA = XX - ZEROCHAN
      IF ( X(5) .LT. 0.0 )  X(5) = 0.0
      SWAVE = X(5) * 11.360 / ( ZETA*ZETA + 11.360 )
C
C BACKGROUND
C
C   Note -- ENDCHAN is the kinematic limit for the reaction
C           X0 is a parameter determined from 3body phase space calculations
C           Both are in a 1024 spectrum
C
      ENDCHAN = 538.1624
      X0 = 237.9954
      ZETA = ( XX - X0 ) / ( ENDCHAN - X0 )
      IF ( XX .LT. ENDCHAN ) THEN
         IF ( X(6) .LT. 0.0 ) X(6) = 0.0
         BACKGROUND = X(6) * SQRT( 1.0 - ZETA*ZETA )
      ELSE
         BACKGROUND = 0.0
      ENDIF
C
C CONSTANT BACKGROUND
C
      IF(X(7).LT.0.0) X(7)=0.0
C
C NOW ADD IT UP
C
      FITFUNC = BACKGROUND + SWAVE + PWAVE1 + PWAVE2 + X(7)
      RETURN
      END
C
CCCCCCCCCCCCCCCCCCCCCCCCCCCCCCCCCCCCCCCCCCCCCCCCCCCCCCCCCCCCCCCCCCCCCCC
CCCCCCCCCCCCCCCCCCCCCCCCCCCCCCCCCCCCCCCCCCCCCCCCCCCCCCCCCCCCCCCCCCCCCCC
C
      SUBROUTINE AMOEBA(P,Y,MP,NP,NDIM,FTOL,FUNK,ITER)
C
CCCCCCCCCCCCCCCCCCCCCCCCCCCCCCCCCCCCCCCCCCCCCCCCCCCCCCCCCCCCCCCCCCCCCCC
C
CCCCCCC -- Input:
C
C
C
```

```
CCCCCCC -- Output:
C
C
C
      PARAMETER (NMAX=20,ALPHA=1.0,BETA=0.5,GAMMA=2.0,ITMAX=500)
      DIMENSION P(MP,NP),Y(MP),PR(NMAX),PRR(NMAX),PBAR(NMAX)
      MPTS=NDIM+1
      ITER=0
1     ILO=1
      IF(Y(1).GT.Y(2))THEN
        IHI=1
        INHI=2
      ELSE
        IHI=2
        INHI=1
      ENDIF
      DO 11 I=1,MPTS
        IF(Y(I).LT.Y(ILO)) ILO=I
        IF(Y(I).GT.Y(IHI))THEN
          INHI=IHI
          IHI=I
        ELSE IF(Y(I).GT.Y(INHI))THEN
          IF(I.NE.IHI) INHI=I
        ENDIF
11    CONTINUE
      RTOL=2.*ABS(Y(IHI)-Y(ILO))/(ABS(Y(IHI))+ABS(Y(ILO)))
      IF(RTOL.LT.FTOL)RETURN
      IF(ITER.EQ.ITMAX) PAUSE 'Amoeba exceeding maximum iterations.'
      ITER=ITER+1
      DO 12 J=1,NDIM
        PBAR(J)=0.
12    CONTINUE
      DO 14 I=1,MPTS
        IF(I.NE.IHI)THEN
          DO 13 J=1,NDIM
            PBAR(J)=PBAR(J)+P(I,J)
13        CONTINUE
        ENDIF
14    CONTINUE
      DO 15 J=1,NDIM
        PBAR(J)=PBAR(J)/NDIM
        PR(J)=(1.+ALPHA)*PBAR(J)-ALPHA*P(IHI,J)
15    CONTINUE
      YPR=FUNK(PR)
      IF(YPR.LE.Y(ILO))THEN
        DO 16 J=1,NDIM
          PRR(J)=GAMMA*PR(J)+(1.-GAMMA)*PBAR(J)
16      CONTINUE
        YPRR=FUNK(PRR)
        IF(YPRR.LT.Y(ILO))THEN
          DO 17 J=1,NDIM
            P(IHI,J)=PRR(J)
17        CONTINUE
          Y(IHI)=YPRR
        ELSE
          DO 18 J=1,NDIM
            P(IHI,J)=PR(J)
18        CONTINUE
          Y(IHI)=YPR
        ENDIF
      ELSE IF(YPR.GE.Y(INHI))THEN
        IF(YPR.LT.Y(IHI))THEN
          DO 19 J=1,NDIM
            P(IHI,J)=PR(J)
19        CONTINUE
          Y(IHI)=YPR
```

```
          ENDIF
          DO 21 J=1,NDIM
            PRR(J)=BETA*P(IHI,J)+(1.-BETA)*PBAR(J)
21        CONTINUE
          YPRR=FUNK(PRR)
          IF(YPRR.LT.Y(IHI))THEN
            DO 22 J=1,NDIM
              P(IHI,J)=PRR(J)
22          CONTINUE
            Y(IHI)=YPRR
          ELSE
            DO 24 I=1,MPTS
              IF(I.NE.ILO)THEN
                DO 23 J=1,NDIM
                  PR(J)=0.5*(P(I,J)+P(ILO,J))
                  P(I,J)=PR(J)
23              CONTINUE
                Y(I)=FUNK(PR)
              ENDIF
24          CONTINUE
          ENDIF
        ELSE
          DO 25 J=1,NDIM
            P(IHI,J)=PR(J)
25        CONTINUE
          Y(IHI)=YPR
        ENDIF
        GO TO 1
        END
```

Bibliography

[Abra 73] S. N. Abramovich, B. Ya. Guzhovskii, A. G. Zvenigorodskii, and S. V. Trusillo, Bull. Acad. Sci. USSR, Phys. Ser. **37**, 144 (1973).

[Amel 90] A. I. Amelin, M. G. Gornov, Yu. B. Gurov, A. L. Il'in, P. V. Morokhov, V. A. Pechkurov, V. I. Savel'ev, F. M. Sergeev, S. A. Smirnov, B. A. Chernyshev, R. R. Shafigullin, and A. V. Shishkov, Sov. J. Nucl. Phys. **52**, 783 (1990).

[Anne 90] R. Anne, S. E. Arnell, R. Bimbot, H. Emling, D. Guillemaud-Mueller, P. G. Hansen, L. Johannsen, B. Jonson, M. Lewitowicz, S. Mattsson, A. C. Mueller, R. Neugart, G. Nyman, F. Pougheon, A. Richter, K. Riisager, M. G. Saint-Laurent, G. Schrieder, O. Sorlin, and K. Wilhelmsen, Phys. Lett. B **250**, 19 (1990).

[Bang 92] J. M. Bang and I. J. Thompson, Phys. Lett. B **279**, 201 (1992). For errata see Surrey University preprint CNP93/4.

[Bark 77] F. C. Barker and G. T. Hickey, J. Phys. G: Nucl. Phys **3**, L23 (1977).

[Barr 93] F. Barranco, Proceedings of Third International Conference on Radioactive Nuclear Beams, East Lansing, Michigan, May 23–27, 1993, D. J. Morrissey, Ed., **Editions Frontières**, (Gif-sur-Yvette, 1993).

[Bert 91] G. F. Bertsch and H. Esbensen, Ann. Phys. (N.Y.) **209**, 327 (1991).

[Bevi 69] P. B. Bevington, *Data Reduction and Error Analysis for the Physical Sciences* (McGraw–Hill, New York, 1969), Chap. 11.

[Blan 91] B. Blank, J.-J. Gaimard, H. Geissel, K.-H. Schmidt, H. Stelzer, K. Sümmerer, D. Bazin, R. Del Moral, J. P. Dufour, A. Fleury, F. Hubert, H.-G. Clerc, and M. Steiner, Z. Phys. A **340**, 41 (1991).

[Blat 52] J. M. Blatt and V. F. Weisskopf, *Theoretical Nuclear Physics* (J. Wiley & Sons, New York, 1952), Chap. 1.

[Bloc 56] M. M. Block, Phys. Rev. **101**, 796 (1956).

[Bohl 93] H. G. Bohlen, B. Gebauer, M. von Lucke–Petsch, W. von Oertzen, A. N. Ostrowski, M. Wilpert, Th. Wilpert, H. Lenske, D. V. Alexandrov, A. S. Demyanova, E. Nikolskii, A. A. Korsheninnikov, A. A. Ogloblin, R. Kalpakchieva, Y. E. Penionzhkevich, and S. Piskor, Z. Phys. A **344**, 381 (1993).

[Boyd 93] R. N. Boyd, Int. J. Mod. Phys. E, to be published.

[Brow 92] B. A. Brown, private communication.

[Esbe 93] H. Esbensen, G. F. Bertsch, and K. Ieki, Phys. Rev. C **48**, 326 (1993).

[Fuku 91] M. Fukuda, T. Ichihara, N. Inabe, T. Kubo, H. Kumagai, T. Nakagawa, Y. Yano, I. Tanihata, M. Adachi, K. Asahi, M. Kouguchi, M. Ishihara, H. Sagawa, and S. Shimoura, Phys. Lett. B **268**, 339 (1991).

[Gold 48] M. Goldhaber and E. Teller, Phys. Rev. **74**, 1046 (1948).

[Gold 74] A. S. Goldhaber, Phys. Lett. B **53**, 306 (1974).

[Grei 75] D. E. Greiner, P. J. Lindstrom, H. H. Heckman, B. Cork, and F. S, Bieser, Phys. Rev. Lett. **35**, 152 (1975).

[Hans 87] P. G. Hansen and B. Jonson, Europhys. Lett. **4**, 409 (1987).

[Heck 76] H. Heckman and P. J. Lindstrom, Phys. Rev. Lett. **37** 56 (1976).

[Hüfn 81] J. Hüfner and M. C. Nemes, Phys. Rev. C **23**, 2538 (1981).

[Ieki 93] K. Ieki, D. Sackett, A. Galonsky, C. A. Bertulani, J. J. Kruse, W. G. Lynch, D. J. Morrissey, N. A. Orr, H. Schulz, B. M. Sherrill, A. Sustich, J. A. Winger, F. Deák, Á. Horváth, Á. Kiss, Z. Seres, J. J. Kolata, R. E. Warner, and D. L. Humphrey, Phys. Rev. Lett. **70**, 730 (1993).

[Joha 90] L. Johannsen, A. S. Jensen, and P. G. Hansen, Phys. Lett. B **244**, 357 (1990).

[Klap 69] R. Klapisch, C. Thibault–Phillipe, C. Détraz, and C. Rigaud, Phys. Rev. Lett. **23** 652 (1969).

[Koba 88] T. Kobayashi, O. Yamakawa, K. Omata, K. Sugimoto, T. Shimoda, N. Takahashi, and I. Tanihata, Phys. Rev. Lett. **60**, 2599 (1988).

[Koba 89] T. Kobayashi, S. Shimoura, I. Tanihata, K. Katori, K. Matsuta, T. Minamisono, K. Sugimoto, W. Müller, D. L. Olson, T. J. M. Symons, and H. Wieman, Phys. Lett. B **232**, 51 (1989).

[Koba 92] T. Kobayashi, Nucl. Phys. **A538**, 343c (1992).

[Koba 93] T. Kobayashi, Proceedings of Third International Conference on Radioactive Nuclear Beams, East Lansing, Michigan, May 23–27, 1993, D. J. Morrissey, Ed., **Editions Frontières**, (Gif-sur-Yvette, 1993).

[Koon 86] S. E. Koonin, *Computational Physics* (Addison–Wesley, New York, 1986), page 50ff.

[Kryg 93] R. Kryger, A. Azhari, A. Galonsky, J. H. Kelley, R. Pfaff, E. Ramakrishnan, D. Sackett, B. M. Sherrill, M. Thoennessen, J. A .Winger, and S. Yokoyama, Phys. Rev. C **47**, 2439 (1993).

[Mant 90] S. A. Mantha and F. Z. Kitters, Phys. Rev. C **38**, 587 (1988).

[Nole 74] J. A. Nolen, Jr., G. Hamilton, E. Kashy, and I. D. Proctor, Nucl. Instr. and Meth. **115**, 189 (1974).

[Orr 92] N. A. Orr, N. Anantaraman, S. M. Austin, C. A. Bertulani, K. Hanold, J. H. Kelley, D. J. Morrissey, B. M. Sherrill, G. A. Souliotis, M. Thoennessen, J. S. Winfield, and J. A. Winger, Phys. Rev. Lett. **69**, 2050 (1992).

[Plic 92] Hans van der Plicht and John Winfield, *The S320 Spectrograph Manual*, unpublished NSCL document.

[Posk 66] A. M. Poskanzer, S. W. Cosper, E. K. Hyde, and J. Cerny, Phys. Rev. Lett. **17** 1271 (1966)

[Pres 86] W. H. Press, B. P. Flannery, S. A. Teukolsky, and W. T. Vetterling, *Numerical Recipes (FORTRAN edition)* (Cambridge University Press, New York, 1986), Chap. 10.

[Pres 92] W. H. Press, S. A. Teukolsky, W. T. Vetterling, and B. P. Flannery, *Numerical Recipes in C* (Cambridge University Press, New York, 1992), Chap. 15.

[Riis 92] K. Riisager, R. Anne, S. E. Arnell, R. Bimbot, H. Emling, D. Guillemaud–Mueller, P. G. Hansen, L. Johannsen, B. Jonson, A. Latimier, M. Lewitowicz, S. Mattsson, A. C. Mueller, R. Neugart, G. Nyman, F. Pougheon, A. Richard, A. Richter, M. G. Saint–Laurent, G. Schrieder, O. Sorlin, and K. Wilhelmsen, Nucl. Phys. **A540**, 365 (1992).

[Sher 85] R. Sherr and G. Bertsch, Phys. Rev. C **32**, 1809 (1985).

[Sher 83] B. M. Sherrill, Ph.D. thesis, Michigan State University (1983).

[Sher 91] B. M. Sherrill, D. J. Morrissey, J. A. Nolen Jr., and J. A. Winger, Nucl. Instr. and Meth. **B56/57**, 1106 (1991).

[Shim 87] S. Shimoura *et al.*, Abstracts of Contributions to the Eleventh International Conference on Particles and Nuclei, Kyoto, 1987.

[Tani 85a] I. Tahihata, H. Hamagaki, O. Hashimoto, Y. Shida, N. Yoshikawa, K. Sugimoto, O. Yamakawa, T. Kobayashi, and N. Takahashi, Phys. Rev. Lett. **55**, 2676 (1985).

[Tani 85b] I. Tanihata, *et al.*, Phys. Lett. B **160**, 380 (1985).

[Tani 92] I. Tanihata, D. Hirata, T. Kobayashi, S. Shimoura, K. Sugimoto, and H. Toki, Phys. Lett. B **289**, 261 (1992).

[Thib 75] C. Thibault, R. Klapisch, C. Rigaud, A. M. Poskanzer, R. Prieels, L. Lessard, and W. Reisdorf, Phys. Rev. C **12** 644 (1975).

[Thom 93a] I. J. Thompson, Proceedings of Third International Conference on Radioactive Nuclear Beams, East Lansing, Michigan, May 23–27, 1993, D. J. Morrissey, Ed., **Editions Frontières**, (Gif-sur-Yvette, 1993).

[Thom 93b] I. J. Thompson and M. V. Zhukov, in preparation.

[Tosa 90] Y. Tosaka and Y. Suzuki, Nucl. Phys. **A512**, 46 (1990).

[Warb 92] E. K. Warburton and B. A. Brown, Phys. Rev. C **46** 923 (1992).

[Wilc 75] K. H. Wilcox, R. B. Weisenmiller, G. J. Wozniak, N. A. Jelley, D. Ashery, and J. Cerny, Phys. Lett. B **59**, 142 (1975).

[Wong 90] S. S. M. Wong, "Introductory Nuclear Physics", Prentice–Hall, 1990, pp. 254–261.

[Wout 88] J. M. Wouters, R. H. Kraus Jr., D. J. Viera, G. W. Butler, and K. E. G. Löbner, Z. Phys. A **331**, 229 (1988).

[Zhuk 91] M. V. Zhukov, B. V. Danilin, D. V. Federov, J. S. Vaagen, F. A. Gareev, and J. Bang, Phys. Lett. B **265**, 19 (1991).

[Zhuk 93] M. V. Zhukov, B. V. Danilin, D. V. Fedorov, J. M. Bang, I. J. Thompson, and V. S. Vaagen, Phys. Rep. **231**, 151 (1993).